Strongly Correlated Electrons in Atomic Liquids:

Gutzwiller Molecular Dynamics Simulations

Chen Cheng

A Thesis submitted to the Graduate Faculty

of the University of Virginia in Candidacy for the Degree of

Doctor of Philosophy

Department of Physics

University of Virginia

May 2024

Prof. Gia-Wei Chern, Advisor, Chair

Prof. Marija Vucelja

Prof. Utpal Chatterjee

Prof. Mona Zebarjadi, GSAS Rep

ii

Strongly Correlated Electrons in Atomic Liquids: Gutzwiller Molecular Dynamics Simulations

Chen Cheng

(ABSTRACT)

In this thesis, we study the intricate interplay between the electronic structure and atomic distribution in liquid metal models featuring electron-electron interaction. In Chapter 2, we introduce the model employed to examine correlated electrons in liquids. Furthermore, we delve into the Gutzwiller variational method, offering an in-depth discussion alongside modern formulations. Additionally, we detail the implementation of Gutzwiller molecular dynamics for our study.

In chapter 3, we study the influence of the atomic distribution on the electronic structure. Our focus lies in the Mott transition in metallic liquids, and draws comparisons to its manifestation in amorphous solids. We demonstrate a rather counter-intuitive phenomenon in metallic fluids where the electrical conductivity of a liquid system can be enhanced by electron correlation effects. We show that while electron hopping is indeed suppressed by a larger Hubbard repulsion, the reduced electronic cohesive forces give rise to atomic clusters with a larger coordination number. The increased atomic connectivity in turn results in an enhanced electrical conductance.

In Chapter 4, we delve into the impact of electron localization on atomic transport properties. Our investigation unveils an unusual peak in atomic diffusion in proximity to the Mott transition in the Hubbard liquid model. To elucidate this intriguing observation, we proposed a general theory based on the Chapman-Enskog method. Remarkably, our theoretical framework successfully replicates this phenomenon in

classical simple liquids.

In chapter 5, we employed the Gutzwiller molecular dynamics to study the liquid-liquid transition in dense hydrogen. We constructed an ab initio tight-binding model tailored specifically for hydrogen. Our simulation results characterise a metal-insulator transition in liquid hydrogen. Notably, this transition arises not from correlated interactions but rather from the dissociation of hydrogen molecules.

Dedication

To my grandparents

Acknowledgments

First, I would like to express my immense gratitude to my supervisor, Prof. Gia-wei Chern, for his unwavering support, guidance, and invaluable insights throughout the entirety of my doctoral research. His expertise, patience, and encouragement have been instrumental in shaping this thesis and my academic journey.

I am also grateful to the members of my thesis committee, Prof. Marija Vucelja, Prof. Utpal Chatterjee and Prof. Mona Zebarjadi, for their constructive feedback and invaluable suggestions, which significantly enriched the quality of this work.

I would like to acknowledge the University of Virginia, for providing the necessary resources and facilities essential for carrying out this research.

I am also thankful to my colleagues and friends for their encouragement, support, and stimulating discussions throughout this journey.

Last but not least, I express my heartfelt gratitude to my family for their unwavering love, without which this accomplishment would not have been possible.

Contents

List of Figures

List of Abbreviations

DC   direct current

DFT   density functional theory

DOS   density of states

GA   Gutzwiller approximation

GMD   Gutzwiller molecular dynamics

GTO   Gaussian-type orbital

GWF   Gutzwiller wave function

HF   Hartree-Fork

LCAO linear combination of atomic orbitals

LDA   local density approximation

LJ   Lennard-Jones

MD   molecular dynamics

MIT   metal-insulator transition

MT   Mott transition

PBC   periodic boundary condition

SCF   self-consistent field

STO   Slater-type orbital

Chapter 1

Introduction

Understanding the metal-insulator transition (MIT) is one of the central problems in condensed matter physics [1, 2]. In 1931, Wilson [3, 4] gave the first successful theoretical depiction of metals, insulators, and the transitions connecting them, based on non-interacting or weakly interacting electron systems. This theory establishes a broad differentiation between metals and insulators at absolute zero temperature, based on the filling of electronic bands. Namely, insulators according to this picture are materials where all energy bands are completely occupied or empty. No current can flow under this situation and the conductivity is zero. A metal, on the other hand, is a material in which one or more energy bands are partially full. In other words, insulators have the Fermi level situated within a band gap, whereas in metals, it resides within a band. According to the non-interacting electron theory, the formation of band structure entirely stems from the periodic lattice arrangement of atoms within crystals.

The correlation induced insulator

This model has been very successful. However, it does not always work. In 1937, de Boer and Verwey [5] were the first to point out; for instance, cubic nickel oxide should be a metal according to the model. In the same year, Peierls first pointed out [6] the

electron-electron interaction could be the origin of the insulating behaviour. Materials with open d and f electron shells, where electrons inhabit confined orbitals, exhibit properties that pose challenges for explanation. In transition metals, such as vanadium, nickel, iron, and their oxides, electrons experience strong Coulomb repulsion because of their spatial confinement in those orbitals. These strongly interacting or correlated electrons cannot be described as embedded in a static mean field generated by other electrons. The impact of each electron on the others is too substantial to permit independent consideration of each.

The effect of correlations on material properties is often profound. The interplay of electrons' internal degrees of freedom, spin, charge, and orbital moment, can give rise to a diverse array of exotic ordering phenomena at low temperatures. The extraordinary phenomena range from huge changes in the conductivity across the metal-insulator transition (MIT) in vanadium oxide, and substantial volume changes across phase transitions in actinides and lanthanides, to high-temperature superconductivity in cuprates. These unique properties contribute to the excitement surrounding the potential applications of strongly correlated materials. Nevertheless, the complexity of these phenomena and their heightened sensitivity to microscopic details present significant challenges for both experimental investigation and analytical study.

Mott [7, 8, 9] took the first important step towards understanding how electron-electron correlations could explain the insulating state, recognized as the Mott insulator. The transition from a metal to a Mott insulator is called Mott transition (MT). A theoretical framework outlining the MT was achieved by using simplified lattice fermion models, notably in the celebrated Hubbard model. The Hubbard model [10, 11, 12, 13, 14] serves as the standard model for electrons with strong short-range interactions, it consists in allowing electron hopping between atoms and considering

a short-ranged on-site electron-electron repulsion while neglecting all other effects of the electron-electron interaction. Despite its simplicity, the Hubbard model does not have exact solutions, except for the one-dimensional lattice systems [15].

The Gutzwiller method

The search for the ground state of a many-electron system is a challenging task for condensed-matter physicists, since the complexity of the exact solution increases exponentially with the number of particles, and in many interesting cases, it is still not affordable with modern computers. One of the most powerful and widely used solver is the quantum Monte-Carlo algorithm [16, 17], it suffers from the well-known sign problem and can provide reliable results only for a limited class of models. Other numerically accurate methods include exact diagonalization, numerical renormalization group, density matrix renormalization group [18] and dynamical mean field theory [19, 20]. Nevertheless, these computationally advanced methods come with a high cost, a factor that becomes more pronounced in larger systems or when aiming to implement them in dynamic simulations.

In the early 1930s, Gutzwiller [21, 22, 23] proposed a variational approach to investigate the Hubbard model. He proposed a simple variational wave function (GWF), which introduces correlations into the non-interacting wave function via a local correlation factor in real space. To compute the ground state energy analytically, he further introduced a Gutzwiller approximation (GA) where spatial correlations are neglected, i.e. the many-body configurations at different lattice sites are assumed to be independent of each other. In the limit of infinite dimensions, for a single band GWF, the results of GA were found to be exact in these works [24, 25]. The results of

the Gutzwiller variational method can also be derived by the Kotliar-Ruckenstein [26] slave-boson mean-field theory, these two approaches are shown to be equivalent on a mean-field level [27, 28, 29].

In 1970, Brinkman and Rice [30] realized that, at half-filling, the Gutzwiller method describes a transition from a paramagnetic metal to a paramagnetic insulator at a finite interaction strength, where all electrons are localized. The Brinkman-Rice theory provides important insight into the Mott insulator. The Gutwiller method is perhaps the most efficient approach to successfully capture the crucial correlation effects. Contrary to a solitary Slater determinant forming the basis for either the Hartree-Fock (HF) or Kohn-Sham (KS) [31, 32] methods, the GWF comprises multiple Slater determinants is variationally optimized, aiming to strike a balance between the kinetic energy gain resulting from electron delocalization and the local Coulomb repulsion that occurs when two electrons occupy the same orbital [33].

Correlated electrons in liquids

While extensive efforts have been devoted to the MIT in crystals and amorphous solids [34, 35, 36, 37, 38], the MIT in liquid is less investigated. Early theoretical models studying liquid assumed no particular short-range order of atoms [39, 40, 41, 42], such approach to MIT in liquid is not much different from those developed for the MIT in amorphous solids.

One of the most unique aspects of MIT in liquids is the interplay between atomic dynamics and electronic structure. The electronic structure naturally depends on the atomic configuration. On the other hand, the distribution of atoms in liquids is determined by the inter-atomic forces, which in turn depend on the electronic

properties and particularly the degree of electron delocalization. Mott [43] pointed out this problem long ago: the difficulty in liquids is that we do not know how the atoms distribute and how they change with volume and temperature.

The development of the density functional theory (DFT) has enabled the ab initio MD simulation. These simulations are capable of capturing the ion dynamics, and have been employed to study the MIT in fluid alkali metals [44, 45]. However, one major drawback of DFT is its inability to capture the strong electron-electron correlation effects, in particular, it fails to describe the Mott transition.

Expanding fluid alkali metals are good examples to study the MIT in liquids [46]. Upon heating and increasing pressure simultaneously along the liquid-vapor coexistence curve up to the critical point, liquid metals can be substantially expanded. Due to the low critical temperatures, e.g. cesium (Cs): 1924 K, 9.25 MPa, rubidium(Rb): 2017 K, 12.45 MPa [47], their properties are accessible under laboratory conditions and have been extensively investigated in the past decades [48, 49, 50, 51, 52]. The MIT in alkali metals occurs at low densities close to their critical temperatures, and are suspected to be the Mott-Hubbard type transition. Various experimental observations support this argument, including the enhanced magnetic susceptibility [53], the increased density of states in nuclear magnetic resonance experiments [54, 55] and the enhancement of the effective optical electron mass [56].

For such correlation-induced MIT in liquid, DFT-MD may be insufficient in accurately capturing the intricate dynamics and electronic correlations involved. Additional computational techniques or advanced methodologies may be required to enhance the predictive capabilities and comprehensively model the complex interplay between electron location and molecular interactions in liquid states. The recently developed Gutzwiller quantum molecular dynamics (GMD) [57] represents a good

step in this direction. In this work [57], the Gutzwiller method was incorporated into MD simulations. This integration revealed a Mott transition in liquids and brought to light the intriguing structural and transport properties of the atoms.

Outline of the thesis

In this thesis, we extend the research initiated by [57], and delve deeper into the study of correlated electrons in liquids with the Gutzwiller quantum molecular dynamics. Chapter 3, 4 and 5 each contains an independent project, accessible for reading subsequent to Chapters 1 and 2.

In **chapter 2**, we give a comprehensive discussion of the model and simulation techniques employed in this study. In section 2.1, we present the model utilized for the investigation of the correlated electrons in liquids. Additionally, we delve into the Gutzwiller variational method, providing a comprehensive discussion with modern formulations in Section 2.2. The implementation of Gutzwiller molecular dynamics is detailed in Section 2.3.

In **chapter 3**, we study the influence of the atomic distribution on the electronic structure. Our focus lies in the Mott transition in metallic liquids, and draw comparisons to its manifestation in amorphous solids. The model and formulas are described in section 3.1, the simulation results and discussion are presented in section 3.2.

In **chapter 4**, we delve into the impact of electron localization on atomic transport properties. In section 4.1, we demonstrate and characterize an unusual maximum of atomic diffusion close to the Mott transition in the Hubbard liquid model. In section 4.2, we introduce a general theory based on the Chapman-Enskog method to elucidate this intriguing observation.

In **chapter 5**, we utilized Gutzwiller molecular dynamics (GMD) to scrutinize the liquid-liquid transition in dense hydrogen. In Section 5.1, we constructed an ab initio tight-binding model specifically tailored for hydrogen, followed by its benchmarking in Section 5.2. Subsequently, we presented and deliberated upon the simulation results in Section 5.3, concluding with a summary in Section 5.4.

Chapter 2

The Hubbard liquid model and the Gutzwiller molecular dynamics

In this chapter, we introduced the model and main theoretical tools exploited in this thesis. These include the Hubbard liquid model, the Gutzwiller variational method, and the Gutzwiller molecular dynamics, each presented in a dedicated section.

2.1 The Hubbard liquid model

The Hubbard model [10, 11, 12, 13, 14] stands as a cornerstone among the canonical models for strongly correlated electron systems. Despite its apparent simplicity, the single-band Hubbard model manifests a diverse spectrum of correlated electron behaviors, encompassing interaction-driven phenomena such as MIT, superconductivity, and magnetism. Within the context of this thesis, we introduce a minimal extension of the Hubbard model, broadening its scope to encompass an atomic liquid, which we call the Hubbard liquid model. A single-band Hubbard liquid model has the following

Hamiltonian:

$$\mathcal{H} = \sum_i \frac{|\mathbf{p}_i|^2}{2m} + \frac{1}{2}\sum_{i\neq j}\phi(|\mathbf{r}_i - \mathbf{r}_j|) + \hat{\mathcal{H}}_e\big(\{\mathbf{r}_i\}\big), \tag{2.1}$$

$$\hat{\mathcal{H}}_e\big(\{\mathbf{r}_i\}\big) = \sum_{ij,\sigma} t_{ij}\hat{c}_{i,\sigma}^\dagger\hat{c}_{j,\sigma} + U\sum_i \hat{n}_{i\uparrow}\hat{n}_{i\downarrow}, \tag{2.2}$$

$$t_{ij} = h(|\mathbf{r}_i - \mathbf{r}_j|), \tag{2.3}$$

where $\mathbf{r}_i$ and $\mathbf{p}_i$ are the classical position and momentum variables, respectively, of the i-th atom. The first term is the classical kinetic energy, while the second term represents the short-range repulsive pair potential. The attractive cohesive forces are provided by itinerant electrons described by Eq. (2.2). Eq. (2.2) is basically the same as a single-band Hubbard model, with a key distinction that the original Hubbard model pertains to a lattice, whereas in this context, it characterizes disordered atoms within a liquid. The first term in Eq. (2.2) describes electron hopping between atoms with $\hat{c}_{i,\sigma}^\dagger$ ($\hat{c}_{i,\sigma}$) being the creation (annihilation) operator of an electron of spin $\sigma =\uparrow, \downarrow$ at the i-th atom, and $\hat{n}_{i,\sigma} = \hat{c}_{i,\sigma}^\dagger\hat{c}_{i,\sigma}$ the corresponding number operator. The Hubbard parameter U in the second term encapsulates the on-site Coulomb repulsion of electrons.

It is worth noting that the above single-band Hubbard liquid model also serves as a minimum model for fluid alkali metals mentioned in chapter 1. Assuming well-localized basis functions, we employ a hopping function which decays exponentially:

$$h(r) = -t_0\, e^{-r/\xi}, \tag{2.4}$$

where ξ and t_0 set the length and energy scales, respectively, of the model. On the

other hand, a faster-decaying function

$$\phi(r) = \phi_0 \exp[-(r/\lambda) - b(r/\lambda)^4] \qquad (2.5)$$

is used for the much sharper repulsive core, where ϕ_0, λ and b are parameters in the model. The form of Eq. (2.5) does not carry specific physical meaning; it merely symbolizes a sharply defined repulsive potential. Alternative forms of $\phi(r)$ can be conceived for different models, but bear in mind, the form of $\phi(r)$ may qualitatively affect the atomic dynamics, and also the electronic structure because they are interdependent. In the work of chapter 3 and chapter 4, the set of model parameters $\phi_0 = 4.17\,t_0$, $\lambda = 0.86\,\xi$, $b = 0.1$ is used.

2.2   The Gutzwiller variational method

Since its original formulation in the early 1960s, the Gutzwiller variational method [21, 22, 23] remains one of the simplest yet effective tools for addressing correlated electron systems. Bünemann, Gebhard, Weber *et. al.* [58, 59, 60] extended the Gutzwiller method to multi-band models. Later, Fabrizio and Lanatà [61, 62, 63] re-formulated and extended the method with practical parametrizations of the Gutzwiller parameter matrix suitable for numerical calculations. The newly formulated parameters are called the Φ matrix. In this chapter, we will employ this formulation, placing particular emphasis on the single-band scenario, as we are simulating a single-band Hubbard liquid model.

2.2.1 The Gutwziller wave function

In the Gutzwiller method, the ground state of the Hubbard Hamiltonian is approximated by the following variational wave function, the Gutzwiller wave function

$$|\Psi_G\rangle = \hat{\mathcal{P}}|\Psi_0\rangle = \prod_i \hat{\mathcal{P}}_i|\Psi_0\rangle, \tag{2.6}$$

where $\mathcal{P}$ is the Gutzwiller operator that can be expressed as a product of the on-site operators $\hat{\mathcal{P}}_i$, and $|\Psi_0\rangle$ is a Slater determinant constructed from the eigenstates of an effective, or renormalized, tight-binding Hamiltonian to be determined self-consistently.

The Slater determinant $|\Psi_0\rangle$, represents an uncorrelated state. A most general many-body wave function can be built from linear combinations of many Slater determinants. We designate a many-body wave function as "correlated" when it cannot be expressed by a single Slater determinant. Conversely, if it can be represented by a single Slater determinant, we define it as "uncorrelated". Ψ_G goes beyond the uncorrelated wave functions, granting it the capability to capture the MT. In contrast, the HF method and DFT search the ground state sorely within the space of uncorrelated states. Additionally, it is also essential to recognize that Ψ_G does not encompass the entire space of all possible wave functions, given its nature as a variational approach.

The local Gutzwiller operator $\hat{\mathcal{P}}_i$ aims to introduce local on-site electron correlation, e.g. by reducing the statistical weight of the double-occupied states. It can be expressed in terms of the local electron Fock states $|i, \Gamma\rangle$,

$$\hat{\mathcal{P}}_i(\Phi_i) = \sum_{\Gamma\Gamma'} \Phi_{i,\Gamma\Gamma'}(P^0_{i,\Gamma})^{-1/2}|i,\Gamma\rangle\langle i,\Gamma'| \equiv \sum_{\Gamma\Gamma'} \lambda_{i,\Gamma\Gamma'}|i,\Gamma\rangle\langle i,\Gamma'|, \tag{2.7}$$

where $P_{i,\Gamma}^0$ is the occupation probability of the uncorrelated state

$$P_{i,\Gamma}^0 \equiv |\langle \Psi_0 | i, \Gamma \rangle|^2 . \tag{2.8}$$

The expansion coefficients $\Phi_{i,\Gamma\Gamma'}$ can be grouped into a Hermitian matrix Φ_i, which serves as the variational parameters to be determined self-consistently [61, 62, 63]. It can be shown that the elements of the Φ_i matrix also correspond to the wave function of slave bosons. For the single-band Hubbard model, the basis $\{|i, \Gamma\rangle\}$ of the local electron Fock space is $\{|0\rangle,\ \hat{c}_{i,\uparrow}^\dagger |0\rangle,\ \hat{c}_{i,\downarrow}^\dagger |0\rangle,\ \hat{c}_{i,\uparrow}^\dagger \hat{c}_{i,\downarrow}^\dagger |0\rangle\}$.

2.2.2 The Gutzwiller approximation and the ground state

The Gutwziller projector $\hat{\mathcal{P}}$ and the variational Slater determinant $|\Psi_0\rangle$ are aslo subject to the Gutzwiller constraints [61, 62, 63],

$$\langle \Phi_0 | \hat{\mathcal{P}}_i^\dagger \hat{\mathcal{P}}_i | \Phi_0 \rangle = 1, \tag{2.9}$$

$$\langle \Phi_0 | \hat{\mathcal{P}}_i^\dagger \hat{\mathcal{P}}_i \hat{c}_{i,\alpha}^\dagger \hat{c}_{i,\beta} | \Phi_0 \rangle = \langle \Phi_0 | \hat{c}_{i,\alpha}^\dagger \hat{c}_{i,\beta} | \Phi_0 \rangle. \tag{2.10}$$

Eq. (2.9) guarantees the normalization of the GWF. In terms of the Φ-matrix, the normalization of the Gutzwiller wave function in Eq. (2.9) becomes

$$\mathrm{Tr}(\Phi_i^\dagger \Phi_i) = 1. \tag{2.11}$$

Eq. (2.10) is introduced for computational convenience, this property of $\hat{\mathcal{P}}$ is extremely useful in infinite-dimensional lattices. In this limit, the expectation value of any local

operator $\hat{O}_i$ becomes [61]

$$\langle\Phi_0|\hat{\mathcal{P}}^\dagger\hat{O}_i\hat{\mathcal{P}}|\Phi_0\rangle = \langle\Phi_0|\hat{\mathcal{P}}_i^\dagger\hat{O}_i\hat{\mathcal{P}}_i|\Phi_0\rangle. \tag{2.12}$$

In the Φ-matrix representation, it becomes

$$\langle\Psi_G|\hat{O}_i|\Psi_G\rangle = \mathrm{Tr}(\Phi_i^\dagger\,\mathbb{O}\,\Phi_i), \tag{2.13}$$

where $\mathbb{O}$ is the matrix representation of operator $\hat{O}_i$ in the local basis, i.e. $\mathbb{O}_{\Gamma\Gamma'} = \langle i,\Gamma|\hat{O}_i|i,\Gamma'\rangle$. We note that since the same basis is used for all atoms, these matrix representations are independent of the site index.

For inter-site hopping operators, the expectation value is [61, 57]

$$\langle\Psi_G|\hat{c}_{i,\sigma}^\dagger\hat{c}_{j,\sigma}|\Psi_G\rangle = \mathcal{R}_{i,\sigma}\mathcal{R}_{j,\sigma}\langle\Psi_0|\hat{c}_{i,\sigma}^\dagger\hat{c}_{j,\sigma}|\Psi_0\rangle. \tag{2.14}$$

This result shows that the expectation of the off-diagonal term is given by a renormalization $\mathcal{R}_{i,\sigma}\mathcal{R}_{j,\sigma}$ of that of the uncorrelated state $|\Psi_0\rangle$. The renormalization factors are given by

$$\mathcal{R}_{i,\sigma} = \frac{\mathrm{Tr}(\Phi_i^\dagger\,\mathbb{M}_\sigma^\dagger\,\Phi_i\,\mathbb{M}_\sigma)}{\sqrt{n_{i,\sigma}(1-n_{i,\sigma})}} \tag{2.15}$$

where $\mathbb{M}_\sigma$ is the matrix representation of the electron annihilation operator $\hat{c}_{i,\sigma}$ in the local basis, and the local electron density is

$$n_{i,\sigma} = \langle\Psi_0|\hat{n}_{i,\sigma}|\Psi_0\rangle = \mathrm{Tr}(\Phi_i^\dagger\,\mathbb{N}_\sigma\,\Phi_i). \tag{2.16}$$

Here $\mathbb{N}_{i,\sigma}$ is similarly the electron number operator in the local basis.

Again, Eq. (2.14) is a result of Eq. (2.10), it is strictly valid only in the limit of infinite-coordination lattices. Nevertheless, it is quite common to use them as approximated formulas for finite-dimensional systems, which is referred to as the Gutzwiller approximation (GA).

The total energy of the Hubbard model is computed from the expectation value $\mathcal{E}\left(|\Psi_0\rangle, \{\Phi_i\}\right) = \langle\Psi_G|\hat{\mathcal{H}}_e|\Psi_G\rangle$, and within the GA it is given by

$$\mathcal{E} = \sum_{ij}\sum_{\sigma} \mathcal{R}_{i\sigma}\mathcal{R}_{j\sigma}\, t_{ij}\, \rho_{ij,\sigma} + U\sum_i \text{Tr}(\Phi_i^\dagger\, \mathbb{D}\, \Phi_i), \tag{2.17}$$

where $\mathbb{D}$ is the matrix representation of the local double occupancy operator

$$\hat{D}_i \equiv \hat{n}_{i,\uparrow}\hat{n}_{i,\downarrow}, \tag{2.18}$$

and we have defined the single-particle density matrix or correlation function

$$\rho_{ij,\sigma} \equiv \langle\Psi_0|\hat{c}_{i,\sigma}^\dagger\hat{c}_{j,\sigma}|\Psi_0\rangle, \tag{2.19}$$

For a single-band model, a general Φ_i matrix can be parametrized by four parameters:

$$\Phi_i = \begin{bmatrix} \phi_{i,0} & 0 & 0 & 0 \\ 0 & \phi_{i,\uparrow} & 0 & 0 \\ 0 & 0 & \phi_{i,\downarrow} & 0 \\ 0 & 0 & 0 & \phi_{i,2} \end{bmatrix}. \tag{2.20}$$

The normalization of the Gutzwiller wave function corresponds to the constraint

$$|\phi_{i,0}|^2 + |\phi_{i,\uparrow}|^2 + |\phi_{i,\downarrow}|^2 + |\phi_{i,2}|^2 = 1. \tag{2.21}$$

From Eq. (2.16), the on-site electron number is

$$n_{i,\sigma} = |\phi_{i,\sigma}|^2 + |\phi_{i,2}|^2, \tag{2.22}$$

and the local double occupancy is given by

$$d_i \equiv \langle \Psi_G | \hat{D}_i | \Psi_G \rangle = |\phi_{i,2}|^2. \tag{2.23}$$

The physical meaning of the ϕ-parameters can be easily read from these identities. First, $|\phi_{i,\sigma}|^2$ and $|\phi_{i,2}|^2$ represent the probability of singly occupied state (with spin σ) and doubly occupied state, respectively, at the i-th site. By interpreting the normalization condition Eq. (2.21) as a probability conservation condition, we can view $|\phi_{i,0}|^2$ as the probability of an empty state at the i-th site.

The total energy in Eq. (2.17) is to be minimized with respect to both the Slater determinant $|\Psi_0\rangle$ and the slave-boson amplitudes expressed as the Φ_i matrices. This minimization has to be carried out by taking into account the normalization condition Eq. (2.21) and the Gutzwiller constraint Eq. (2.16). To this end, we introduce two local Lagrangian multipliers and consider the following energy functional

$$\begin{aligned}
\mathcal{E}' = \mathcal{E} &+ \sum_{i,\sigma} \mu_{i,\sigma}(|\phi_{i,\sigma}|^2 + |\phi_{i,2}|^2 - \langle \Psi_0 | \hat{n}_{i,\sigma} | \Psi_0 \rangle) \\
&+ \sum_i \epsilon_i \left[1 - (|\phi_{i,0}|^2 + |\phi_{i,\uparrow}|^2 + |\phi_{i,\downarrow}|^2 + |\phi_{i,2}|^2) \right],
\end{aligned} \tag{2.24}$$

The minimization of $\mathcal{E}'$ with respect to the Slater determinant, $\partial \mathcal{E}'/\partial |\Psi_0\rangle = 0$, leads to the following renormalized quasi-particle tight-binding Hamiltonian

$$\mathcal{H}^{\text{qp}} = \sum_{ij} \sum_{\sigma} t_{ij} \mathcal{R}_{i,\sigma} \mathcal{R}_{j,\sigma} \, \hat{c}_{i,\sigma}^\dagger \hat{c}_{j,\sigma} + \sum_i \mu_i \, \hat{n}_{i,\sigma}. \tag{2.25}$$

The optimal Slater determinant is then obtained from the eigenstates of this renormalized single-particle Hamiltonian. The minimization with respect to the slave bosons, $\partial \mathcal{E}'/\partial \Phi_i = 0$, can be cast into local eigenvalue problem [63]:

$$
\mathcal{H}_i^{sb}
\begin{bmatrix}
\phi_{i,0} \\
\phi_{i,\uparrow} \\
\phi_{i,\downarrow} \\
\phi_{i,2}
\end{bmatrix}
= \epsilon_i
\begin{bmatrix}
\phi_{i,0} \\
\phi_{i,\uparrow} \\
\phi_{i,\downarrow} \\
\phi_{i,2}.
\end{bmatrix}
\tag{2.26}
$$

The effective slave-boson Hamiltonian is

$$
\mathcal{H}_i^{\text{sb}} = \sum_\sigma \frac{\Delta_{i,\sigma}\mathbb{M}_\sigma + \Delta_{i,\sigma}^*\mathbb{M}_\sigma^\dagger}{\sqrt{n_{i,\sigma}(1-n_{i,\sigma})}} + \sum_\sigma \mu_{i,\sigma}\mathbb{N}_\sigma + U\mathbb{D},
\tag{2.27}
$$

Here the parameter $\Delta_{i,\sigma}$ characterizes the local electron bonding and is given by

$$
\Delta_{i,\sigma} = \sum_j t_{ij}\, \mathcal{R}_{j,\sigma}\rho_{ij,\sigma}.
\tag{2.28}
$$

Due to the interdependence between the quasi-particle and slave-boson Hamiltonians, the two eigenvalue problems of solving $\mathcal{H}^{\text{qp}}$ and $\mathcal{H}_i^{\text{sb}}$ are carried out iteratively until convergence is reached.

2.2.3 The Gutzwiller method at finite temperatures

In this subsection, we discuss the generalization of the Gutzwiller method to finite temperatures, following the works of Refs. [64, 65]. While the zero-temperature formulation aims to obtain the Gutzwiller wave function $|\Psi_G\rangle$ variationally, at finite

temperatures, we seek a variational form for the many-electron density operator

$$\hat{\varrho}_G = \hat{\mathcal{P}} \hat{\varrho}_0 \hat{\mathcal{P}}^\dagger \tag{2.29}$$

where $\hat{\varrho}_0$ denotes the density operator of the quasi-particles in thermal equilibrium. Effectively, it is described by the following Boltzmann distribution

$$\hat{\varrho}_0 = \frac{e^{-\beta \hat{\mathcal{H}}^{\mathrm{qp}}}}{\mathrm{Tr}(e^{-\beta \hat{\mathcal{H}}^{\mathrm{qp}}})} \tag{2.30}$$

Here $\mathcal{P}$ is the Gutzwiller operator parametrized in the same way as Eq. (2.6).

Importantly, the various variational parameters at finite temperatures are obtained from the minimization of the free energy of the system, $\mathcal{F} = \mathcal{E} - T\mathcal{S}$, instead of just the energy. The total energy at finite-T is obtained from the trace $\mathcal{E} = \mathrm{Tr}(\hat{\varrho}_G \hat{\mathcal{H}}_e)$, and is given by the same expression Eq. (2.17), except the single-electron correlation function is now computed from the trace with the quasi-particle density operator

$$\rho_{ij,\sigma} \equiv \mathrm{Tr}\left(\hat{\varrho}_0 \, \hat{c}_{i,\sigma}^\dagger \hat{c}_{j,\sigma} \right). \tag{2.31}$$

The entropy of the system $\mathcal{S} = -\mathrm{Tr}(\hat{\varrho}_G \ln \hat{\varrho}_G)$ cannot be computed analytically even within the GA. In order to efficiently compute the entropy for MD simulations, it is estimated by a analytical lower bound, which can be separated into contributions from the quasi-particles and the slave bosons [64, 65]

$$\mathcal{S} = \mathcal{S}^{\mathrm{qp}}(\hat{\varrho}_0) + \mathcal{S}^{\mathrm{sb}}(\{\Phi_i\}). \tag{2.32}$$

Here the first term is the entropy of free fermions described by the density operator $\hat{\varrho}_0$, which can be expressed in terms of the occupation probabilities of the quasi-particle

Hamiltonian

$$\mathcal{S}^{\mathrm{qp}} = -\mathrm{Tr}(\hat{\varrho}_0 \ln \hat{\varrho}_0) \tag{2.33}$$
$$= -\sum_m \left[f_m \ln f_m + (1 - f_m) \ln(1 - f_m) \right],$$

where $f_m = f_{\mathrm{FD}}(\epsilon_m)$, $f_{\mathrm{FD}}(\varepsilon)$ is the Fermi-Dirac function, ϵ_m are eigenenergies of the renormalized Hamiltonian $\hat{\mathcal{H}}^{\mathrm{qp}}$ in Eq. (2.25). The entropy of the slave-bosons is estimated from the relative entropy between the distribution $\Phi_i^\dagger \Phi_i$ of the local correlated state and P_i^0 of the uncorrelated one:

$$\mathcal{S}^{\mathrm{sb}} = \sum_i S(\Phi_i^\dagger \Phi_i || P_i^0) \tag{2.34}$$
$$= -\sum_i \mathrm{Tr}[\Phi_i^\dagger \Phi_i \ln((P_i^0)^{-1} \Phi_i^\dagger \Phi_i)],$$

The free-energy of the system $\mathcal{F}(\hat{\varrho}_0, \{\Phi_i\})$ depends on both the quasi-particle density operator and the slave-boson amplitudes. The optimized uncorrelated density operator is again obtained from the eigenstates of a self-consistently determined quasi-particle Hamiltonian Eq. (2.25), while the minimization of $\mathcal{F}$ with respect to slave-bosons is similarly recast into an eigenvalue problem with an additional entropy term added to the slave-boson Hamiltonian Eq. (2.27).

2.3 The Gutzwiller molecular dynamics

In this section, we outline the application of the Gutzwiller MD method to simulate the Mott metal-insulator transition in the Hubbard liquid model [57]. The atomic

liquid is described by the Hamiltonian

$$\mathcal{H}' = \sum_i \frac{|\mathbf{p}_i|^2}{2m} + \frac{1}{2} \sum_{i \neq j} \phi(|\mathbf{r}_i - \mathbf{r}_j|) + \mathcal{V}_e(\{\mathbf{r}_i\}) \tag{2.35}$$

where $\mathbf{r}_i$ and $\mathbf{p}_i$ are the classical position and momentum variables, respectively, of the i-th atom. The first term is the classical kinetic energy, while the second term represents the short-range repulsive pair potential. The last term denotes the electron-mediated potential energy which provides the cohesive forces for the atoms. As in standard quantum MD approaches, the adiabatic or Born-Oppenheimer approximation is employed, which assumes a fast electronic relaxation compared with the atomic dynamics. The electron potential with this approximation is given by the expectation of the disordered Hubbard model $\hat{\mathcal{H}}_e$ in Eq. (2.2):

$$\mathcal{V}_e(\{\mathbf{r}_i\}) = \langle \hat{\mathcal{H}}_e \rangle = \text{Tr}(\hat{\varrho}_G \hat{\mathcal{H}}_e). \tag{2.36}$$

As discussed above, the Gutzwiller method is used to compute the above expectation. The atomic dynamics is described by the classical Newtonian dynamics in MD simulations [66, 67]. Here we employ the NVT scheme, which means the atomic number N, system volume V, and temperature T are kept constant in the MD simulations [66, 67]. With the Langevin thermostat for controlling the simulation temperature, the atomic trajectories are governed by the Langevin equation [66]

$$m\ddot{\mathbf{r}}_i = -\gamma \dot{\mathbf{r}}_i - \frac{\partial \mathcal{H}'}{\partial \mathbf{r}_i} + \boldsymbol{\eta}_i(t), \tag{2.37}$$

where γ is the dissipation coefficient, $\boldsymbol{\eta}_i(t)$ are stochastic forces with statistical properties

$$\langle \eta_i^\alpha(t) \rangle = 0, \tag{2.38}$$

$$\langle \eta_i^\alpha(t) \eta_j^\beta(t') \rangle = 2\gamma k_B T \delta_{ij}\, \delta_{\alpha\beta}\, \delta(t - t'),$$

where α, β denote the $x,\ y,\ z$ Cartesian component of the stochastic forces.

The deterministic forces, the second term in Eq. (2.37), have two contributions. The first is the repulsive forces due to the pair potential

$$\mathbf{F}_i^{\text{rep}} = -\sum_j \frac{\partial \phi(r_{ij})}{\partial \mathbf{r}_i} \tag{2.39}$$

This repulsive component comes from the exclusion of core electrons around the atomic nuclei. The attractive atomic forces are provided by the electron Hamiltonian, which can be computed using the Hellmann-Feynman theorem

$$\mathbf{F}_i^{\text{elec}} = -\frac{\partial \mathcal{V}_e}{\partial \mathbf{r}_i} = -\left\langle \frac{\partial \hat{\mathcal{H}}_e}{\partial \mathbf{r}_i} \right\rangle \tag{2.40}$$

$$= -\sum_{j,\sigma} \left[\mathcal{R}_{i,\sigma} \mathcal{R}_{j,\sigma} \rho_{ij,\sigma} \frac{\partial h(r_{ij})}{\partial \mathbf{r}_i} + \text{c.c.} \right].$$

This expression indicates that the force acting on a particular atom can be partitioned into contributions from the neighboring atoms: $\mathbf{F}_i^{\text{elec}} = \sum_j \mathbf{f}_{ij}^{\text{elec}}$. From Eq. (2.40), the inter-atomic forces of an atomic pair can be written as

$$f_{ij}^{\text{elec}} = -\sum_\sigma \mathcal{R}_{i,\sigma} \mathcal{R}_{j,\sigma}\, \rho_{ij,\sigma} h'(r_{ij}), \tag{2.41}$$

where $h'(r) = dh/dr$. Assuming well-localized basis functions, here we employ a hopping function which decays exponentially: $h(r) = -t_0\, e^{-r/\xi}$, where ξ and t_0 set

the length and energy scales, respectively, of the model. While the forces are mostly determined by the inter-atomic distance r_{ij} through the hopping function, both the renormalization factors $\mathcal{R}_{i,\sigma}$ and the electron correlation function $\rho_{ij,\sigma}$ depend on the immediate neighborhood of the atomic pair (ij), giving rise to a finite distribution of forces around the curve of an isolated pair $f_{ij}^{\text{pair}} = -\langle\mathcal{R}^2\rangle h'(r_{ij})$, $\mathcal{R}^2$ is the average value over different orbitals. This finite distribution underscores the many-body nature of the cohesive forces mediated by electrons.

Chapter 3

Electrical conductivity in the Hubbard liquid model

Metal-insulator transition (MIT) remains at the forefront of condensed matter research [68, 1, 69]. Contrary to conventional phase transitions which can be described by order parameters associated with the broken symmetries, a transition from metals to insulators is characterized by different dynamical behaviors of electrons. Of particular interest are MITs induced by the localization of electrons through either strong disorder or electron interaction. In the former case, which is known as the Anderson localization [70], the transition to an insulator is caused by the destructive wave interference between multiple scattering paths of electrons, leading to a complete localization of all wave functions in the strong scattering limit even in the absence of electron-electron interaction. In the second scenario, known as the Mott transition, suppression of electron hopping is induced by strong electron correlations, as exemplified by a large on-site Coulomb repulsion. Such correlation-induced MITs are characterized by the enhancement of the electron effective mass and the opening of a spectral gap.

Understanding the interplay between these two mechanisms has been a subject of intense activity over the past few decades [69, 71, 35, 72]. One particularly intriguing phenomenon reported in several studies is the enhancement of electrical conductance

caused by repulsive electron-electron interactions. The suppression of disordered-induced electronic localization can be attributed to partial screening of the random potential. In the weak-coupling regime, this results from a smoother random potential as the density of the electrons can adjust well to the given disorder configuration [73, 74, 75]. The resultant disorder screening is more prominent in low dimensions and is sensitive to both temperatures and magnetic field. On the other hand, a different screening mechanism, which can be traced to the nonperturbative Kondo-like processes that lead to strong mass enhancements, is suggested for the screening of on-site disorder potential in the strong coupling regime.

In this paper, we report a novel mechanism for the enhancement of electrical conductance that is unique for correlated electrons in an atomic liquid system. It is worth noting that fluid metals have played an important role in the theoretical development of Anderson localization and Mott transition phenomena [76]. Of particular interest is the MIT in expanded metallic alkali fluids. Various experimental studies also hinted at a correlation-driven metal-nonmetal transition in supercritical alkali liquid [47, 77, 78, 79, 80]. In particular, experiments on liquid cesium and rubidium observed an enhancement of magnetic susceptibility close to the critical density [53, 81, 55], indicating the emergence of localized magnetic moments which is a telltale sign of Mott-Hubbard type transition.

3.1 Model and formulas

The electron transport in such fluid metals depends on the instantaneous atomic configurations. On the other hand, within the Born-Oppenheimer approximation [82], the adiabatic motion of atoms is governed by covalent forces that are mediated by

itinerant electrons. The fluctuating atomic structures in a liquid can be viewed as a dynamic disorder for electrons. To incorporate the effects of electron correlations in such fluid metals, we employ a molecular dynamics scheme where the electronic structure is solved by the Gutzwiller method. We show that, in the presence of strong electron correlations, this nontrivial interplay leads to a rearrangement of atoms that increases the coordination numbers, which in turn enhances the electron transport.

We consider the Hubbard liquid Hamiltonian (2.1), with the model parameters are described in chapter 2.1,

$$\mathcal{H} = \sum_i \frac{|\mathbf{p}_i|^2}{2m} + \frac{1}{2}\sum_{i \neq j} \phi(|\mathbf{r}_i - \mathbf{r}_j|) + \sum_{ij,\sigma} h(|\mathbf{r}_i - \mathbf{r}_j|)\hat{c}_{i,\sigma}^\dagger \hat{c}_{j,\sigma} + U\sum_i \hat{n}_{i\uparrow}\hat{n}_{i\downarrow}. \tag{3.1}$$

For random atomic configurations in a liquid, the electron subsystem of Eq. (2.1) corresponds to a tight-binding model with off-diagonal disorder, contrary to the diagonal on-site disorder in the well-studied Anderson-Hubbard model. In order to highlight the dynamical nature of the off-diagonal disorder in a liquid state, an amorphous-Hubbard model with random, yet static, atoms is introduced to serve as a reference system. The atomic positions $\mathbf{r}_i$ of the amorphous solid are random variables uniformly distributed with a cube of linear size L, but subject to the hard-core condition that the distance between any atomic pair is greater than a_c. The resultant radial distribution function $g(r)$ of the amorphous solid is shown in Fig. 3.1. The radial distribution function is defined as

$$g(r) = \frac{\rho(r)}{\rho_0}, \tag{3.2}$$

where $\rho(r)$ is the density of the shell at distance r from a reference atom and $\rho_0 = N/V$ is the system's overall density. The radial distribution function reflects how density

varies as a function of distance from a reference particle. For a given random configuration $\{\mathbf{r}_i\}$, the hopping coefficients are given by the same exponential decaying function. In this work, we focus on Mott transitions at half-filling for both models.
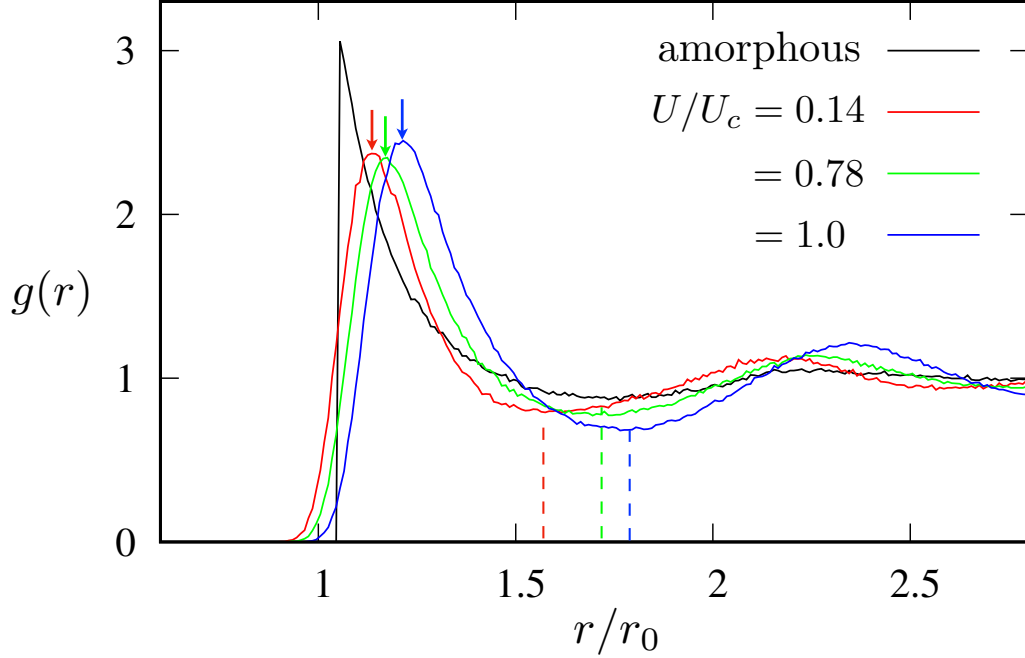
Figure 3.1: The radial distribution functions of the amorphous model as well as the liquid Hubbard at $k_B T/t_0 = 0.00825$ for three different Hubbard parameters. $r_0 = 0.526\xi$, it is the equilibrium distance of an isolated dimer at $U = 0$. t_0 and ξ are the energy and length scale of the system given in Eq. (2.4). U_c is the critical value of U at which the Mott transition occurs, $U_c \sim 1.3t_0$. The $g(r)$ for both cases is obtained by averaging 10^3 disorder realizations from direct sampling in the case of the amorphous model, and from GMD simulations of the atomic liquid. The sharp cutoff is a result of the hard-core condition for the amorphous model. The arrows mark the most probable nearest-neighbor distance, while the dashed lines indicate the extent of the first coordination shell.

For a given atomic configuration, the electron structure of the amorphous and liquid Hubbard models is solved by the Gutzwiller method. It is worth noting that this electronic structure calculation has to be repeated at every time step of the MD simulations of the liquid system. Compared with other computationally more expensive methods, the relative simplicity of the Gutzwiller approximation is crucial for effi-

cient integration with MD simulations [57]. In this approach, the collective electron behaviors such as the local double-occupation are encoded in the slave-boson degrees of freedom [26], while the quasi-particles are described by an effective or renormalized tight-binding Hamiltonian

$$\hat{\mathcal{H}}^{\mathrm{qp}} = \sum_{ij} \sum_{\sigma} t_{ij}^* \hat{c}_{i\sigma}^\dagger \hat{c}_{j\sigma} + \sum_i \lambda_i \hat{n}_i. \tag{3.3}$$

Here $t_{ij}^* = \mathcal{R}_i \mathcal{R}_j h(|\mathbf{r}_i - \mathbf{r}_j|)$ is the renormalized hopping coefficient and λ_i denotes an effective on-site potential in the Gutzwiller method. The renormalization factors $\mathcal{R}_i$ depend on the slave-boson amplitudes and need to be solved self-consistently with the quasi-particles solutions [63, 65].

To characterize the electron transport properties of the two disordered systems, we use the Kubo-Greenwood formula [83, 84] to compute the electrical conductivity. Given our focus on DC conductivity, we specifically consider the real component of electrical conductivity given by [85]

$$\sigma(\omega) = \frac{\pi \hbar}{V} \sum_{mn} \left(\frac{f_n - f_m}{\epsilon_m - \epsilon_n} \right) \Re(\langle m|\hat{\mathbf{j}}|n\rangle \langle n|\hat{\mathbf{j}}|m\rangle) \delta(\epsilon_m - \epsilon_n - \omega), \tag{3.4}$$

where ω is the frequency, V is the volume, f_m is the Fermi-Dirac factor, ϵ_m and $|m\rangle$ are the eigenenergy and eigenstate of the quasi-particle Hamiltonian Eq. (3.3), $\Re()$ denotes the real part. The current operator is defined as [86, 87]

$$\hat{\mathbf{j}} = i \frac{e}{\hbar} \sum_{ij} \sum_{\sigma} (\mathbf{r}_j - \mathbf{r}_i) \, t_{ij}^* \, \hat{c}_{i,\sigma}^\dagger \hat{c}_{j,\sigma}. \tag{3.5}$$

Note $\sigma(\omega)$ is a tensor, its component is

$$\sigma_{\mu\nu}(\omega) = \frac{\pi\hbar}{V} \sum_{mn} \left(\frac{f_n - f_m}{\epsilon_m - \epsilon_n} \right) \Re(\langle m|\hat{\mathbf{j}}_\mu|n\rangle \langle n|\hat{\mathbf{j}}_\nu|m\rangle)\delta(\epsilon_m - \epsilon_n - \omega), \qquad (3.6)$$

where μ and ν represent the x, y, z directions.

In practical calculations, due to the finite size effect, the δ function in the formula can be replaced by a Lorentzian $L(x) = \frac{\eta}{\pi}/(x^2 + \eta^2)$, with a finite small η. An alternative approach is to compute $\sigma(\omega)$ by averaging over a narrow frequency range of $2\Delta\omega$. [88, 89],

$$\sigma(\omega) = \frac{1}{2\Delta\omega} \int_{\omega-\Delta\omega}^{\omega+\Delta\omega} \sigma(\omega')d\omega', \qquad (3.7)$$

This method is equivalent to replacing the δ function with a rectangular function of width $2\Delta\omega$. The value of $\Delta\omega$ cannot be too small so that some energy levels can be included in the δ function, it should also not be too big to give a good resolution. In this work, we use Eq. (3.7) and choose $\Delta\omega$ to be twice the average gap between neighboring energy levels near the chemical potential. The DC conductivity σ_0 is the conductivity at zero frequency, for isotropic systems,

$$\sigma_0 = \sigma_{xx}(0) = \sigma_{yy}(0) = \sigma_{zz}(0). \qquad (3.8)$$

3.2 Simulation results and discussion

The Gutzwiller MD method is used to simulate the bandwidth-controlled MIT in the half-filled liquid Hubbard model. Fig. 3.1 shows the pair distribution functions $g(r)$ at various Hubbard U obtained from GMD simulations. Notably, while the extent

of the first coordination shell expands slightly with increasing U, the strength of the first coordination peaks remains roughly the same.
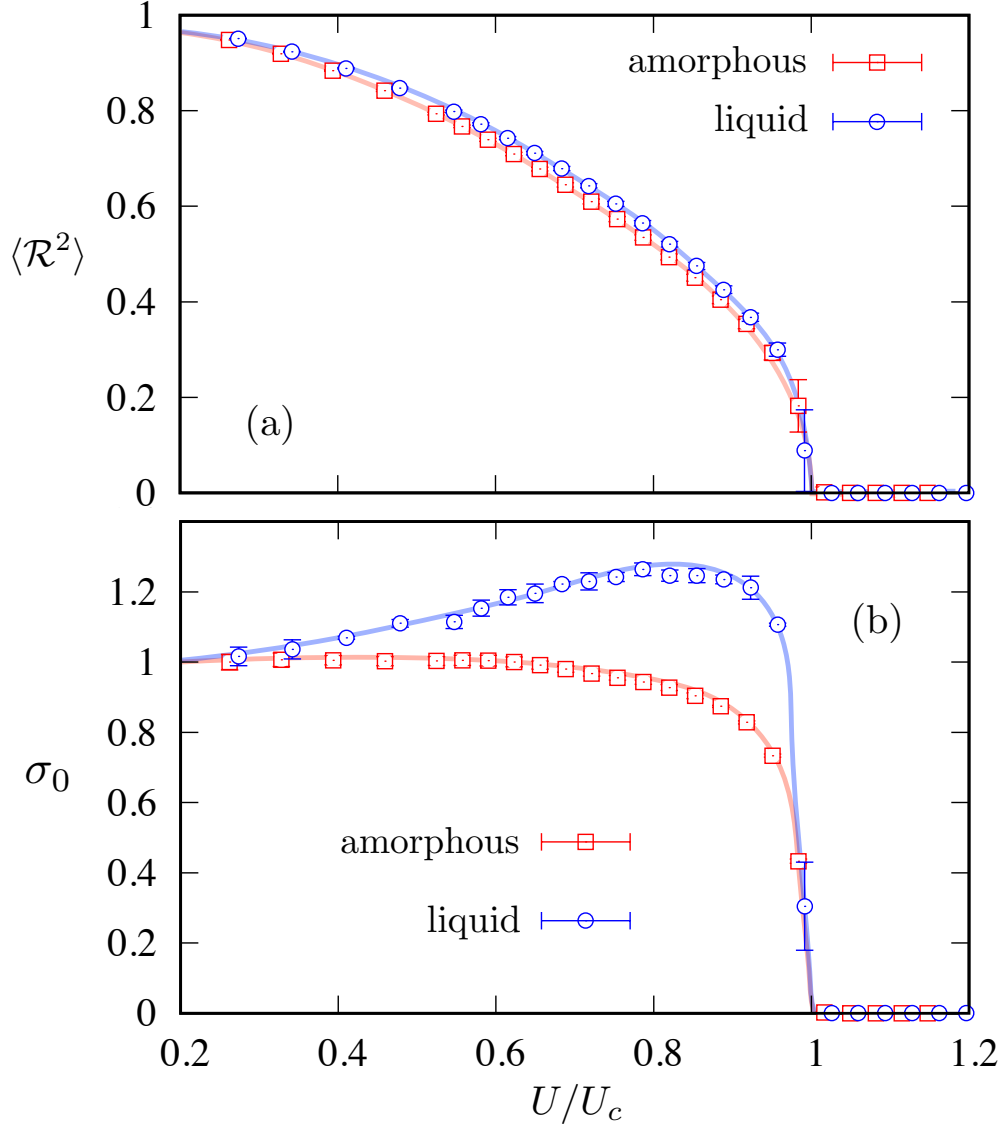
Figure 3.2: (a) the ensemble and spatially averaged renormalization factor $\langle \mathcal{R}^2 \rangle$ as a function of the Hubbard parameter U for the amorphous and liquid Hubbard models. The U dependences of the ensemble averaged DC conductivity σ_0 for the two models are shown in panel (b). U_c is the critical value of U at which the Mott transition occurs, $U_c \sim 1.3t_0$, t_0 is the energy scale of the system given in Eq. (2.4). The two systems have the same temperature $k_B T / t_0 = 0.00825$.

We next compare the bandwidth-controlled Mott transitions in the amorphous and liquid Hubbard models at half-filling. The correlation-induced bandwidth reduction in both systems can be characterized by the ensemble and spatially averaged renormalization factor $\langle \mathcal{R}^2 \rangle$. As shown in Fig. 3.2(a), the averaged renormalization factor in both cases decreases monotonically from the uncorrelated limit $\langle \mathcal{R}^2 \rangle \sim 1$ to zero for $U \geq U_c$. The double occupancy $\langle \hat{n}_\uparrow \hat{n}_\downarrow \rangle$ also shows a similar monotonically decreasing trend with increasing U for both models. The vanishing of the double occupancy indicates a metal insulator transition driven by electronic localization due to strong Hubbard repulsion. These results also show that the Mott transition in the atomic liquid seems to follow a similar scenario as in the well-studied amorphous systems.

Yet, despite the similarity in the evolution of bandwidth renormalizations, the liquid systems exhibit dramatically different electron transport behaviors, compared with that of amorphous solid. As shown in Fig. 3.2(b), the DC conductivity of the liquid metal is enhanced by Hubbard U before the rapid drop at the Mott transition. On the other hand, the conductivity of the amorphous system gradually decreases before a significant drop near the critical U_c. The behavior in the amorphous case is consistent with the statistical DMFT calculations [90, 91]. Indeed, it is argued that the DC conductivity of the metallic phase is pinned at its value in the uncorrelated $U \to 0$ limit for any model obeying a local particle-hole symmetry, which applies to tight-binding systems at half-filling with arbitrary form of hopping randomness [90].
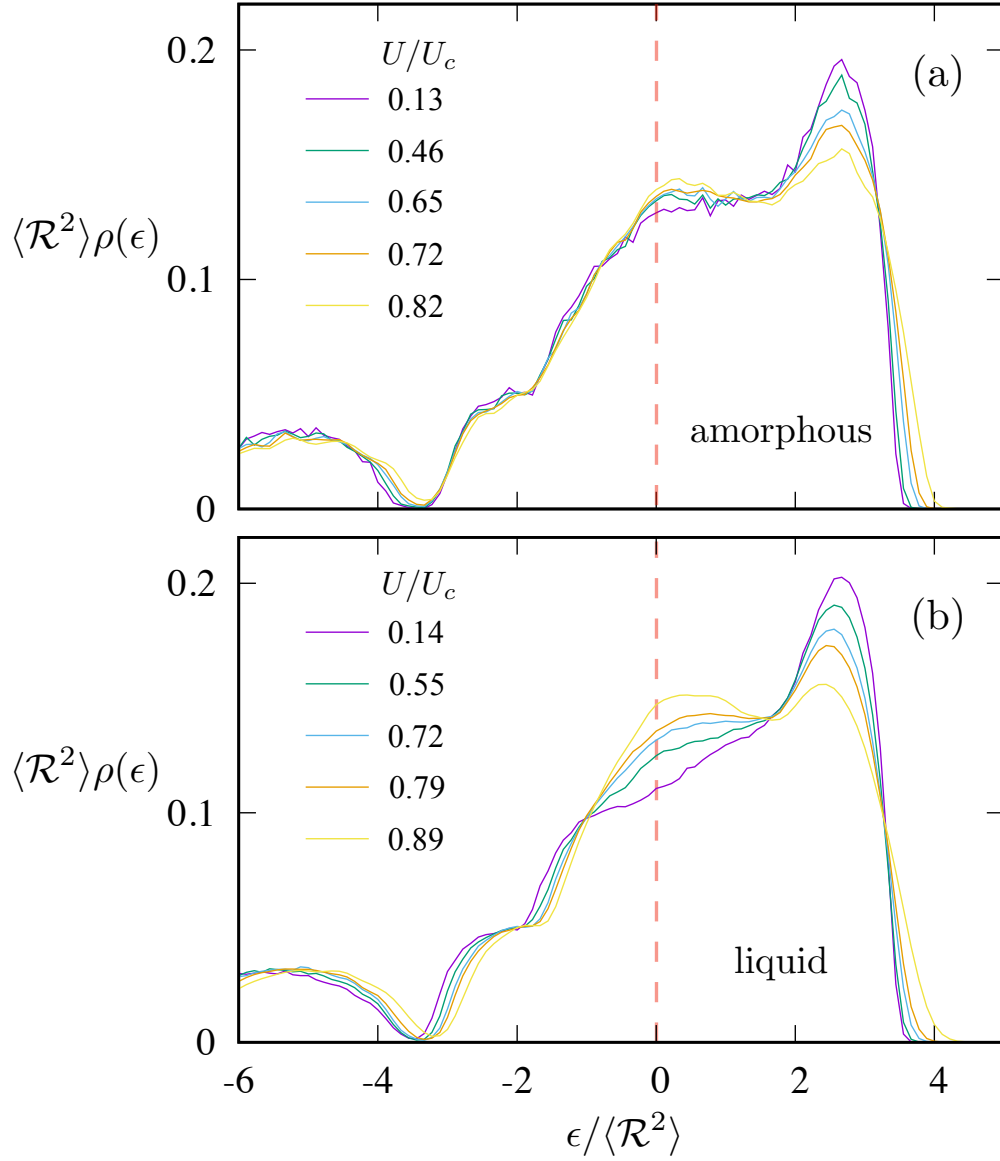
Figure 3.3: Effective density of states $\rho^*(\epsilon) = \langle \mathcal{R}^2 \rangle \rho(\epsilon)$ at various Hubbard U for (a) the amorphous solid and (b) the Hubbard liquid. The Fermi level is fixed at $\epsilon = 0$ shown by the red dashed line.

The DC conductivity of the amorphous solid can also be understood from the picture of a renormalized Fermi liquid. Applying the Kubo-Greenwood formula to a $T = 0$ degenerate Fermi gas in the presence of randomly distributed scatterers, one obtains

DC conductivity [92]:

$$\sigma_0 = \frac{2\pi e^2 \hbar}{m^{*2}} \overline{|\langle \hat{\mathbf{p}} \rangle|^2} \, \rho_F^2, \tag{3.9}$$

where m^* is the effective mass, ρ_F is the density of states (DOS) at the Fermi level, $\langle \hat{\mathbf{p}} \rangle$ denotes a matrix element between two different eigenstates at the Fermi level, and the overline indicates averaging over such states. In the presence of the Hubbard repulsion, the electron correlation effect results in an enhanced effective mass

$$m^* = \frac{m}{\langle \mathcal{R}^2 \rangle}, \tag{3.10}$$

where the bracket in $\langle \mathcal{R}^2 \rangle$ denotes the average of the renormalization at different orbitals. On the other hand, as the electron bandwidth is reduced, the conservation of total states implies an enlarged DOS. The increased effective mass and the increased DOS at the Fermi level are driving the conductivity in opposite directions, whichever factor prevails dictates the change of the conductivity. For instance, in the case of amorphous solids, their effects counterbalance each other, resulting in a levelled conductivity as depicted in Fig. 3.2(b).

To enhance our understanding of this condition, we reformulate Eq. (3.9) as

$$\sigma_0 = \frac{2\pi e^2 \hbar}{m^2} \overline{|\langle \hat{\mathbf{p}} \rangle|^2} \, \rho_F^{*2}, \tag{3.11}$$

$$\rho_F^* = \langle \mathcal{R}^2 \rangle \rho_F, \tag{3.12}$$

where ρ_F^* is the effective DOS at the Fermi level. In the form of Eq. (3.11), the change of conductivity solely depends on the change of the effective density of states ρ_F^*. The effective DOS for both the amorphous solid and the Hubbard liquid at various U are
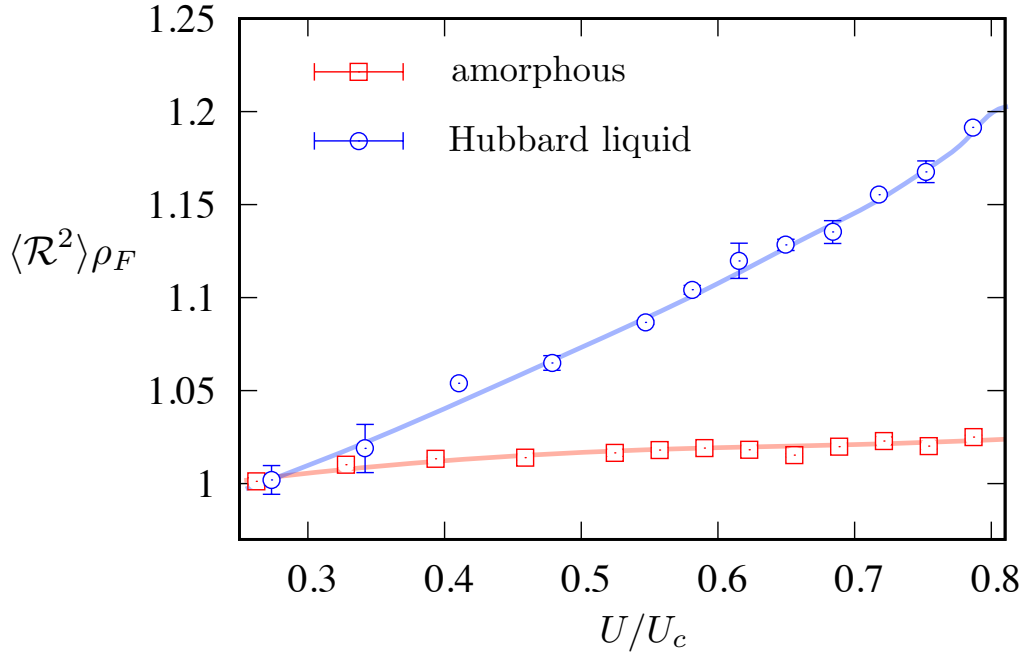
Figure 3.4: The effective density of states at the Fermi level ρ_F^* versus U, for the amorphous solid and the Hubbard liquid.

shown in Fig. 3.3. The two figures Fig. 3.3(a) and Fig. 3.3(b) show distinct behaviour at the Fermi level as the interaction U increases. In contrast to the amorphous case, the Hubbard liquid exhibits a notable surge in the effective density of states (DOS) at the Fermi level as U increases, which elucidates the observed enhancement in conductivity as illustrated in Fig. 3.2. The variation of the effective DOS at the Fermi level with respect to U is also depicted in Fig. 3.4. It illustrates a substantial increase for the Hubbard liquid, whereas only a minimal change is observed for the amorphous solid.

The different behaviour of the electronic structure between the amorphous solid and Hubbard liquid is attributed to the alteration in atomic distribution within the Hubbard liquid as the interaction strength increases. We explore the change of atomic distribution by computing the coordination number and average nearest-neighbor dis-
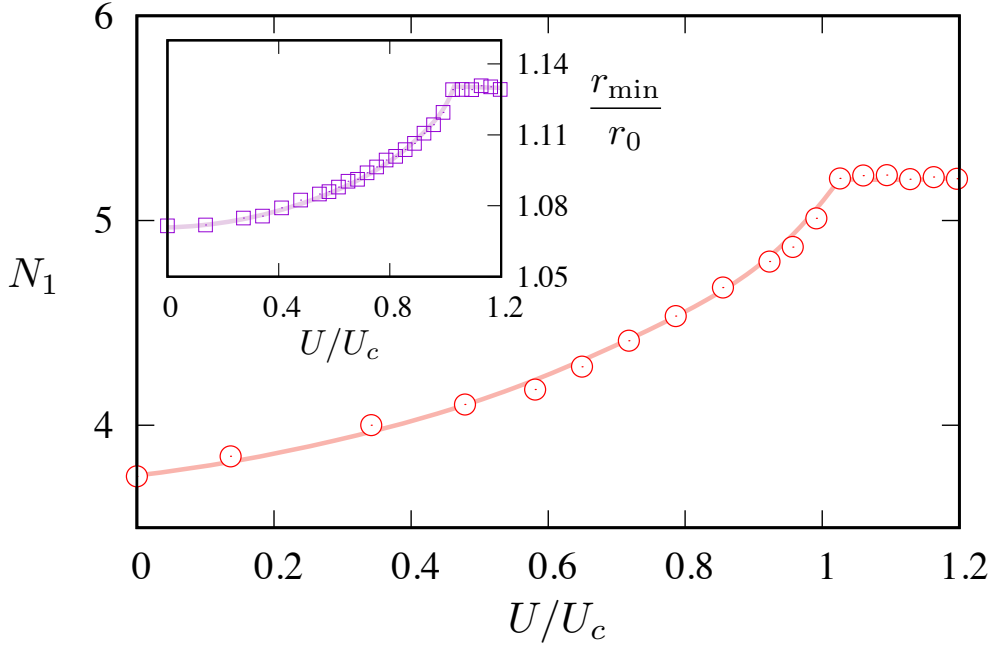
Figure 3.5: The coordination number N_1 versus U for the Hubbard liquid, at $k_B T/t_0 = 0.00825$. $r_0 = 0.526\xi$, t_0 and ξ are the energy and length scale of the system given in Eq. (2.4). The inset: the average inter-atomic nearest-neighbor distance versus the interaction for the Hubbard liquid.

tance in the liquid, as shown in Fig. 3.5. The coordination number in liquid refers to the average number of nearest-neighbor atoms surrounding a central atom, it reflects the packing efficiency of particles in the liquid. The coordination number is defined as

$$N_1 = 2 \int_0^{r_{\max}} dr 4\pi r^2 g(r)\rho_0, \tag{3.13}$$

the integral is integrated from 0 to the position of the first peak $r_{\max}$ in $g(r)$, $\rho_0 = N/V$ is the system's overall density. The coordination number N_1 as a function of U is depicted in Fig. 3.5. It demonstrates a rise with increasing U until the occurrence of the Mott transition, beyond which the system exhibits no further changes and inter-atomic force is purely from the classical repulsive potential $\phi(|\mathbf{r}_i - \mathbf{r}_j|)$ in Eq. (3.1).

The inset in Fig. 3.5 shows the average inter-atomic nearest-neighbor distance versus U. As interaction increases, the cohesive inter-atomic force provided by the electron hopping is reduced, leading to a further nearest-neighbor distance. At higher U, despite the increased distance between near-neighbors, the liquid attains a higher coordination number. The higher coordination number means the atomic clusters are better connected, resulting in an enhanced electrical conductivity. it is worth mentioning that the conductivity of a perfect lattice at $T = 0$ is infinite, for a reference atom all its near-neighbors are equidistant from it. Moreover, expanding the lattice, i.e. increasing the lattice constant, will have no impact on conductivity in the absence of electron interaction.

3.3   Summary

We studied the DC conductivity of amorphous solids and Hubbard liquid with the Kubo-Greenwood formula. We demonstrate a rather counterintuitive phenomenon in metallic fluids where the electrical conductivity of a liquid system can be enhanced by electron correlation effects. Typically, strong electron correlation tends to localize electrons, which commonly leads to diminished electrical conductivity. We compared the effective density of states at the Fermi level between the amorphous solid and the Hubbard liquid at various U, and discovered a substantial increase for the Hubbard liquid, whereas only a minimal change is observed for the amorphous solid. The discrepancy is attributed to the alteration of atomic distribution in the Hubbard liquid due to the reduction of cohesive force at high U. The reduced cohesive force gives rise to atomic clusters with a larger coordination number, the increased atomic connectivity in turn results in an enhanced electrical conductance.

Chapter 4

Atomic diffusion enhancement due to electron delocalization

The kinetic properties of liquids, such as self-diffusion, viscosity, and thermal conductivity, are a subject of both fundamental interest as well as technological importance [93, 94, 95]. In particular, the diffusivity is a fundamental property that encodes the information of how inter-atomic interactions affect the random atomic motion in a fluid. For example, the Einstein equation, $D = k_B T/\zeta$, relates the atomic self-diffusion D to the friction coefficient ζ which partially quantifies the forces between atoms [96, 97]; here the temperature T underscores the stochastic nature of the thermally activated diffusive motion. Qualitatively, a stronger interatomic force is thus expected to increase the viscosity, hence giving rise to a reduced atomic diffusion.

The inter-atomic potential in liquids generally consists of a short-distance sharp repulsion originating from Pauli exclusion of overlapping electron orbitals and a longer-ranged attraction which provides the cohesive energy [98, 99]. Phenomenologically, the inter-atomic forces in simple liquids consisting of noble-gas atoms are well approximated by the familiar Lennard-Jones (LJ) potential [100, 101]. Monatomic liquid metals such as alkali fluids comprise another important family of simple liquids [102, 103]. The inter-atomic interactions in liquid metals, however, are significantly more complicated due to the formation of metallic bonds [104, 105, 106, 107, 108]. Their

effective potential exhibits a softer core [109, 110, 111, 112] compared with LJ-type potentials and a long-range oscillating tail.

While the repulsive core is mostly responsible for the emergence of short-range order that is characteristic of a liquid state [113, 114], extensive works over past decades have shown that the repulsive force also dominates the dynamical properties, especially in the dense limit [115, 116, 117]. The addition of an attractive tail to the repulsion generally leads to further friction and a reduced self-diffusion coefficient [118, 119, 120, 121]. However, the intricate interplay between the repulsive and attractive interactions has yet to be studied in detail, especially in the context of liquid-state Mott metal-insulator transitions [122], where the localization of electrons results in a diminished attractive inter-atomic interaction. Such study is particularly important for understanding the metal-insulator transition in expanding alkali fluids along the liquid-vapor coexistence line [80, 123], where several experiments have suggested the important role played by the electron correlation [53, 54, 55].

More generally, the effects of electron correlation on the atomic dynamics in a liquid metal remain a largely uncharted territory in the research of both liquid-state physics and correlated electron systems. This is partly due to the lack of proper molecular dynamics methods to study such effects. The widely used classical MD [124] methods which rely on empirical inter-atomic potentials fail to describe electronic phase transitions. On the other hand, state-of-the-art quantum MD [125, 82] methods based on density functional theory cannot properly include the strong electron correlation effects and, hence are inadequate for simulating the Mott transition.

In this chapter, we present a comprehensive theory for the effects of electron correlation on the self-diffusion coefficient of liquid metals with correlated electrons. We demonstrate and characterize an unusual maximum of atomic diffusion near the

Mott transition by employing a new quantum MD scheme [57, 126] based on the Gutzwiller method, which offers an efficient and qualitatively correct description of the Mott transition [21, 22, 23, 26]. This non-monotonic behavior is counter-intuitive since the addition of the attractive interaction is expected to increase the friction, hence reducing the atomic diffusivity. We show that the enhanced diffusion originates from a reduced repulsive core when the effect of the attractive tail is suppressed by thermal fluctuations.

4.1 Diffusion in a Hubbard liquid model

To investigate the effects of electron correlations on the motion of atoms in a liquid, we consider the Hubbard liquid Hamiltonian (2.1), with the model parameters described in Chapter 2.1,

$$\mathcal{H} = \sum_i \frac{|\mathbf{p}_i|^2}{2m} + \frac{1}{2} \sum_{i \neq j} \phi(|\mathbf{r}_i - \mathbf{r}_j|) + \sum_{ij,\sigma} h(|\mathbf{r}_i - \mathbf{r}_j|)\hat{c}_{i,\sigma}^\dagger \hat{c}_{j,\sigma} + U \sum_i \hat{n}_{i\uparrow}\hat{n}_{i_\downarrow}. \quad (4.1)$$

We perform the GMD simulations on systems of $N = 50$ atoms, with periodic boundary conditions. The system volume is fixed by setting the Wigner-Seitz radius

$$r_s = (3V/4\pi N)^{1/3} \quad (4.2)$$

to be $r_s = 1.9\xi$. The temperature T is controlled by the Langevin thermostat with a small damping. The atomic forces, computed using the Hellmann-Feynman formula $\mathbf{F}_i = -\langle \partial \mathcal{H}/\partial \mathbf{r}_i \rangle$, can also be derived from an effective pair-like potential $\mathbf{F}_i =$
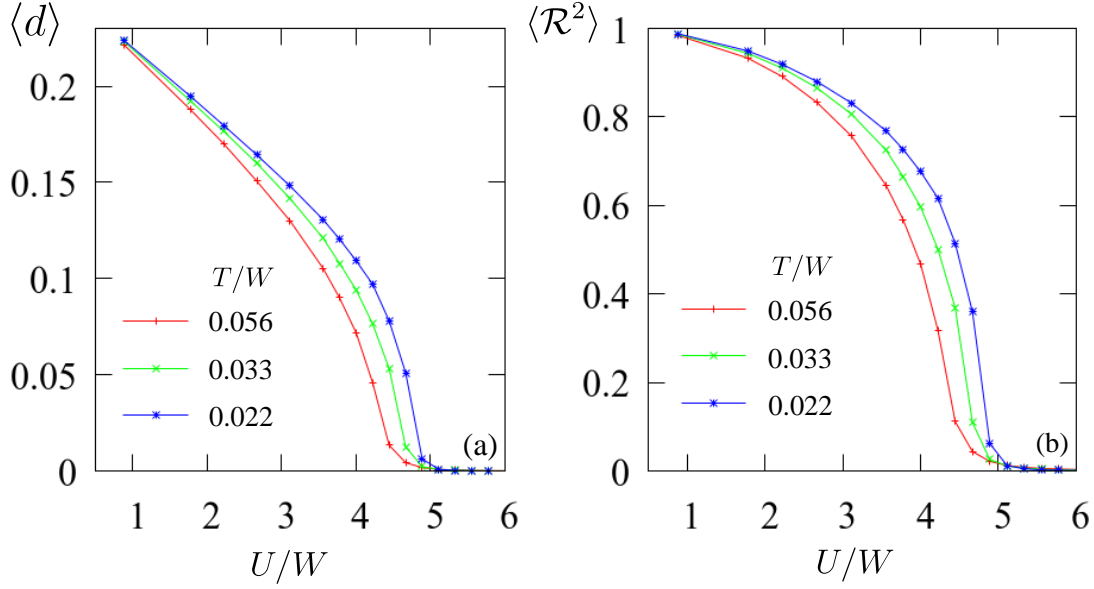
Figure 4.1: (a) The average double occupancy $\langle d \rangle$ and (b) the average renormalization $\langle \mathcal{R}^2 \rangle$ versus the Hubbard interaction at three different temperatures obtained from GMD simulations of the Hubbard liquid model. $W \approx 0.1875 t_0$ is the energy scale of the disordered tight-binding model at low temperatures.

$-\partial V(r_{ij})/\partial \mathbf{r}_i$. It consists of two parts:

$$V(r_{ij}) = \phi(r_{ij}) - 2\big(\langle \hat{c}_i^\dagger \hat{c}_j \rangle + \langle \hat{c}_j^\dagger \hat{c}_i \rangle\big) h(r_{ij}), \tag{4.3}$$

where the factor 2 accounts for the spin degeneracy, and $\langle \hat{A} \rangle = \text{Tr}(\hat{\varrho}_G \hat{A})$, with $\hat{\varrho}_G$ being the many-body electron density matrix within the Gutzwiller approximation, denotes the quantum average of operator $\hat{A}$. The first term describes the short-range repulsive core, while the second term denotes a renormalized attractive force. It should be noted the forces here are not exactly pair-wise since the electron reduced density matrix $\langle \hat{c}_i^\dagger \hat{c}_j \rangle$ depends also on atoms in the neighborhood of bond (ij). Given the atomic forces, a velocity-Verlet algorithm is used to integrate the Langevin equation, and the self-diffusion coefficient is computed from the velocity autocorrela-
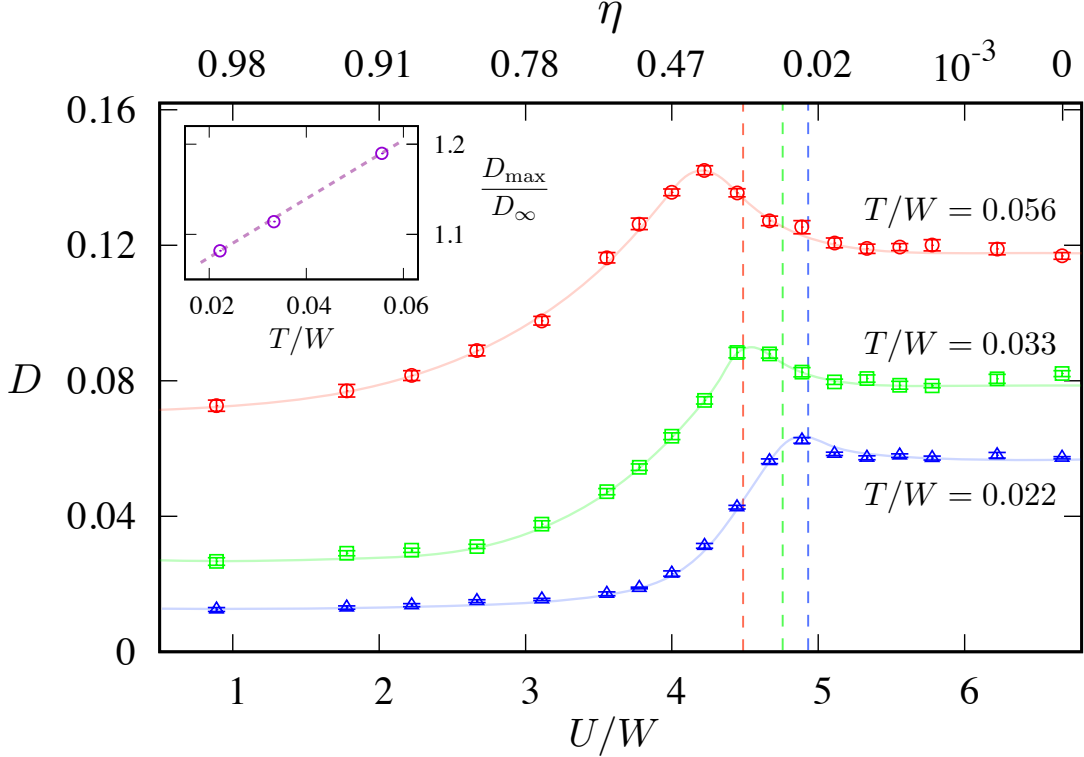
Figure 4.2: The atomic self-diffusion coefficient coefficient D versus the Hubbard parameter U from the GMD simulations of the Hubbard liquid model at three different temperatures. The dashed lines indicate an estimate of the critical U_c for the Mott transition. W is the absolute value of electron band energy at $U = 0$ at $T = 0.0042t_0$, $W = 0.1875t_0$. The inset shows the temperature dependence of $D_{\max}/D_\infty$, which provides a measure of the enhancement; here $D_{\max}$ is the maximum diffusion coefficient and D_∞ is the value in the large U limit.

tion: [66, 67]

$$D = \frac{1}{3N} \sum_{i=1}^{N} \int_0^\infty \langle \mathbf{v}_i(0) \cdot \mathbf{v}_i(t) \rangle dt. \tag{4.4}$$

Fig. 4.2 shows the atomic self-diffusion coefficient D as a function of Hubbard repulsion U obtained from the GMD simulations for three temperatures. The critical U_c of the Mott transition, estimated by the vanishing of the double occupancy shown in Fig. 4.1, are indicated by the vertical lines in Fig. 4.2. Perhaps the most re-

markable feature is the non-monotonic behavior of the diffusion coefficient which was first reported in Ref. [57]. The diffusion behavior at small U can be understood within the framework of Stokes-Einstein relation. Assuming that atomic dynamics in this regime is dominated by the electron-mediated attraction, the increase of self-diffusion coefficient thus comes from a weakened attractive force. As indicated in Eq. (4.3), the effective attractive interaction relies on the delocalization of electrons, we thus introduce the following renormalization factor to characterize the weakening of the attractive force: $\eta \equiv \langle \hat{c}_i^\dagger \hat{c}_j \rangle / \langle \hat{c}_i^\dagger \hat{c}_j \rangle_{U=0}$, where $\langle \cdots \rangle$ denotes both quantum averages as well as spatial and ensemble averages from MD simulations. Within the Gutzwiller approximation, this factor is approximated as $\eta \sim \langle \mathcal{R}_i \mathcal{R}_j \rangle$. The top horizontal axis of Fig. 4.2 shows the η at $T/W = 0.056$, increasing the Hubbard U leads to a reduced η and a weakened attractive force, which in turn increases the atomic diffusion. As the Hubbard parameter is greater than the critical U_c, the nearly complete localization of electrons leads to a pure repulsive inter-atomic interaction. The resultant diffusion coefficient is thus independent of U in this Mott insulating phase, giving rise to the leveled curves on the right side of Fig. 4.2.

The weakening of the electronic forces by the electron correlation is evidenced by Fig. 4.3, which exhibits the density plots of the magnitude of electronic force f_{ij}^{elec} between an atomic pair versus the pair distance r_{ij} for various values of Hubbard U. In contrast to forces due to a classical potential, the data points do not fall on a single curve. Nonetheless, the distribution of the inter-atomic forces does follow a well-defined underlying curve related to the hopping function, described by Eq. (2.41):

$$f_{ij}^{\text{elec}} = -\sum_{\sigma} \mathcal{R}_{i,\sigma} \mathcal{R}_{j,\sigma} \, \rho_{ij,\sigma} h'(r_{ij}).$$

The suppressed renormalization factor $\mathcal{R}_{i,\sigma}$, originates from the correlation-induced
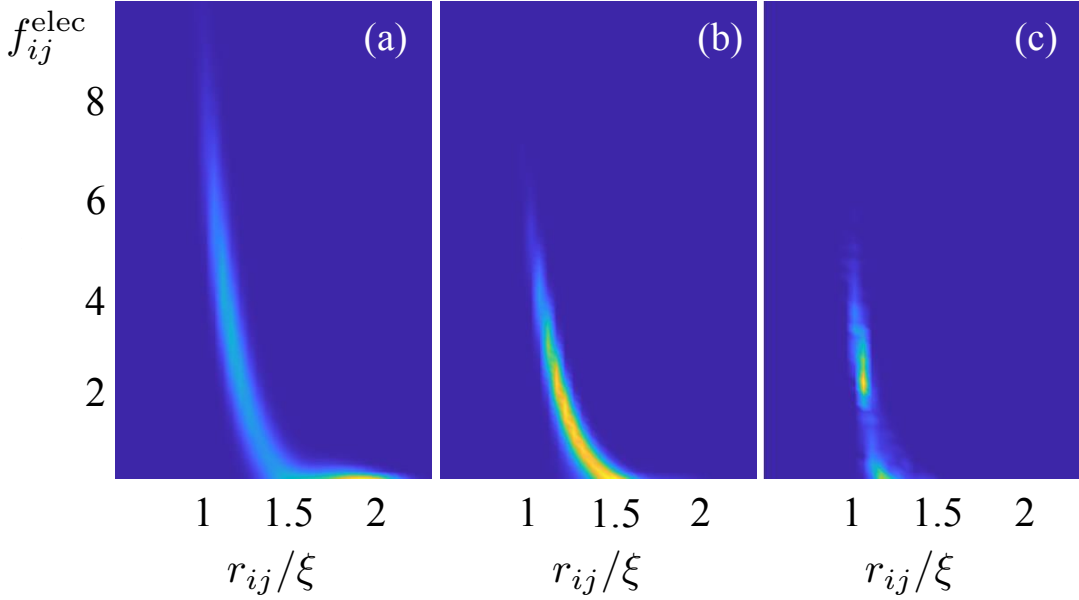
Figure 4.3: Density plots of the electronic forces between atomic pairs f_{ij}^{elec} versus the pair distance r_{ij} from the Gutzwiller MD simulations for various Hubbard parameter: (a) $U/t_0 = 0.167$, (b) $U/t_0 = 0.833$, (c) $U/t_0 = 1.08$. The number of atoms in the MD simulations is $N = 100$. The force is shown with arbitrary units, while the distance is measured in terms of ξ. Here t_0 and ξ are characteristic energy and length scales, respectively, of the hopping function $h(r)$. The temperature is set at $k_B T/t_0 = 0.0063$. The system density is fixed by setting the Wigner-Seitz radius $r_s = (3V/4\pi N)^{1/3}$ to be $r_s = 1.9\xi$.

localization of electrons, is shown in Fig. 4.1(b). The simulation results clearly show that as the Hubbard repulsion increases, the electrons become more localized, giving rise to a reduced average double occupancy and suppressed electron hopping. This in turn causes the reduction of attractive inter-atomic forces.

The above scenario based on a weakened attraction, however, could not explain the maximum of diffusion coefficient D in the vicinity of the Mott transition. In particular, due to the opposite signs of attractive and repulsive forces, their interplay near U_c could lead to interesting dynamical behaviors. To this end, we will introduce a simpler classical model to reproduce and elucidate this non-monotonic behavior of the diffusion coefficient in the subsequent section.

4.2 Diffusion in a classical Morse potential

We consider an effective inter-atomic pair potential which can be viewed as a generalization of the well-known Morse potential [127, 128]

$$V(r) = \varepsilon_0\big(e^{-r/\ell_+} - \eta\, e^{-r/\ell_-}\big), \qquad (4.5)$$

where ε_0 sets the energy scale, $\ell_\pm$ denote the ranges of the repulsive/attractive interactions. Importantly, we introduce a dimensionless parameter η to mimic the renormalization of the attractive forces discussed above. The range of the repulsive core is in general smaller than that of attraction, for simplicity we set $\ell \equiv \ell_- = 2\ell_+$. With this ratio, the special point $\eta = 2/e$ corresponds to the Morse potential

$$V(r) = \varepsilon_0\{1 - \exp[-(r - \ell)/\ell]\}^2. \qquad (4.6)$$

The generalized Morse potential is studied using standard classical MD simulations in the NVT ensemble with up to $N = 1000$ atoms. We consider a relatively dilute system with an $r_s = 4.5\ell$. Fig. 4.4 shows the self-diffusion coefficient versus the renormalization parameter η for three different temperatures. At large η, the strong attraction binds the atoms into a liquid state, it has a much smaller diffusion coefficient due to its high density. Upon reducing the parameter η, the system undergoes a first-order liquid-gas transition, as indicated by the vertical lines in Fig. 4.4. More relevant to our main interest here is the non-monotonic behavior of the diffusion coefficient as η is further reduced in the gas phase. Importantly, this result which is similar to that of the Hubbard liquid model indicates that the mechanism of the diffusion maximum can be understood from this relatively simple classical liquid
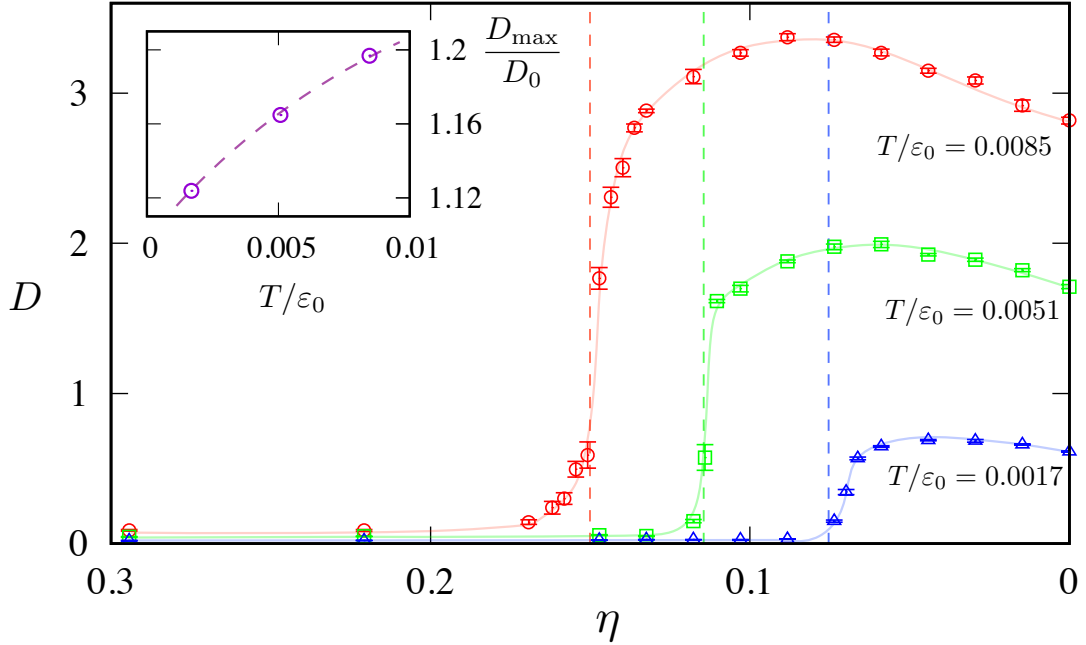
Figure 4.4: The self-diffusion coefficient D versus the renormalization parameter η obtained from classical MD simulation of the generalized Morse potential Eq. (4.5). The dashed lines indicate the liquid-gas transitions at the corresponding temperatures. The inset shows the enhancement of self-diffusion defined as $D_{\max}/D_0$, where $D_{\max}$ is the maximum diffusion coefficient and D_0 is the value at $\eta = 0$.

model.

To this end, we employ the Chapman-Enskog theory [129], which provides an accurate description for dilute liquids or gases based on binary collisions, to study the kinetic properties of the generalized Morse potential. Importantly, the Chapman-Enskog approach also demonstrates a clear maximum of atomic diffusivity when the attractive component of the interatomic forces is reduced.

Here we briefly review the application of this theory to the calculation of diffusion coefficient. The Chapman-Enskog method [129, 130] is an analytical approach for solving the Boltzmann equation. It provides a systematic method for calculating the transport coefficients of a gas from the knowledge of inter-molecular interactions.
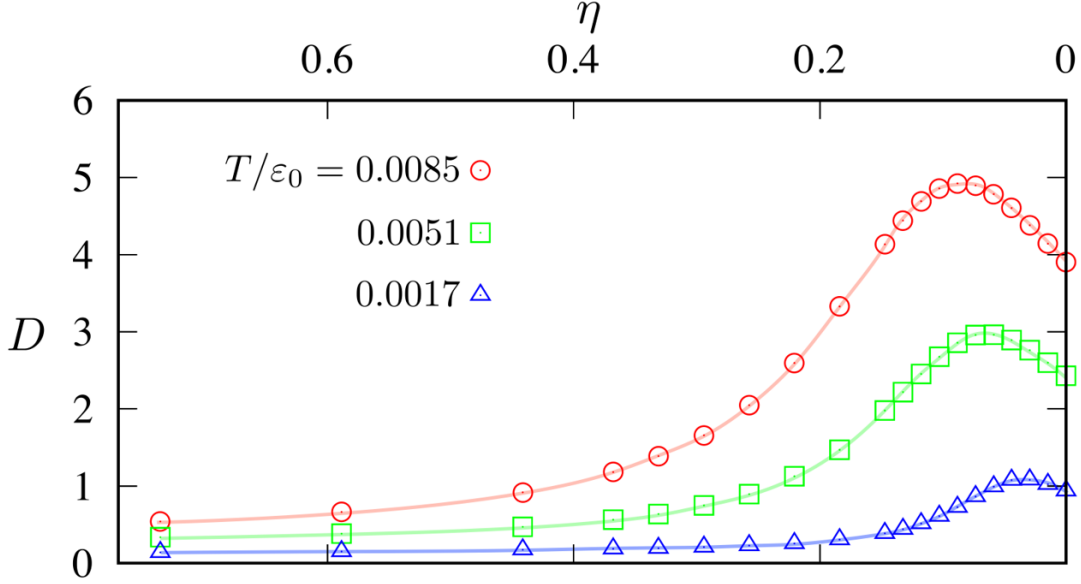
Figure 4.5: The diffusion coefficient of the generalized Morse potential Eq. (4.5) versus the weakening factor η computed using the Chapman-Enskog theory.

The transport properties of an atomic liquid, such as the diffusion coefficient and thermal conductivity, can be expressed by a set of collision integrals $\Omega^{(l,s)}$, where the superscript (l, s) denotes the order in a systematic expansion based on a small parameter which is the ratio of the mean-free path between collisions to the scale length of macroscopic variations.

Relevant to our work, the self-diffusion coefficient of a mono-atomic gas to the first order is given by

$$D = \frac{3}{8m\rho} \frac{k_B T}{\Omega^{(1,1)}},\tag{4.7}$$

where m is the atom mass, and $\rho = N/V$ is the atomic density. The first-order collision integral is computed as

$$\Omega^{(1,1)} = \left(\frac{k_B T}{2\pi\mu}\right)^{1/2} \int_0^\infty e^{-\frac{\epsilon}{k_B T}} \left(\frac{\epsilon}{k_B T}\right)^2 Q(\epsilon) \frac{d\epsilon}{2k_B T},\tag{4.8}$$

where $\mu = m/2$ is the reduced mass. The integration variable ϵ is related to the kinetic energy of an atomic pair $\epsilon = \mu v^2/2$ during the collision. For a given incoming energy ϵ of the atomic pair, the effective cross-section of the collision is

$$Q(\epsilon) = 2\pi \int_0^\infty (1 - \cos \chi) b \, db, \tag{4.9}$$

This integral is essentially the summation of cross sections $2\pi b \, db$ at different impact parameter b weighted by the factor $(1 - \cos \chi)$ to account for the momentum transfer. Here χ is the deflection angle of the atomic trajectory during the binary collision. It depends on both the impact parameter and the incoming energy

$$\chi(b, \epsilon) = \pi - 2b \int_{r_m}^\infty \frac{dr/r^2}{\left[1 - \frac{b^2}{r^2} - \frac{V(r)}{\epsilon}\right]^{1/2}}. \tag{4.10}$$

where the minimum distance r_m also depends on both b and ϵ.

In general, this set of integrals cannot be computed analytically, except for the case of the hard-sphere model. The inter-atomic potential for a hard sphere of diameter σ is defined as infinite repulsion $V(r) = +\infty$ for pair distance $r < \sigma$, and $V(r) = 0$ outside. The collision integral of the hard-sphere model can be seen to be given by the circular area

$$Q(\epsilon) = \pi \sigma^2, \tag{4.11}$$

which is independent of the incoming energy. Substituting this into Eq. (4.8) for the collision integral, one obtains the following Enskog formula for the diffusion coefficient

of hard-sphere gas

$$D = \frac{3}{8} \left(\frac{\pi k_B T}{m} \right)^{1/2} \frac{1}{\pi \sigma^2 \rho}.$$ (4.12)

This formula can be used to extract an effective cross-section radius $r_{\text{eff}} = \sigma$ for other inter-atomic potentials.

In this work of Morse potential, we define

$$r_{\text{eff}} = (m/\pi k_B T)^{1/4} \Omega_{(1,1)}^{1/2}$$ (4.13)

as the effective radius of the scattering cross-section, so that the diffusion coefficient is given by

$$D = \frac{3}{8} \left(\frac{\pi k_B T}{m} \right)^{1/2} \frac{1}{\pi r_{\text{eff}}^2 \rho}.$$ (4.14)

Employing the Chapman-Enskog method, Fig. 4.5 shows the diffusion coefficient D versus η at different temperatures. The curves exhibit a clear maximum, which becomes more prominent with increasing temperature, consistent with the classical MD simulations in Fig. 4.4. We note that the condensation phenomena in the strong attraction region, however, is beyond the Chapman-Enskog theory which is valid only for dilute systems.

It is worth noting that this non-monotonic behavior is unexpected since even a small attractive interaction, which operates at a longer range, immediately introduces an additional friction, which in turn results in a reduced atomic diffusion. While the enlarged diffusion coefficient is obviously due to a smaller r_{eff}, we find that the intriguing reduction of the effective radius is well captured by a shrinking repulsive
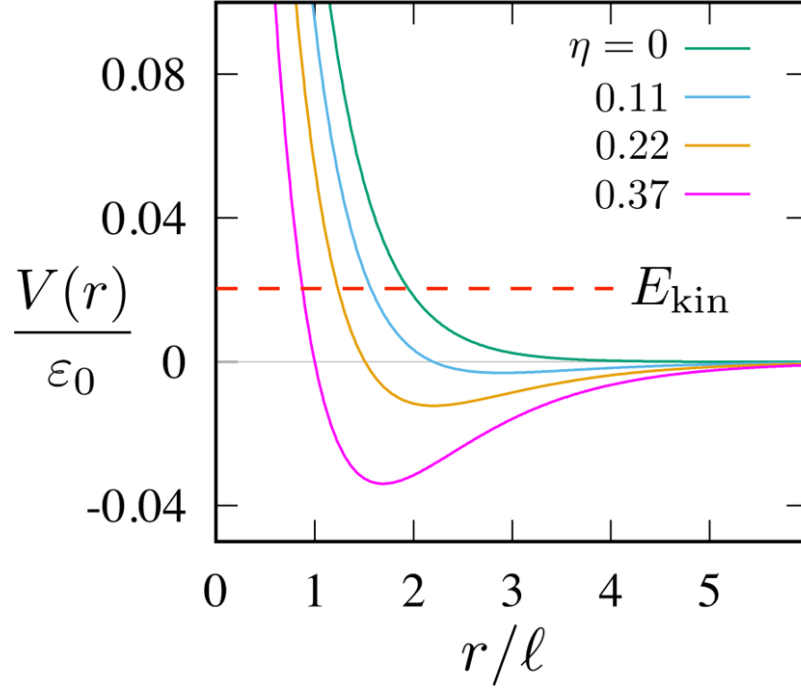
Figure 4.6: The generalized Morse potential Eq. (4.5), versus the weakening factor η computed using the Chapman-Enskog theory. The red dashed line shows the radius of repulsive core determined by condition $V(r_{\text{core}}) = E_{\text{kin}} = 3k_B T/2$.

core. To see this, we define an effective core radius r_{core}, which is similar to the so-called Boltzmann's hard-sphere diameter [131], as the distance at which the potential energy equals the average kinetic energy of atoms, i.e.

$$V(r_{\text{core}}) = E_{\text{kin}} = 3k_B T/2, \tag{4.15}$$

see Fig. 4.6. As shown by the dashed lines in Fig. 4.7, the η dependence of the effective radius r_{eff} is well approximated by r_{core} almost all the way up to the minimum.

Based on this observation, a theory of the diffusion maximum is presented in the following. As discussed in the introduction, an inter-atomic potential in general consists of a short-distance repulsive interaction V_+ and a longer-ranged attraction V_-; see Fig. 4.8(a). Physically, these two components $V_\pm$ are of rather distinct origins.
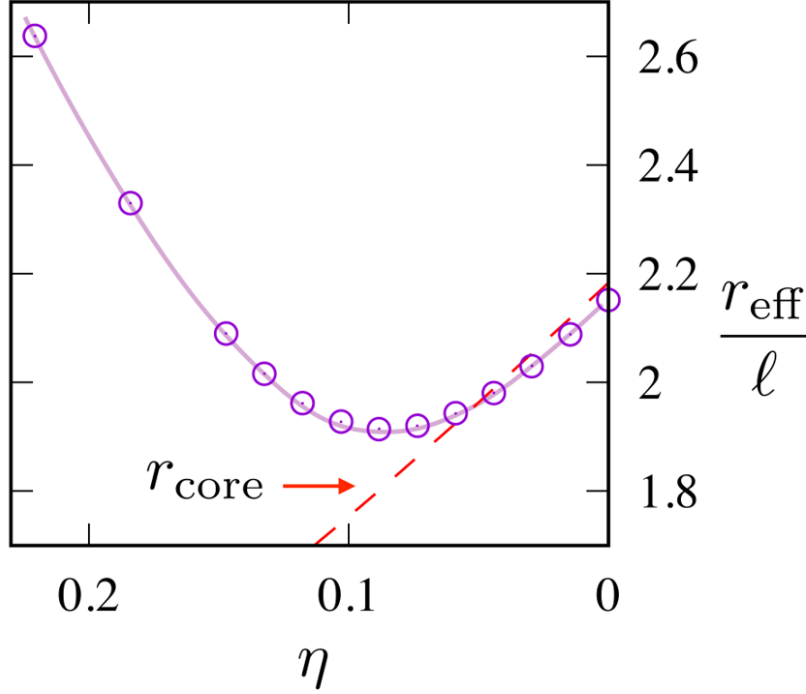
Figure 4.7: Effective radius r_{eff} of the scattering cross-section versus η for $T/\varepsilon_0 = 0.0085$, shown by the purple circles and line in the figure. The red dashed line shows r_core defined in Eq. (4.15).

On the other hand, the importance of the inner repulsive core in determining the short-range correlation suggests a different decomposition $V = V_{\text{core}} + V_{\text{tail}}$ [114] as shown in Fig. 4.8(b). The force is purely repulsive inside the core region, and is entirely attractive outside the core. Based on the Einstein relation, the self-diffusion coefficient can then be expressed as $D = k_B T/(\zeta_{\text{core}} + \zeta_{\text{tail}})$. The friction coefficients ζ are given by the force auto-correlation function, and here ζ_{core} denotes the friction due to the repulsive core, while the effects of the attractive tail (including the cross terms) are subsumed into ζ_{tail} [118, 119, 120, 121]. It is the cancellation between V_+ and V_- that leads to a reduction of ζ_{core}, resulting in an enhanced D. However, as V_- continues to increase, ζ_{tail} becomes predominant, causing a subsequent decline in the diffusion coefficient.
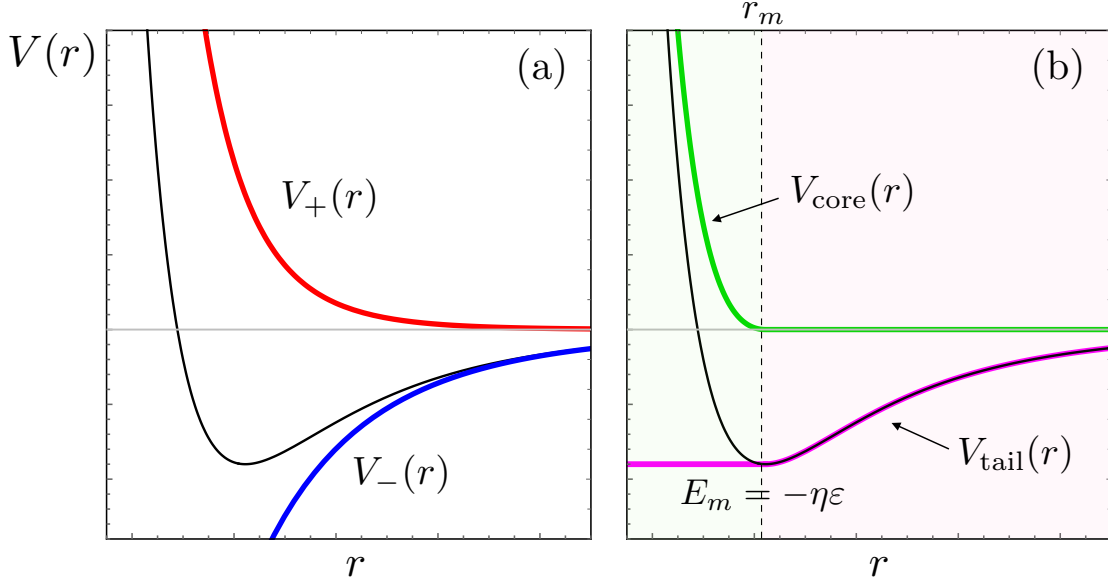
Figure 4.8: (a) Decomposition of an interatomic potential $V(r)$ into its physical repulsive $V_+(r)$ and attractive $V_-(r)$ components. (b) The same interaction potential can also be spatially separated into a repulsive core $V_{\text{core}}(r)$ for $r < r_m$, and an attractive tail $V_{\text{tail}}(r)$ for $r > r_m$.

4.3 Summary

To summarize, we have presented a comprehensive theory for the intriguing phenomenon of attraction facilitated enhancement of atomic diffusion in simple liquids. In general, while both the structural and dynamical properties of simple liquids at high densities are dominated by the repulsive core [115, 116, 117], our work highlights interesting kinetic phenomena in the intermediate and dilute regime that results from the nontrivial interplay between repulsive core and the longer-ranged attractive interaction. In particular, our theory naturally explains a maximum atomic diffusivity in the vicinity of a Mott metal-insulator transition in liquid metals, a phenomenon that is demonstrated by quantum molecular dynamics simulations on correlated-electron liquid models.

Chapter 5

GMD simulation of hydrogen under extreme conditions

Our preliminary works on the Gutzwiller-MD simulations of the liquid Hubbard model, provide crucial proof of concept for incorporating electron correlation into quantum MD simulations. In particular, we show that the Gutzwiller-MD. is able to describe the MIT dynamics, which is beyond the conventional DFT-MD. The next step naturally is to implement this framework on real correlated electron materials. In principle, this can be achieved through the combination of well-established DFT techniques, such as the local density approximation (LDA), with the Gutzwiller method. This so-called LDA+G approach has recently been proposed as a high-throughput electronic structure method for real correlated electron compounds [132, 133, 134, 135, 64].

However, there are still obstacles that must be overcome to integrate the LDA+G into MD simulations. For example, because of the different basis functions used in the LDA and Gutzwiller methods, technical details of the force calculation have yet to be worked out. Moreover, since the number of different electron configurations grows exponentially with the number of correlated orbitals, a huge set of variational parameters is required in the Gutzwiller calculation of multi-orbital atoms. For instance, this number is in the order of 10^4 for atoms with d-orbitals in transition metal
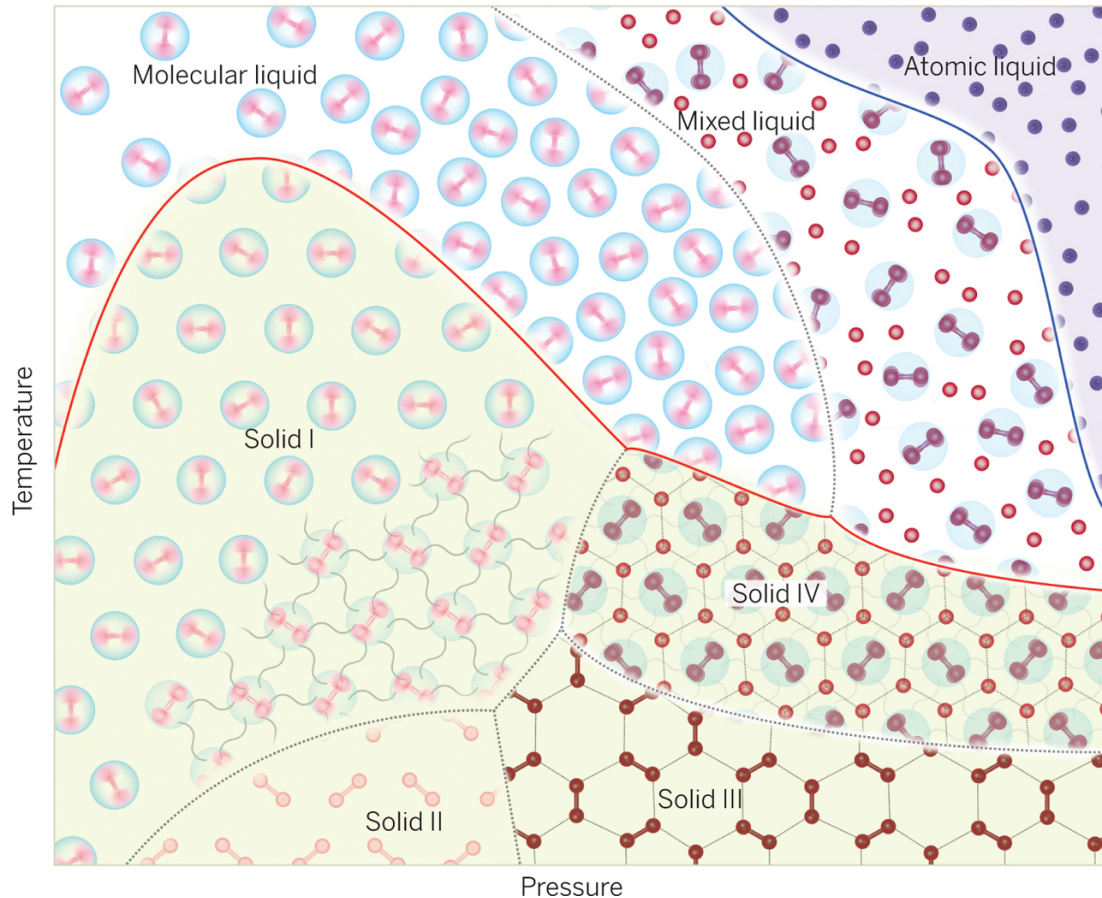
Figure 5.1: Schematic phase diagram of hydrogen adopted from Ref. [136]. The figure shows the four known solid phases I to IV and two observed liquid phases, together with the predicted atomic liquid. The liquid-liquid MIT corresponds to the transition from molecular to atomic liquid hydrogen. The mixed liquid corresponds to the co-existence region of the first-order MIT.

compounds such as VO_2. Consequently, direct quantum MD simulation of the MIT for such complex atoms is almost impossible even with the already efficient Gutzwiller method.

Instead of tackling the complex correlated systems head-on, in this thesis we propose to first develop a linear-scaling ab initio MD framework based on the Gutzwiller and the ML methods for liquid metallic hydrogen under extreme conditions. In fact, the liquid Hubbard model used in our pilot study can be viewed as a highly simplified

version of the liquid hydrogen [57]. Despite being the simplest element of the periodic table, hydrogen continues to fascinate researchers in condensed-matter physics, energy application, and planetary science [137, 138]. This is because hydrogen exhibits a rich phase diagram [136], which contains at least four different solid phases as well as several liquid phases; see Fig. 5.1. Furthermore, it is predicted to display remarkable properties such as low-temperature quantum fluidity and high-pressure superconductivity [139, 140, 141, 142].

In particular, it was conjectured by Wigner and Huntington in the early days of quantum mechanics that hydrogens might undergo a liquid-liquid insulator to metal transition with increasing pressure [143]; see Fig. 5.1. The liquid metallic hydrogen at high pressures is also special in the sense that it is an atomic liquid. Indeed, all other phases of hydrogen, including the solid phases and the insulating liquid, consist of hydrogen H2 molecule as the basic unit. The insulator-to-metal transition thus also corresponds to the dissociation of the hydrogen molecules, which results in the diminishing of the molecule peak in the radial distribution function $g(r)$, a phenomenon already observed in our Gutzwiller-MD simulations of the liquid Hubbard model [57].

Tantalizing evidences of this liquid-liquid MIT in hydrogen have been reported in recent experiments [144, 145, 146, 147]. Moreover, various quantum MD simulations, with many-body solvers ranging from state-of-the-art DFT to expensive brute-force quantum Monte Carlo optimization, have been applied to study this intriguing phenomenon [148, 149, 150, 151, 152]. These previous studies thus provide ample numerical data that can be used to benchmark our ab initio Gutzwiller-MD simulations.

5.1 Ab initio tight-binding model for hydrogen

Instead of using an ad hoc function for $t(R_{ij})$ and a parameter U as in the liquid Hubbard model, the starting point of our ab initio MD is the following fundamental Hamiltonian for hydrogen atoms in a cubic super-cell system with periodic boundary condition (PBC):

$$H = -\frac{\hbar^2}{2m} \sum_{\mathbf{p}} \sum_{\mu=1}^{N_e} \nabla^2_{\mathbf{r}_{\mathbf{p},\mu}} - \sum_{\mathbf{n},\mathbf{p}} \sum_{\mu=1}^{N_e} \sum_{i=1}^{N_a} \frac{e^2}{|\mathbf{r}_{\mathbf{p},\mu} - \mathbf{R}_i - \mathbf{n}L|} + \frac{1}{2} \sum_{\mathbf{p},\mathbf{q}} \sum_{\mu,\nu=1}^{N_e} \frac{e^2}{|\mathbf{r}_{\mathbf{p},\mu} - \mathbf{r}_{\mathbf{q},\nu}|}$$

$$+ \frac{1}{2} \sum_{\mathbf{n},\mathbf{m}} \sum_{i,j=1\,(i \neq j\,\text{if}\,\mathbf{n}=\mathbf{m})}^{N_a} \frac{e^2}{|\mathbf{R}_i + \mathbf{n}L - \mathbf{R}_j - \mathbf{m}L|} + \sum_{\mathbf{n}} \sum_{i=1}^{N_a} \frac{\mathbf{P}_i^2}{2M}, \tag{5.1}$$

where N_e and N_a are the number of electrons and atoms in a super-cell, in the case of hydrogen, $N_e = N_a$. L is the box length of the super-cell, i.e. lattice constant. $\mathbf{n}$, $\mathbf{m}$, $\mathbf{p}$, $\mathbf{q}$ are 3D vectors denoting the super-cells, e.g. $\mathbf{n} = (1,0,0)$, $(-1,0,0)...$, $\mathbf{n}L$ is the central position of the super-cell with index $\mathbf{n}$. Define $\mathcal{N}$ as the total number of super-cells in the system, $\mathbf{n}$, $\mathbf{m}$, $\mathbf{p}$, $\mathbf{q}$ iterate through all the $\mathcal{N}$ super-cells, we work in the thermodynamic limit with $\mathcal{N} \to \infty$. $\mathbf{R}_i$ is the position of the i-th ion in the original super-cell, i.e. the cell with index $\mathbf{n} = (0,0,0)$. m and M are the mass of the electron and the ion. $\mathbf{P}_i$ is the momentum of the i-th ion, the i-th ion has identical momentum in every super-cell in the PBC setup. $\mathbf{r}_{\mathbf{p},\mu}$ denotes the position of μ-th electron in the super-cell with $\mathbf{p}$.

We introduce a set of Bloch-like basis functions,

$$|\tilde{w}_j^{\mathbf{k}}\rangle = \frac{1}{\sqrt{\mathcal{N}}} \sum_{\mathbf{n}} e^{-i\mathbf{k}\cdot\mathbf{n}L} |w_j^{\mathbf{n}}\rangle, \tag{5.2}$$

satisfying the orthogonal condition

$$\langle \tilde{w}_i^{\mathbf{k}} | \tilde{w}_j^{\mathbf{k}'} \rangle = \delta_{ij} \delta_{\mathbf{k}\mathbf{k}'}. \tag{5.3}$$

$w_i^{\mathbf{n}}(r) \equiv \langle r | w_i^{\mathbf{n}} \rangle$ is a localized wave function in the super-cell of index $\mathbf{n}$ with the translational symmetry

$$w_i^{\mathbf{n}}(\mathbf{r}) = w_i(\mathbf{r} - \mathbf{n}L). \tag{5.4}$$

The basis functions are constructed from the Slater-type orbitals (STOs) with the Löwdin orthogonalization method, which is discussed in appendix A.

Using the standard procedure of second-quantization based on the basis functions $|\tilde{w}_j^{\mathbf{k}}\rangle$, we derive the following second-quantized Hamiltonian for $\mathcal{N}$ super-cells

$$\mathcal{H}_{\mathcal{N}} = \int_{\mathrm{BZ}} d\mathbf{k} \sum_{ij} \sum_{\alpha} \mathcal{T}_{ij}^{\mathbf{k}} c_{\mathbf{k},i\alpha}^{\dagger} c_{\mathbf{k},j\alpha} + \frac{1}{2} \int_{\mathrm{BZ}} d\mathbf{k}_1 \int_{\mathrm{BZ}} d\mathbf{k}_2 \sum_{ijkl} \sum_{\alpha\beta} \mathcal{V}_{ijkl}^{\mathbf{k}_1,\mathbf{k}_2,\mathbf{k}_1,\mathbf{k}_2}$$

$$c_{\mathbf{k}_1,i\alpha}^{\dagger} c_{\mathbf{k}_2,j\beta}^{\dagger} c_{\mathbf{k}_2,l\beta} c_{\mathbf{k}_1,k\alpha} + \frac{1}{2} \sum_{\mathbf{n},\mathbf{m}} \sum_{i,j=1 \,(i \neq j \,\mathrm{if}\, \mathbf{n}=\mathbf{m})}^{N_a} \frac{e^2}{|\mathbf{R}_i + \mathbf{n}L - \mathbf{R}_j - \mathbf{m}L|} + \sum_{\mathbf{n}} \sum_{i=1}^{N_a} \frac{\mathbf{P}_i^2}{2M}, \tag{5.5}$$

where $\mathbf{k}$ is integrated over the Brillouin Zone (BZ), α and β denote electron spins.

Numerically, it is impossible to solve the eigenstates for all $\mathbf{k}$ points, since the $\mathbf{k}$ values are continuous. In conventional methods, the Hamiltonian is typically computed solely at some selected high-symmetry points within the Brillouin zone. In this work, since we are working on super-cells, we exclusively choose the Γ point within the Brillouin Zone, i.e. $\mathbf{k} = \mathbf{0}$ point. Choosing the $\mathbf{k} = \mathbf{0}$ point is equivalent to requiring the electronic wave function to be periodic across the super-cells, which is a periodic

boundary condition for electrons. In the thermodynamic limit of a very large super-cell $N_a \to \infty$, the eigenstates of $\mathbf{k} = \mathbf{0}$ point are equivalent to the eigenstates of all $\mathbf{k}$ points in the Brillouin zone. In that limit, we have $\mathcal{H}_\mathcal{N} = \mathcal{N}\mathcal{H}_1$, where $\mathcal{H}_1$ is the Hamiltonian of a single super-cell:

$$\mathcal{H}_1 = \sum_{ij} \sum_\alpha \mathcal{T}_{ij} c_{i\alpha}^\dagger c_{j\alpha} + \frac{1}{2} \sum_{ijkl} \sum_{\alpha\beta} \mathcal{N} \, \mathcal{V}_{ijkl} c_{i\alpha}^\dagger c_{j\beta}^\dagger c_{l\beta} c_{k\alpha}$$
$$+ \frac{1}{2} \sum_\mathbf{n} \sum_{i,j=1(i\neq j \, \text{if} \, \mathbf{n}=\mathbf{0})}^{N_a} V_{ij,\mathbf{n}}^{\text{coul}} + \sum_{i=1}^{N_a} \frac{\mathbf{P}_i^2}{2M}, \tag{5.6}$$

$$V_{ij,\mathbf{n}}^{\text{coul}} \equiv \frac{e^2}{|\mathbf{R}_i - \mathbf{R}_j - \mathbf{n}L|}, \tag{5.7}$$

$$c_{i\alpha}^\dagger = c_{\mathbf{0},i\alpha}^\dagger, \quad c_{i\alpha} = c_{\mathbf{0},i\alpha},$$

$$\mathcal{T}_{ij} = \mathcal{T}_{ij}^\mathbf{0}, \quad \mathcal{V}_{ijkl} = \mathcal{V}_{ijkl}^{\mathbf{0},\mathbf{0},\mathbf{0},\mathbf{0}}.$$

At $\mathbf{k} = \mathbf{0}$ point, the basis functions are

$$|\tilde{w}_j\rangle \equiv |\tilde{w}_j^\mathbf{0}\rangle = \frac{1}{\sqrt{\mathcal{N}}} \sum_\mathbf{n} |w_j^\mathbf{n}\rangle, \tag{5.8}$$

The hopping coefficient is given by

$$\mathcal{T}_{ij} = \int d\mathbf{r} \, \tilde{w}_i^*(\mathbf{r}) \left[-\frac{\hbar^2}{2m} \nabla_\mathbf{r}^2 - \sum_{k,\mathbf{p}} \frac{e^2}{|\mathbf{r} - \mathbf{R}_k - \mathbf{p}L|} \right] \tilde{w}_j(\mathbf{r})$$
$$= \sum_\mathbf{n} \int d\mathbf{r} \, w_i^*(\mathbf{r}) \left[-\frac{\hbar^2}{2m} \nabla_\mathbf{r}^2 - \sum_{k,\mathbf{p}} \frac{e^2}{|\mathbf{r} - \mathbf{R}_k - \mathbf{p}L|} \right] w_j(\mathbf{r} - \mathbf{n}L), \tag{5.9}$$

and the interaction potential coefficient is

$$
\begin{aligned}
\frac{1}{2}\mathcal{N}\,\mathcal{V}_{ijkl} &= \frac{1}{2}\mathcal{N}\int\int d\mathbf{r}_1 d\mathbf{r}_2 \tilde{w}_i^*(\mathbf{r}_1)\tilde{w}_j^*(\mathbf{r}_2)\frac{e^2}{|\mathbf{r}_1-\mathbf{r}_2|}\tilde{w}_k(\mathbf{r}_1)\tilde{w}_l(\mathbf{r}_2). \\
&= \sum_{\mathbf{n},\mathbf{p},\mathbf{q}}\int\int d\mathbf{r}_1 d\mathbf{r}_2 w_i^*(\mathbf{r}_1)w_j^*(\mathbf{r}_2-\mathbf{p}L)\frac{e^2}{|\mathbf{r}_1-\mathbf{r}_2|}w_k(\mathbf{r}_1-\mathbf{n}L)w_l(\mathbf{r}_2-\mathbf{q}L).
\end{aligned}
$$

$$(5.10)$$

Define the integer vector $\boldsymbol{\nu}_{ij}$ as the $\mathbf{n}$ that minimizes the distance $|\mathbf{R}_i-\mathbf{R}_j-\mathbf{n}L|$.

$$
\boldsymbol{\nu}_{ij}\equiv\{\mathbf{n}:\text{minimize}|\mathbf{R}_i-\mathbf{R}_j-\mathbf{n}L|\} \tag{5.11}
$$

Intuitively, one can think of $\mathbf{R}_j+\boldsymbol{\nu}_{ij}L$ as the copy of the j-th atom of the super-lattice that is closest to the i-th atom.

Assume the functions $w_i(\mathbf{r})$ are well-localized, and the super-cell box length is larger than the range of $w_i(\mathbf{r})$, we expect the overlapping $w_i^*(\mathbf{r})w_j(\mathbf{r}-\mathbf{n}L)=0$ unless at $\mathbf{n}=\boldsymbol{\nu}_{ij}$. Then Eq. (5.9) and Eq. (5.10) is simplified as

$$
\mathcal{T}_{ij}=\int d\mathbf{r}\, w_i^*(\mathbf{r})\left[-\frac{\hbar^2}{2m}\nabla_{\mathbf{r}}^2-\sum_{k,\mathbf{p}}\frac{e^2}{|\mathbf{r}-\mathbf{R}_k-\mathbf{p}L|}\right]w_j(\mathbf{r}-\boldsymbol{\nu}_{ij}L), \tag{5.12}
$$

$$
\frac{1}{2}\mathcal{N}\,\mathcal{V}_{ijkl}=\frac{1}{2}\sum_{\mathbf{p}}\int\int d\mathbf{r}_1 d\mathbf{r}_2 w_i^*(\mathbf{r}_1)w_j^*(\mathbf{r}_2-\mathbf{p}L)\frac{e^2}{|\mathbf{r}_1-\mathbf{r}_2|}w_k(\mathbf{r}_1-\boldsymbol{\nu}_{ik}L)w_l(\mathbf{r}_2-\mathbf{p}_{jl}^*L), \tag{5.13}
$$

$$
\mathbf{p}_{jl}^*\equiv\mathbf{p}+\boldsymbol{\nu}_{jl} \tag{5.14}
$$

In Eq. (5.12), the sum over $\mathbf{p}$ blows up the hopping coefficient $\mathcal{T}_{ij}$, since the electron-ion Coulomb interaction is long-range. Whereas, the sum over $\mathbf{n}$ causes no problem

because the local basis $w_i(\mathbf{r})$ decays fast with distance. Eq. (5.13) shares the same problem, the sum over $\mathbf{p}$ blows up $\mathcal{N}\mathcal{V}_{ijkl}$ due to the long-range electron-electron Coulomb interaction. The rescue to this problem lies in recognizing that these infinities will cancel out each other.

Effective tight-binding Hubbard model with finite coefficients

So far, the results derived above in this section are exact, at least in the thermodynamic limit $N_a \to \infty$, $\mathcal{N} \to \infty$. Yet, as previously discussed, the tight-binding coefficients Eq. (5.12) and Eq. (5.13) become infinite in the PBC setup. In this subsection, We derive an effective tight-binding model with finite coefficients by investigating the cancellation among the infinite terms presented in Eq. (5.6), utilizing certain approximations.

On-site hopping

First, decompose the on-site hopping in Eq. (5.12) as

$$\mathcal{T}_{ii} = t_{ii} + \sum_{\mathbf{p} \neq \mathbf{0}} T_{ii}^{i\mathbf{p}} + \sum_{k,\mathbf{p}\,(k \neq i)} T_{ii}^{k\mathbf{p}}, \tag{5.15}$$

$$t_{ii} \equiv \int d\mathbf{r}\, w_i^*(\mathbf{r}) \left[-\frac{\hbar^2}{2m}\nabla_{\mathbf{r}}^2 - \frac{e^2}{|\mathbf{r} - \mathbf{R}_i|} \right] w_i(\mathbf{r}), \tag{5.16}$$

$$T_{ii}^{k\mathbf{p}} \equiv \int d\mathbf{r}\, w_i^*(\mathbf{r}) \left[-\frac{e^2}{|\mathbf{r} - \mathbf{R}_k - \mathbf{p}L|} \right] w_i(\mathbf{r}), \tag{5.17}$$

where $T_{ii}^{k\mathbf{p}}$ is the hopping from atom i to itself in the original cell due to the atom k located in super-cell $\mathbf{p}$. t_{ii} and $T_{ii}^{k\mathbf{p}}$ are both finite.

For the interaction terms, decompose $\frac{1}{2}\mathcal{N}\mathcal{V}_{iiii}$ as

$$\frac{1}{2}\mathcal{N}\mathcal{V}_{iiii} = \frac{1}{2}(U_i + \sum_{\mathbf{p}\neq\mathbf{0}} V_{iiii}^{\mathbf{0p0p}}), \tag{5.18}$$

$$U_i \equiv V_{iiii}^{\mathbf{0000}}, \tag{5.19}$$

$$V_{iiii}^{\mathbf{0p0p}} \equiv \int\int d\mathbf{r}_1 d\mathbf{r}_2 w_i^*(\mathbf{r}_1)w_i^*(\mathbf{r}_2 - \mathbf{p}L)\frac{e^2}{|\mathbf{r}_1 - \mathbf{r}_2|}w_i(\mathbf{r}_1)w_i(\mathbf{r}_2 - \mathbf{p}L). \tag{5.20}$$

In general, define

$$V_{ikjl}^{\mathbf{npmq}} \equiv \int\int d\mathbf{r}_1 d\mathbf{r}_2 w_i^*(\mathbf{r}_1 - \mathbf{n}L)w_i^*(\mathbf{r}_2 - \mathbf{p}L)\frac{e^2}{|\mathbf{r}_1 - \mathbf{r}_2|}w_i(\mathbf{r}_1 - \mathbf{m}L)w_i(\mathbf{r}_2 - \mathbf{q}L). \tag{5.21}$$

Again, since $w_i(\mathbf{r})$ is a localized function, assume the super-cell box length is larger than the range of $w_i(\mathbf{r})$, we realize

$$T_{ii}^{i\mathbf{p}} = -V_{iiii}^{\mathbf{0p0p}}, \quad (\mathbf{p}\neq\mathbf{0}). \tag{5.22}$$

Eq. (5.22) has a clear physical picture, at a distant range, the electron cloud completely shields the ion, leading to a cancellation of their effects. With Eq. (5.22), the second last term on the right side of Eq. (5.15) could to cancel out the last term on the right side of Eq. (5.18). But there is still a factor of $\frac{1}{2}$ with the interaction term $V_{iiii}^{\mathbf{0p0p}}$ in Eq. (5.6), only half of $T_{ii}^{i\mathbf{p}}$ is canceled out. Fortunately, we have the ion-ion interaction $V_{ij,\mathbf{n}}^{\text{coul}}$ in Eq. (5.6) to compensate the other half:

$$T_{ii}^{i\mathbf{p}} + \frac{1}{2}V_{iiii}^{\mathbf{0p0p}} + \frac{1}{2}V_{ii,\mathbf{p}}^{\text{coul}} = 0, \quad (\mathbf{p}\neq\mathbf{0}). \tag{5.23}$$

The finite coefficients t_{ii} and U_i are used to define the effective tight-binding Hubbard model.

Similarly, decompose $\frac{1}{2}\mathcal{N}\mathcal{V}_{ijij}$ $(i \neq j)$ as

$$\frac{1}{2}\mathcal{N}\mathcal{V}_{ijij} = \frac{1}{2}(V_{ijij}^{\mathbf{0}\boldsymbol{\nu}_{ij}\mathbf{0}\boldsymbol{\nu}_{ij}} + \sum_{\mathbf{p}\neq\boldsymbol{\nu}_{ij}} V_{ijij}^{\mathbf{0p0p}}), \quad (i \neq j) \tag{5.24}$$

the definition of $V_{ijij}^{\mathbf{0p0p}}$ is give in Eq. (5.21), we have

$$T_{ii}^{j\mathbf{p}} = -V_{ijij}^{\mathbf{0p0p}}, \quad (i \neq j, \ \mathbf{p} \neq \boldsymbol{\nu}_{ij}), \tag{5.25}$$

the reasoning and physical picture of this equation is similar to that of Eq. (5.22). Again, there is a factor of $\frac{1}{2}$ with the interaction term $V_{ijij}^{\mathbf{0p0p}}$, the other half is canceled by the ion-ion Coulomb interaction,

$$T_{ii}^{j\mathbf{p}} + \frac{1}{2}V_{ijij}^{\mathbf{0p0p}} + \frac{1}{2}V_{ij,\mathbf{p}}^{\text{coul}} = 0, \quad (i \neq j, \ \mathbf{p} \neq \boldsymbol{\nu}_{ij}). \tag{5.26}$$

What happens if $i \neq j$, $\mathbf{p} = \boldsymbol{\nu}_{ij}$ in Eq. (5.26)? It results in a strong short-range inter-atomic core-core repulsion. At a significant distance between atom i and atom j, the ion-ion interaction is shielded by the ion-electron interaction. Nonetheless, as they approach, the ion begins to penetrate the electron cloud of the other atom. At this point, the screening effect diminishes, and the ion-ion interaction begins to dominate. This phenomenon underpins the short-range core-core repulsion, originating from the breakdown of the screening effect. Based on this picture, we define a pair-wise inter-

atomic repulsive potential

$$\phi_{ij} \equiv T_{ii}^{j\boldsymbol{\nu}_{ij}} + T_{jj}^{i\boldsymbol{\nu}_{ji}} + V_{ijij}^{\mathbf{0}\boldsymbol{\nu}_{ij}\mathbf{0}\boldsymbol{\nu}_{ij}} + V_{ij,\boldsymbol{\nu}_{ij}}^{\text{coul}}, \quad (i \neq j)$$

$$= T_{ii}^{j} + T_{jj}^{i} + V_{ijij} + V_{ij}^{\text{coul}}, \tag{5.27}$$

with the definitions

$$T_{ii}^{j} \equiv T_{ii}^{j\boldsymbol{\nu}_{ij}}, \ V_{ijij} \equiv V_{ijij}^{\mathbf{0}\boldsymbol{\nu}_{ij}\mathbf{0}\boldsymbol{\nu}_{ij}}, \ V_{ij}^{\text{coul}} \equiv V_{ij,\boldsymbol{\nu}_{ij}}^{\text{coul}} \tag{5.28}$$

The definition of ϕ_{ij} in Eq. (5.27) has taken advantage of these relations

$$V_{ijij}^{\mathbf{0}\boldsymbol{\nu}_{ij}\mathbf{0}\boldsymbol{\nu}_{ij}} = V_{jiji}^{\mathbf{0}\boldsymbol{\nu}_{ji}\mathbf{0}\boldsymbol{\nu}_{ji}}, \tag{5.29}$$

$$V_{ij,\boldsymbol{\nu}_{ij}}^{\text{coul}} = V_{ji,\boldsymbol{\nu}_{ji}}^{\text{coul}}, \tag{5.30}$$

but in general $T_{ii}^{j\boldsymbol{\nu}_{ij}} \neq T_{jj}^{i\boldsymbol{\nu}_{ji}}$, since $w_i(\mathbf{r})$ and $w_j(\mathbf{r})$ have different distributions.

Off-site hopping

Similar to the on-site hopping $\mathcal{T}_{ii}$, decompose the off-site hopping $\mathcal{T}_{ij}(i \neq j)$ in Eq. (5.12) as

$$\mathcal{T}_{ij} = t_{ij} + \sum_{k,\mathbf{p} \ (k \neq i \text{ if } \mathbf{p}=\mathbf{0}, \, k \neq j \text{ if } \mathbf{p}=\boldsymbol{\nu}_{ij})} T_{ij}^{k\mathbf{p}}, \quad (i \neq j), \tag{5.31}$$

$$t_{ij} \equiv \int d\mathbf{r} w_i^*(\mathbf{r}) \left[-\frac{\hbar^2}{2m} \nabla_{\mathbf{r}}^2 - \frac{e^2}{|\mathbf{r} - \mathbf{R}_i|} - \frac{e^2}{|\mathbf{r} - \mathbf{R}_j - \boldsymbol{\nu}_{ij}L|} \right] w_j(\mathbf{r} - \boldsymbol{\nu}_{ij}L), \tag{5.32}$$

$$T_{ij}^{k\mathbf{p}} \equiv \int d\mathbf{r} w_i^*(\mathbf{r}) \left[-\frac{e^2}{|\mathbf{r} - \mathbf{R}_k - \mathbf{p}L|} \right] w_j(\mathbf{r} - \boldsymbol{\nu}_{ij}L), \tag{5.33}$$

The finite hopping coefficient t_{ij} considers only the kinetic term and the hopping induced by atom i and atom j, disregarding contribution from other ions. This simplification, known as the two-center approximation [153, 154], allows for a more computationally tractable representation of the system's electronic behavior while retaining essential physics. Many writers on tight-binding models have assumed that three-center integrals, i.e. Eq. (5.33) involving three distinct atoms, were negligible compared to two-center integrals Eq. (5.32). While they are certainly smaller than the two-center integrals, they are not entirely negligible. Especially in the PBC setup, the summation of all three-center integrals blows up $\mathcal{T}_{ij}$. Nevertheless, we will still use the two-center approximation. The justification is that the three-center integrals will be canceled by the interaction terms.

Decompose $\frac{1}{2}\mathcal{N}\,\mathcal{V}_{ikjk}$ as

$$\frac{1}{2}\mathcal{N}\,\mathcal{V}_{ikjk} = \frac{1}{2}\sum_{\mathbf{p}} V_{ikjk}^{\mathbf{0p\nu}_{ij}\mathbf{p}}, \tag{5.34}$$

the definition of $V_{ikjk}^{\mathbf{0p\nu}_{ij}\mathbf{p}}$ is give in Eq. (5.21). Assume the functions $w_i(\mathbf{r})$ are localized, and the super-cell box length is larger than the range of the $w_i(\mathbf{r})$, we have

$$T_{ij}^{k\mathbf{p}} = -V_{ikjk}^{\mathbf{0p\nu}_{ij}\mathbf{p}} = -V_{kikj}^{\mathbf{0},-\mathbf{p},\mathbf{0},(-\mathbf{p})^*_{ij}} \quad (k \neq i \text{ if } \mathbf{p} = \mathbf{0},\, k \neq j \text{ if } \mathbf{p} = \boldsymbol{\nu}_{ij}), \tag{5.35}$$

which gives

$$T_{ij}^{k\mathbf{p}} + \frac{1}{2}V_{ikjk}^{\mathbf{0p\nu}_{ij}\mathbf{p}} + \frac{1}{2}V_{kikj}^{\mathbf{0},-\mathbf{p},\mathbf{0},(-\mathbf{p})^*_{ij}} = 0 \quad (k \neq i \text{ if } \mathbf{p} = \mathbf{0},\, k \neq j \text{ if } \mathbf{p} = \boldsymbol{\nu}_{ij}), \tag{5.36}$$

Then the terms in Eq. (5.34) could cancel with the last term on the right side of Eq. (5.31).

The Hubbard liquid model of hydrogen

With the finite coefficients defined, t_{ii} from Eq. (5.16), t_{ij} from Eq. (5.32), U_i from Eq. (5.19), ϕ_{ij} from Eq. (5.27), we have the effective Hubbard liquid model extracted from Eq. (5.6),

$$
\mathcal{H} = \sum_{ij} \sum_{\alpha} t_{ij} c_{i\alpha}^\dagger c_{j\alpha} + \sum_i U_i \hat{n}_{i\uparrow} \hat{n}_{i\downarrow} + \frac{1}{2} \sum_{i \neq j} \phi_{ij}
$$
$$
- \frac{1}{2} \sum_{i \neq j} \sum_{\alpha} V_{ijij} (\rho_{ij} c_{i\alpha}^\dagger c_{j\alpha} + \rho_{ji} c_{j\alpha}^\dagger c_{i\alpha} - |\rho_{ij,\alpha}|^2) + \sum_{i=1}^{N_a} \frac{\mathbf{P}_i^2}{2M}. \qquad (5.37)
$$

With the definitions

$$
\rho_{ji,\alpha} \equiv \langle c_{i\alpha}^\dagger c_{j\alpha} \rangle, \qquad (5.38)
$$

$$
n_{i,\alpha} \equiv \rho_{ii,\alpha}, \qquad (5.39)
$$

which has the property:

$$
\rho_{ji} = \rho_{ij}^*, \qquad (5.40)
$$

in this work the basis functions are real, we have $\rho_{ji} = \rho_{ij}$.

Moreover, we are working on half-filling and non-magnetic systems,

$$
\rho_{ji} \equiv \rho_{ji,\uparrow} = \rho_{ji,\downarrow}, \qquad (5.41)
$$

$$
n_i \equiv n_{i,\uparrow} = n_{i,\downarrow}. \qquad (5.42)
$$

In obtaining Eq. (5.37), we applied a Hartree-Fock mean-field method on the inter-

action terms $V_{ijij}c_i^\dagger c_j^\dagger c_j^\dagger c_i^\dagger$ $(i \neq j)$ and assumed the charge density $\langle \hat{n}_{i\alpha} \rangle = 0.5$. These approximations enable the cancellations based on Eq. (5.23), Eq. (5.26), Eq. (5.36) to be valid, since the system's energy not only depends on the tight-binding coefficients but also on the charge density matrix ρ_{ij}.

For example, the energy associated with Eq. (5.26) in the HF mean-field method is

$$\sum_\alpha T_{ii}^{j\mathbf{p}} n_i + \sum_{\alpha\beta} \frac{1}{2} V_{ijij}^{\mathbf{0p0p}} (\frac{1}{2} n_i n_j - |\rho_{ij}|^2) + \frac{1}{2} V_{ij,\mathbf{p}}^{\text{coul}}, \quad (i \neq j, \; \mathbf{p} \neq \boldsymbol{\nu}_{ij}), \qquad (5.43)$$

where the spin summation α, β gives a factor of 2 for the first term and a factor of 4 for the second term. Assume $n_i = n_j = 0.5$, Eq. (5.43) equals

$$-\sum_{\alpha\beta} \frac{1}{2} V_{ijij}^{\mathbf{0p0p}} |\rho_{ij}|^2, \qquad (5.44)$$

which is just the exchange energy in the HF method, all other terms cancel out thanks to Eq. (5.26). This exchange energy gives rise to the last term in Eq. (5.37). Note in this work, when solving for the wave function, we only optimize the Hubbard model, i.e. hopping term t_{ij} and on-site interaction U_i term, in Eq. (5.37).

There are other terms in $\frac{1}{2} \sum_{ijkl} \mathcal{N} \mathcal{V}_{ijkl}$ that are not used, e.g. the four-center integrals, we will neglect those in this work. With these formulations and approximations discussed, eventually we get Eq. (5.37). The last question that remains is how to construct the orthogonal basis functions and obtain the tigh-binding coefficients? We construct the basis functions with the Slater-type orbitals (STOs) in this work, the formulations and their derivatives with respect to the atomic positions are presented in appendix A. Another possibility is to use the Wannier functions constructed from the band structures of the DFT-LDA computation, but we shall not discuss this method
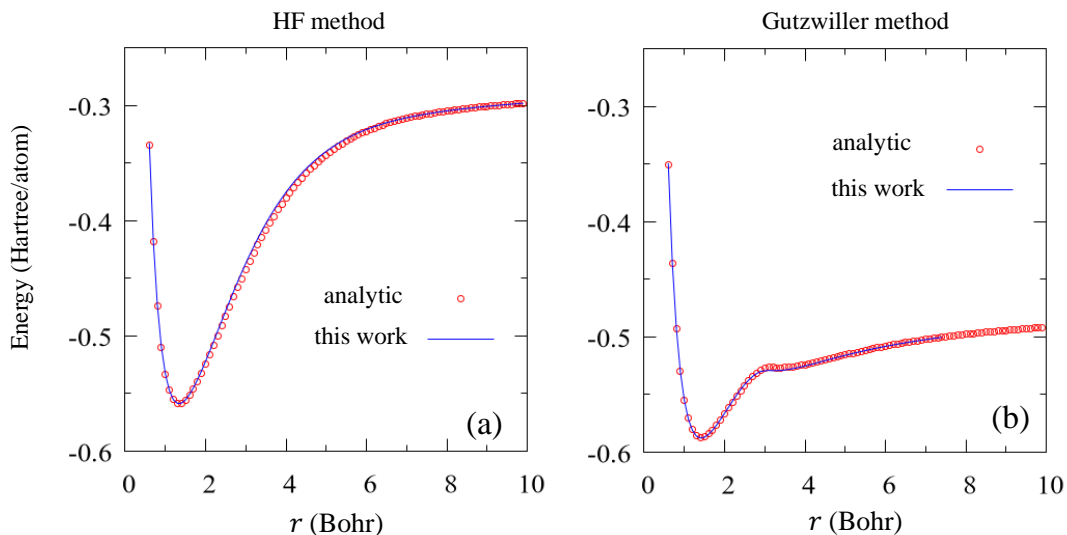
Figure 5.2: Energy binding curves of the H_2 molecule of different methods, x-axis is the distance of the two hydrogen atoms and y-axis is the energy per atom. (a) HF method, the red circle is the analytic result from [155], the blue line is our result from the Hamiltonian Eq. (5.37) with numerical SCF solution. (b) Gutzwiller method, the red circle is the analytic result from [155], the blue line is our result from the Hamiltonian Eq. (5.37) with numerical SCF solution.

extensively here, interested readers are encouraged to refer to these papers [132, 133, 134, 135, 64].

5.2 Benchmarks of the ab initio tight-binding model

Binding energy curve of the H_2 molecule

This work [155] gives the analytic solutions of the H_2 molecule for various methods. This provides an important benchmark for our constructed tight-binding Hamiltonian Eq. (5.37). In our PBC Hamiltonian, the H_2 molecule can be computed by setting a very large super-cell size and placing two atoms in the super-cell. Fig. 5.2 shows the energy binding curves of different methods, with a comparison of the analytic result

and our result that is obtained from the Hamiltonian Eq. (5.37) with a numerical self-consistent field (SCF) solution. Fig. 5.2(a) shows the HF method results, the red circles show the analytic solution in [155], the blue line shows the numerical solution of our constructed Hamiltonian Eq. (5.37). Similarly, Fig. 5.2(b) shows the Gutzwiller method results, the red circles show the analytic solution in [155], the blue line shows the numerical solution of our constructed Hamiltonian Eq. (5.37). Fig. 5.2 also shows in the strong correlation limit, i.e. at large inter-atomic distance r, the HF result deviates significantly from the Gutzwiller result.

Force benchmark, total energy in MD simulation

The forces are computed from the derivatives of the tight-binding coefficients given in appendix A.4. These are sophisticated formulas. To ensure the implementation of the forces is accurate, we plot the system's total energy over time. Of course, the SCF method always has some convergence error. To eliminate the error from the SCF solver, we only minimize the first term $\sum_{ij} \sum_{\alpha} t_{ij} c_{i\alpha}^{\dagger} c_{j\alpha}$ in the Hamiltonian Eq. (5.37), i.e. diagonalize the t_{ij} matrix just once without SCF computations. Moreover, the double occupancies d_i is fixed at 0.25 on all atoms, the charge density n_i is fixed at 0.5 on all atoms when computing the inter-atomic potential ϕ_{ij}, and the exchange energy in Eq. (5.37) is not included in this benchmark simulation.

Fig. 5.3 shows the system's electronic energy, atomic kinetic energy and total energy versus time. Initially, 10 atoms are randomly positioned in a super-cell of side length 16 Bohr, the system's total energy is shown to be conservative throughout. Of course, the Langevin noise is turned off in this simulation. Fig. 5.3 verifies the force is conservative and our implementation is accurate.
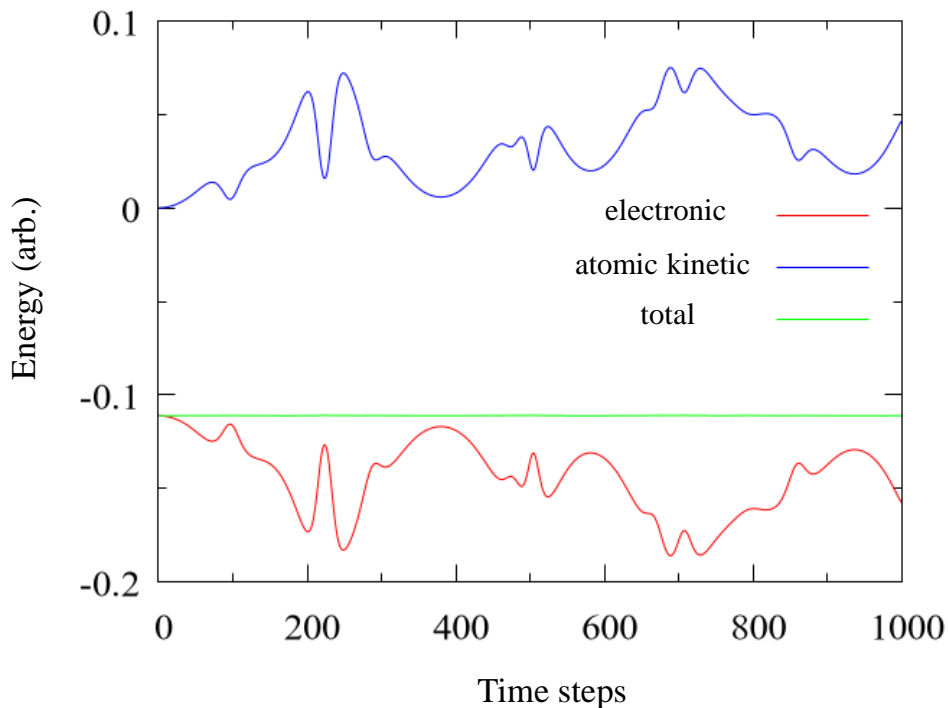
Figure 5.3: The system's electronic energy (red line), atomic kinetic energy (blue line) and total energy (green line) versus time. Initially, 10 atoms are randomly placed in a super-cell of side length 16 Bohr. The Langevin dynamics was turned off in the simulation.

5.3   Simulation results of dense hydrogen

To investigate the liquid-liquid transition between the molecular and atomic fluids in dense hydrogen. We perform NVT simulations at different densities, observing the occurrence of a liquid-liquid transition as the system is compressed. The number of atoms is set as $N = 64$, the density is determined by the Wigner-Seitz radius

$$r_s = (3V/4\pi N)^{1/3}. \tag{5.45}$$

The temperature T is controlled by the Langevin thermostat with a small damping. The simulation time is ~ 1 picosecond, long enough to reach equilibrium and gather
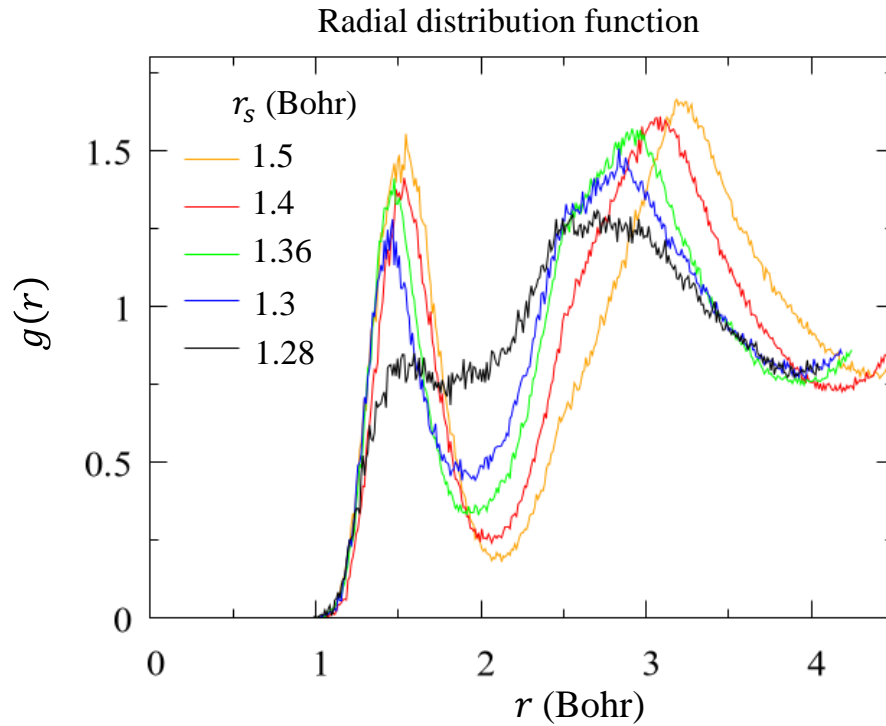
Radial distribution function

Figure 5.4: The radial distribution function $g(r)$ at various densities specified by the Wigner-Seitz radius r_s. The definition of $g(r)$ is given in Eq. (3.2). The system temperature is $T = 2600$ K.

sufficient data thereafter.

To identify the liquid-liquid transition, we simulate at different densities with the same temperature. Fig. 5.4 shows the radial distribution functions $g(r)$ of different densities from $r_s = 1.5$ Bohr to $r_s = 1.28$ Bohr, the temperature is set at $T = 2600$ K. At the lower densities, the g(r) exhibits a prominent peak slightly above 1.4 Bohr, which coincides with the molecular bond length of H_2. At room temperature, this bond length is approximately 1.4 Bohr. However, at higher temperatures, it is expected to be slightly longer due to thermal expansion. With increasing density, the prominence of the molecular peak diminishes, indicating the gradual dissociation of H2 molecules. This transition signifies the transformation of hydrogen into a monatomic liquid state.
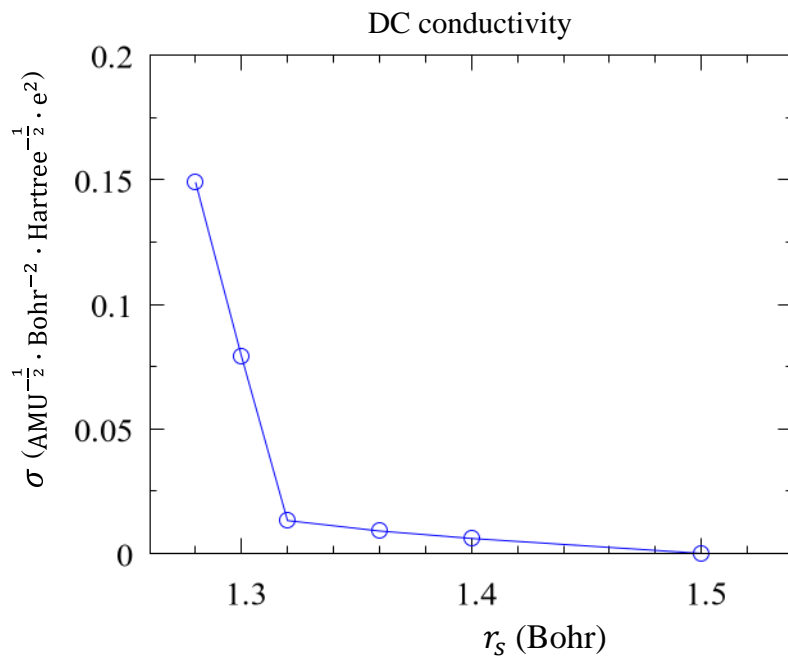
Figure 5.5: The DC conductivity σ versus the system density. In the unit of σ, AMU is the atomic mass unit, e is the elementary charge. The system temperature is $T = 2600$ K.

The direct current conductivity is evaluated across various densities, with the results depicted in Fig. 5.5 showcasing conductivity plotted against r_s. The formulas we use to compute the DC conductivity is given in section 3.1. Notably, as density rises from $r_s = 1.5$ Bohr, the conductivity increases by a few orders of magnitude. This observed behaviour indicates a metal-insulator transition in hydrogen.

The density of states at different atomic densities are shown in Fig. 5.6 At the molecular end, there is a large gap between the bonding states and anti-bonding states, this is responsible for high resistivity. As the density increases, the molecular H_2 gradually dissociates, the distinction between bonding and anti-bonding states becomes less defined, thus the energy gap narrows, resulting in an amplified conductivity.

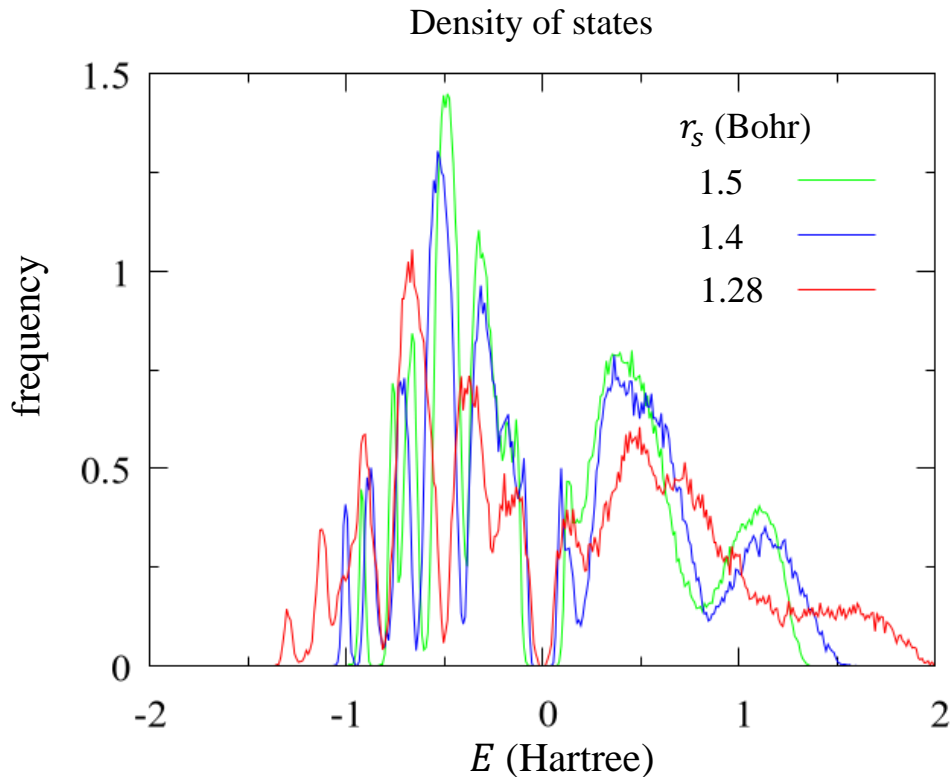The molecular dissociation offers a convincing explanation for the observed band

Density of states

Figure 5.6: The density of states at various densities specified by the Wigner-Seitz radius r_s. The energy spectrum is set to be 0 at the system's chemical potential. The system temperature is $T = 2600$ K, $k_B T = 0.00823$ Hartree.

narrowing in the liquid-liquid transition. However, it's also essential to investigate whether electron correlation influences this process. Fig. 5.7 shows the average double occupancy and renormalization factor at different densities in the GMD simulations. The results show the renormalization factor $\langle \mathcal{R}^2 \rangle$ is close to 1 and the double occupancy is significantly lower from 0.25, suggesting that the system is not strongly correlated. Despite the double occupancy and renormalization factor showing weak dependence on density, there is a slight increase observed as density rises. This is anticipated because as hydrogen atoms get closer, the hopping becomes stronger, leading to a decrease in electron correlation.
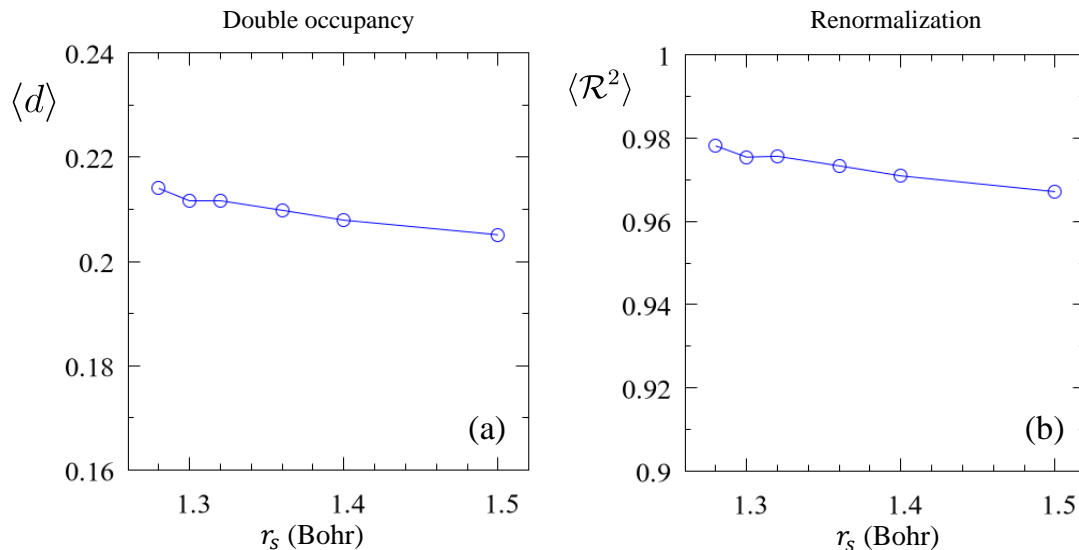
Figure 5.7: The average double occupancy $\langle d \rangle$ and (b) the average renormalization factor $\langle \mathcal{R}^2 \rangle$ versus the system density, where $\langle ... \rangle$ denotes both quantum and ensemble averages in MD simulations. The system temperature is $T = 2600$ K.

5.4   Summary

We developed an ab initio tight-binding Hubbard model using local STO-3G orbitals to describe liquid hydrogen. Employing the GMD, we simulated the liquid-liquid transition in dense hydrogen, during which a metal-insulator transition is observed. We attribute this MIT to the narrowing of the band gap between the bonding and anti-bonding states, stemming from the dissociation of H_2 molecules. Investigation into the double occupancy across various densities under study revealed that the system does not exhibit strong correlation effects.

Appendices

Appendix A

Basis functions and tight-binding coefficients, and derivatives

The orthogonal basis functions used in chapter 5 are built from the linear combination of atomic orbitals (LCAO). There are two types of functions commonly used for atomic functions, the Slater-type orbitals (STOs) and Gaussian-type orbitals (GTOs) [156]. A $1s$ STO has the form

$$\phi_\zeta(\mathbf{r}) = (\zeta^3/\pi)^{1/2} e^{-\zeta|\mathbf{r}|}, \tag{A.1}$$

A $1s$ GTO has the form

$$g_\alpha(\mathbf{r}) = (2\alpha/\pi)^{3/4} e^{-\alpha|\mathbf{r}|^2}, \tag{A.2}$$

where ζ is the Slater orbital exponent, α is the Gaussian orbital exponent. The major differences between the two functions occur at $r = 0$ and large r. At $r = 0$, the STO has a finite slope, whereas the GTO has a zero slope. At large r, the GTO decays much faster than the STO.

For electronic wave function calculations, the STO is usually preferred. Since at large distance molecular orbitals decay as $\sim e^{\zeta r}$, and STOs usually yield better results than GTOs for the same number of basis functions. The advantage of GTOs is that the

integrals are analytic, thus much more efficient than the STOs. One is faced with a dilemma here. A compromise is to emulate an STO with linear combinations of GTOs of different exponents, this approach is widely used in the quantum chemistry community. These bases are denoted as STO-LG, where $L = 1, 2, 3\ldots$ denotes how many Gaussians are used to emulate an STO.

A popular choice is STO-3G [156], which is presented in section A.2. In this work, only $1s$ orbitals are used for hydrogens. Section A.1 gives the GTO integrals and their derivatives with respect to the atomic positions. Section A.3 introduces the Löwdin orthogonalization method. Section A.4 gives the tight-binding coefficients in the orthogonal basis functions constructed from the STOs and Löwdin orthogonalization, and their derivatives with respect to the atomic positions.

A.1 Gaussian-type orbitals

A normalized $1s$ primitive Gaussian-type orbital (GTO) is

$$g_\alpha(\mathbf{r}) = (2\alpha/\pi)^{3/4} e^{-\alpha|\mathbf{r}|^2}, \tag{A.3}$$

where α is the orbital exponent, the center is at $\mathbf{r} = \mathbf{0}$. The following integrals involves four different GTOs centering at $\mathbf{R}_A, \mathbf{R}_B, \mathbf{R}_C, \mathbf{R}_D$, with corresponding ex-

ponents $\alpha, \beta, \gamma, \delta$, we simply denote them as A, B, C, D.

$$(A|B) = \int d\mathbf{r}\, g_\alpha^*(\mathbf{r} - \mathbf{R}_A) g_\beta(\mathbf{r} - \mathbf{R}_B), \tag{A.4a}$$

$$(A| - \frac{1}{2}\nabla^2|B) = \int d\mathbf{r}\, g_\alpha^*(\mathbf{r} - \mathbf{R}_A)(-\frac{1}{2}\nabla^2) g_\beta(\mathbf{r} - \mathbf{R}_B), \tag{A.4b}$$

$$(A| - \frac{1}{|r - \mathbf{R}_C|}|B) = \int d\mathbf{r}\, g_\alpha^*(\mathbf{r} - \mathbf{R}_A)(-\frac{1}{|\mathbf{r} - \mathbf{R}_C|}) g_\beta(\mathbf{r} - \mathbf{R}_B), \tag{A.4c}$$

$$(AB|CD) = \int d\mathbf{r}_1 \mathbf{r}_2\, g_\alpha^*(\mathbf{r}_1 - \mathbf{R}_A) g_\beta^*(\mathbf{r}_1 - \mathbf{R}_B) \frac{1}{|\mathbf{r}_1 - \mathbf{r}_2|} g_\gamma(\mathbf{r}_2 - \mathbf{R}_C) g_\delta(\mathbf{r}_2 - \mathbf{R}_D), \tag{A.4d}$$

where the electron charge is set as $e = 1$.

Define

$$\mathbf{R}_P \equiv (\alpha \mathbf{R}_A + \beta \mathbf{R}_B)/(\alpha + \beta), \tag{A.5a}$$

$$\mathbf{R}_Q \equiv (\gamma \mathbf{R}_C + \delta \mathbf{R}_D)/(\gamma + \delta), \tag{A.5b}$$

$$F_0(t) \equiv \frac{\sqrt{\pi}}{2} \frac{1}{\sqrt{t}}\, \mathrm{erf}(\sqrt{t}) = \frac{1}{\sqrt{t}} \int_0^{\sqrt{t}} dx\, e^{-x^2}, \tag{A.5c}$$

where erf() is the error function, $F_0(t)$ has the property

$$\lim_{t \to 0} F_0(t) = 1. \tag{A.6}$$

The normalized GTO integrals are [156],

$$(A|B) = (\alpha\beta)^{3/4}[2/(\alpha+\beta)]^{3/2}\exp[-\frac{\alpha\beta}{\alpha+\beta}|\mathbf{R}_A - \mathbf{R}_B|^2], \tag{A.7a}$$

$$(A| - \frac{1}{2}\nabla^2|B) = \frac{\alpha\beta}{\alpha+\beta}[3 - 2\frac{\alpha\beta}{\alpha+\beta}|\mathbf{R}_A - \mathbf{R}_B|^2](A|B), \tag{A.7b}$$

$$(A| - \frac{1}{|r - \mathbf{R}_C|}|B) = -\frac{2}{\sqrt{\pi}}\frac{(4\alpha\beta)^{3/4}}{(\alpha+\beta)}\exp[-\frac{\alpha\beta}{\alpha+\beta}|\mathbf{R}_A - \mathbf{R}_B|^2] \times F_0[(\alpha+\beta)|\mathbf{R}_P - \mathbf{R}_C|^2], \tag{A.7c}$$

$$(AB|CD) = \frac{16}{\pi^{1/2}}\frac{(\alpha\beta\gamma\delta)^{3/4}}{(\alpha+\beta)(\gamma+\delta)(\alpha+\beta+\gamma+\delta)^{1/2}} \times \exp[-\frac{\alpha\beta}{\alpha+\beta}|\mathbf{R}_A - \mathbf{R}_B|^2$$

$$-\frac{\gamma\delta}{\gamma+\delta}|\mathbf{R}_C - \mathbf{R}_D|^2] \times F_0[\frac{(\alpha+\beta)(\gamma+\delta)}{\alpha+\beta+\gamma+\delta}|\mathbf{R}_P - \mathbf{R}_Q|^2]. \tag{A.7d}$$

Where the integral $(AB|CD)$ is in the chemists' notation,

$$(AB|CD) = \int\int d\mathbf{r}_1 d\mathbf{r}_2 g_\alpha(\mathbf{r}_1 - \mathbf{R}_A)g_\beta(\mathbf{r}_1 - \mathbf{R}_B)\frac{1}{|\mathbf{r}_1 - \mathbf{r}_2|}g_\gamma(\mathbf{r}_2 - \mathbf{R}_C)g_\delta(\mathbf{r}_2 - \mathbf{R}_D), \tag{A.8}$$

it would have been $\langle AC|BD \rangle = (AB|CD)$ in the physists' notation.

The derivatives of the GTO overlap integrals are

$$\frac{\partial(A|B)}{\partial\mathbf{R}_A} = -2\frac{\alpha\beta}{\alpha+\beta}(\mathbf{R}_A - \mathbf{R}_B) \times (A|B), \tag{A.9a}$$

$$\frac{\partial(A|B)}{\partial\mathbf{R}_B} = -\frac{\partial(A|B)}{\partial\mathbf{R}_A}. \tag{A.9b}$$

For the kinetic term

$$
\frac{\partial(A| - \frac{1}{2}\nabla^2|B)}{\partial \mathbf{R}_A} = -4(\frac{\alpha\beta}{\alpha + \beta})^2(\mathbf{R}_A - \mathbf{R}_B) \times (A|B)
$$

$$
- 2\frac{\alpha\beta}{\alpha + \beta}(\mathbf{R}_A - \mathbf{R}_B) \times (A| - \frac{1}{2}\nabla^2|B), \tag{A.10a}
$$

$$
\frac{\partial(A| - \frac{1}{2}\nabla^2|B)}{\partial \mathbf{R}_B} = -\frac{\partial(A| - \frac{1}{2}\nabla^2|B)}{\partial \mathbf{R}_A}. \tag{A.10b}
$$

For the nuclear-electron interaction

$$
F_1(t) \equiv \frac{\partial F_0(t)}{\partial t} = -\frac{\sqrt{\pi}}{4}t^{-3/2}\,\mathrm{erf}(\sqrt{t}) + \frac{1}{2t}e^{-t} = \frac{1}{2t}(-F_0(t) + e^{-t}), \tag{A.11a}
$$

$$
\frac{\partial(A| - 1/|r - \mathbf{R}_C||B)}{\partial \mathbf{R}_A} = -2\frac{\alpha\beta}{\alpha + \beta}(\mathbf{R}_A - \mathbf{R}_B) \times (A| - \frac{1}{|r - \mathbf{R}_C|}|B)
$$

$$
- \frac{2}{\sqrt{\pi}}\frac{(4\alpha\beta)^{3/4}}{(\alpha + \beta)}\exp[-\frac{\alpha\beta}{\alpha + \beta}|\mathbf{R}_A - \mathbf{R}_B|^2] \times F_1[(\alpha + \beta)|\mathbf{R}_P - \mathbf{R}_C|^2]2\alpha(\mathbf{R}_P - \mathbf{R}_C),
$$

$$
\tag{A.11b}
$$

$$
\frac{\partial(A| - 1/|r - \mathbf{R}_C||B)}{\partial \mathbf{R}_C} = -\frac{2}{\sqrt{\pi}}\frac{(4\alpha\beta)^{3/4}}{(\alpha + \beta)}\exp[-\frac{\alpha\beta}{\alpha + \beta}|\mathbf{R}_A - \mathbf{R}_B|^2]
$$

$$
\times F_1[(\alpha + \beta)|\mathbf{R}_P - \mathbf{R}_C|^2]2(\alpha + \beta)(\mathbf{R}_C - \mathbf{R}_P), \tag{A.11c}
$$

we have

$$
\lim_{t \to 0} F_1(t) = -\frac{1}{3}. \tag{A.12}
$$

$\frac{\partial(A| - 1/|r - \mathbf{R}_C||B)}{\partial \mathbf{R}_B}$ can be obtained by the symmetry

$$
\frac{\partial(A| - 1/|r - \mathbf{R}_C||B)}{\partial \mathbf{R}_A} = \frac{\partial(B| - 1/|r - \mathbf{R}_C||A)}{\partial \mathbf{R}_A}, \tag{A.13}
$$

expand the left side with Eq. (A.11b) and swap the symbol "A" with "B", "α" with "β" throughout the equation.

For the electron-electron interaction

$$\frac{\partial(AB|CD)}{\partial \mathbf{R}_A} = -2\frac{\alpha\beta}{\alpha+\beta}(\mathbf{R}_A - \mathbf{R}_B) \times (AB|CD) + \frac{16}{\pi^{1/2}}\frac{(\alpha\beta\gamma\delta)^{3/4}}{(\alpha+\beta)(\gamma+\delta)(\alpha+\beta+\gamma+\delta)^{1/2}}$$

$$\times \exp[-\frac{\alpha\beta}{\alpha+\beta}|\mathbf{R}_A - \mathbf{R}_B|^2 - \frac{\gamma\delta}{\gamma+\delta}|\mathbf{R}_C - \mathbf{R}_D|^2] \times F_1\left[\frac{(\alpha+\beta)(\gamma+\delta)}{\alpha+\beta+\gamma+\delta}|\mathbf{R}_P - \mathbf{R}_Q|^2\right]$$

$$\times \frac{2\alpha(\gamma+\delta)}{\alpha+\beta+\gamma+\delta}(\mathbf{R}_P - \mathbf{R}_Q), \tag{A.14}$$

the derivative with respect to other atoms can be obtained with the symmetries

$$\frac{\partial(AB|CD)}{\partial \mathbf{R}_A} = \frac{\partial(BA|CD)}{\partial \mathbf{R}_A} = \frac{\partial(CD|AB)}{\partial \mathbf{R}_A} = \frac{\partial(CD|BA)}{\partial \mathbf{R}_A}, \tag{A.15}$$

and similarly swap corresponding symbols in a manner that is demonstrated on Eq. (A.13).

A.2 STO-3G

Denote the $1s$ STOs as $\phi_1, \phi_2, ..., \phi_i$ represents the orbital centered at the i-th atom. In the STO-3G basis,

$$\phi_i = d_1\, g_{i1} + d_2\, g_{i2} + d_3\, g_{i3}, \tag{A.16}$$

g_{i1}, g_{i2}, g_{i3} are the three GTOs used to construct ϕ_i with exponents $0.109818\zeta^2$, $0.405771\zeta^2$, $2.22766\zeta^2$. The standard value of the orbital exponent ζ for hydrogen is $\zeta = 1.24$ [156], we use this value in this work. $\{d_1, d_2, d_3\} = \{0.444635, 0.535328, 0.154326\}$

are the GTO coefficients in STO-3G.

The STO integrals are given by the GTO integrals

$$(\phi_i|\phi_j) = \sum_{ab=1}^{3} d_a d_b (g_{ia}|g_{jb}), \tag{A.17a}$$

$$(\phi_i| - \frac{1}{2}\nabla^2|\phi_i) = \sum_{ab=1}^{3} d_a d_b (g_{ia}| - \frac{1}{2}\nabla^2|g_{jb}), \tag{A.17b}$$

$$(\phi_i| - \frac{1}{|r - \mathbf{R}_C|}|\phi_i) = \sum_{ab=1}^{3} d_a d_b (g_{ia}| - \frac{1}{|r - \mathbf{R}_C|}|g_{jb}), \tag{A.17c}$$

$$(\phi_i\phi_j|\phi_k\phi_l) = \sum_{abcd=1}^{3} d_a d_b d_c d_d (g_{ia}g_{jb}|g_{kc}g_{ld}). \tag{A.17d}$$

A.3 Löwdin orthogonalization

The Löwdin orthogonalization method is a symmetric orthogonalization (as opposed to the Schmidt orthogonalization), it treats all the wave functions on an equal footing [157]. An important feature of the Löwdin orthogonalization is that it ensures

$$\sum_i |\phi_i - \phi_i'|^2 = \text{minimum}, \tag{A.18}$$

where ϕ_i is the original vector, ϕ_i' is the vector obtained from Löwdin Orthogonalization. This means the symmetrically orthogonalized vectors ϕ_i' are the least distant in the Hilbert space from the original vector ϕ_i, it is the gentlest push on the vectors to get them orthogonal [158].

Formulas

For a set of normalized but non-orthogonal vectors $\boldsymbol{\phi} = [\phi_1 \ \phi_2 \ ...]^T$. Define S as the overlap matrix with elements $S_{ij} = \langle \phi_i | \phi_j \rangle$, U is the unitary matrix that diagonalize S,

$$S_{\text{diag}} = U^\dagger S U. \tag{A.19}$$

Since S is a Gram matrix, its eigenvalues are always positive, we define $S_{\text{diag}}^{\frac{1}{2}}$ as the matrix that S_{diag} replacing all its diagonal elements by their square roots. Define

$$S^{\frac{1}{2}} \equiv U S_{\text{diag}}^{\frac{1}{2}} U^\dagger, \tag{A.20}$$

$$S^{-\frac{1}{2}} \equiv (S^{\frac{1}{2}})^{-1} = U S_{\text{diag}}^{-\frac{1}{2}} U^\dagger, \tag{A.21}$$

$S^{-\frac{1}{2}}$ is the transformation matrix that symmetrically orthogonalize $\boldsymbol{\phi}$:

$$\boldsymbol{\phi}' = S^{-\frac{1}{2}} \boldsymbol{\phi}, \tag{A.22}$$

$\boldsymbol{\phi}'$ is the set of ortho-normal vectors obtained from Löwdin orthogonalization. Note $S^{-\frac{1}{2}}$ is symmetric [157],

$$(S^{-\frac{1}{2}})_{ij} = (S^{-\frac{1}{2}})_{ji}. \tag{A.23}$$

Derivatives

To our purpose, we also compute the derivative of the Löwdin transformation matrix $S^{-\frac{1}{2}}$ [159],

$$\frac{\partial (S^{-1/2})_{ij}}{\partial \mathbf{R}_X} = \sum_{pq} \frac{-T_{ip} S^X_{pq} T_{jq}}{s_p^{1/2} s_q^{1/2} (s_p^{1/2} + s_q^{1/2})}, \tag{A.24}$$

where

$$S^X_{pq} \equiv \sum_{mn} T_{mp} \frac{\partial S_{mn}}{\partial \mathbf{R}_X} T_{nq}, \tag{A.25}$$

s_p are eigenvalues and the matrix T are the eigenvectors of the overlap matrix S. Note, S^X_{pq} is symmetric $S^X_{pq} = S^X_{qp}$.

Plug in

$$\frac{\partial S_{mn}}{\partial \mathbf{R}_X} = \frac{\partial S_{mn}}{\partial \mathbf{R}_m} \frac{\partial \mathbf{R}_m}{\partial \mathbf{R}_X} + \frac{\partial S_{mn}}{\partial \mathbf{R}_n} \frac{\partial \mathbf{R}_n}{\partial \mathbf{R}_X} = \frac{\partial S_{Xn}}{\partial \mathbf{R}_X} \delta_{mX} + \frac{\partial S_{mX}}{\partial \mathbf{R}_X} \delta_{nX}, \tag{A.26}$$

we have

$$\begin{aligned}
S^X_{pq} &= \sum_{mn} T_{mp} \frac{\partial S_{mn}}{\partial \mathbf{R}_X} T_{nq} \\
&= \sum_{n} T_{Xp} \frac{\partial S_{Xn}}{\partial \mathbf{R}_X} T_{nq} + \sum_{m} T_{mp} \frac{\partial S_{mX}}{\partial \mathbf{R}_X} T_{Xq} \\
&= \sum_{n} T_{Xp} \frac{\partial S_{Xn}}{\partial \mathbf{R}_X} T_{nq} + \sum_{n} T_{np} \frac{\partial S_{nX}}{\partial \mathbf{R}_X} T_{Xq} \\
&= \sum_{n} \frac{\partial S_{Xn}}{\partial \mathbf{R}_X} (T_{Xp} T_{nq} + T_{np} T_{Xq}),
\end{aligned} \tag{A.27}$$

where we changed the dummy variable $m \to n$, and in the last step we used

$$\frac{\partial S_{Xn}}{\partial \mathbf{R}_X} = \frac{\partial S_{nX}}{\partial \mathbf{R}_X}, \tag{A.28}$$

since the wave functions are real in this work.

A.4   The tight-binding coefficients

The Bloch-like wave functions in a cubic super-cell lattice are

$$\tilde{\phi}_i(\mathbf{r}) = \frac{1}{\sqrt{\mathcal{N}}} \sum_{\mathbf{n}} \phi_i(\mathbf{r} - \mathbf{n}L), \tag{A.29}$$

where $\mathcal{N}$ is the number of super-cells, L is the box length, $\mathbf{n}$ iterates through all super-cells. $\phi_i(\mathbf{r})$ is the normalized STO centered at the i-th atom. Apply the Löwdin orthogonalization to Eq. (A.29), and assume the Löwdin transformation matrix is $\mathbf{L}$, which is the $S^{-\frac{1}{2}}$ matrix in section A.3. We have the ortho-normal basis functions:

$$\tilde{w}_i(\mathbf{r}) = \sum_j \tilde{\phi}_j(\mathbf{r}) L_{ji}. \tag{A.30}$$

The local functions can be chosen as

$$w_i(\mathbf{r}) = \sum_j \phi_j(\mathbf{r}) L_{ji}. \tag{A.31}$$

or alternatively,

$$w_i(\mathbf{r}) = \sum_j \phi_j(\mathbf{r} - \boldsymbol{\nu}_{ij}) L_{ji}, \tag{A.32}$$

where ν_{ij} is defined in Eq. (5.11). They both satisfy

$$\tilde{w}_i(\mathbf{r}) = \frac{1}{\sqrt{\mathcal{N}}} \sum_{\mathbf{n}} w_i(\mathbf{r} - \mathbf{n}L), \tag{A.33}$$

here we choose Eq. (A.32) as the definition because it is more localized than Eq. (A.31).

A.4.1 Hopping terms

Define the simplified symbols

$$K \equiv -\frac{1}{2}\nabla^2, \tag{A.34}$$

$$V_{\text{ion}}(\mathbf{R}_i) \equiv -\frac{1}{|\mathbf{r} - \mathbf{R}_i|}. \tag{A.35}$$

For off-site terms $i \neq j$,

$$t_{ij} = \langle w_i(\mathbf{r})|K + V_{\text{ion}}(\mathbf{R}_i) + V_{\text{ion}}(\mathbf{R}_j + \boldsymbol{\nu}_{ij})L|w_j(\mathbf{r} - \boldsymbol{\nu}_{ij})\rangle$$

$$= \sum_{mn} L_{mi}L_{nj}\langle \phi_m(\mathbf{r} - \boldsymbol{\nu}_{im})|K + V_{\text{ion}}(\mathbf{R}_i) + V_{\text{ion}}(\mathbf{R}_j + \boldsymbol{\nu}_{ij})L|\phi_n(\mathbf{r} - \boldsymbol{\nu}_{ij} - \boldsymbol{\nu}_{jn})\rangle, \tag{A.36}$$

To simplify the notation, define

$$\langle \phi_m|T(ij)|\phi_n\rangle \equiv \langle \phi_m(\mathbf{r} - \boldsymbol{\nu}_{im})|K + V_{\text{ion}}(\mathbf{R}_i) + V_{\text{ion}}(\mathbf{R}_j + \boldsymbol{\nu}_{ij})L|\phi_n(\mathbf{r} - \boldsymbol{\nu}_{ij} - \boldsymbol{\nu}_{jn})\rangle, \tag{A.37}$$

we have

$$t_{ij} = \sum_{mn} L_{mi} L_{nj} \langle \phi_m | T(ij) | \phi_n \rangle. \tag{A.38}$$

It has the symmetry property

$$\langle \phi_m | T(ij) | \phi_n \rangle = \langle \phi_m (\mathbf{r} - \boldsymbol{\nu}_{im}) | K + V_{\text{ion}}(\mathbf{R}_i) + V_{\text{ion}}(\mathbf{R}_j + \boldsymbol{\nu}_{ij}) L | \phi_n (\mathbf{r} - \boldsymbol{\nu}_{ij} - \boldsymbol{\nu}_{jn}) \rangle$$

$$= \langle \phi_m (\mathbf{r} + \boldsymbol{\nu}_{ij} - \boldsymbol{\nu}_{im}) | K + V_{\text{ion}}(\mathbf{R}_i - \boldsymbol{\nu}_{ij} L) + V_{\text{ion}}(\mathbf{R}_j) | \phi_n (\mathbf{r} - \boldsymbol{\nu}_{jn}) \rangle$$

$$= \langle \phi_n (\mathbf{r} - \boldsymbol{\nu}_{jn}) | K + V_{\text{ion}}(\mathbf{R}_j) + V_{\text{ion}}(\mathbf{R}_i + \boldsymbol{\nu}_{ji}) L | \phi_m (\mathbf{r} - \boldsymbol{\nu}_{ji} - \boldsymbol{\nu}_{im}) \rangle$$

$$= \langle \phi_n | T(ji) | \phi_m \rangle, \tag{A.39}$$

where we used $\boldsymbol{\nu}_{ij} = -\boldsymbol{\nu}_{ji}$.

The derivative

$$\sum_{ij:i\neq j} \frac{\partial t_{ij}}{\partial \mathbf{R}_X} \rho_{ij} = \sum_{ijmn:i\neq j} L_{mi} L_{nj} \frac{\partial \langle \phi_m | T(ij) | \phi_n \rangle}{\partial \mathbf{R}_X} \rho_{ij} + \sum_{ijmn:i\neq j} \frac{\partial L_{mi}}{\partial \mathbf{R}_X} L_{nj} \langle \phi_m | T(ij) | \phi_n \rangle \rho_{ij}$$

$$+ \sum_{ijmn:i\neq j} L_{mi} \frac{\partial L_{nj}}{\partial \mathbf{R}_X} \langle \phi_m | T(ij) | \phi_n \rangle \rho_{ij}. \tag{A.40}$$

The first term on the right side of Eq. (A.40) can be simplified, with

$$\frac{\partial \langle \phi_m | T(ij) | \phi_n \rangle}{\partial \mathbf{R}_X}$$

$$= \frac{\partial \langle \phi_m | T(ij) | \phi_n \rangle}{\partial \mathbf{R}_m} \frac{\partial \mathbf{R}_m}{\partial \mathbf{R}_X} + \frac{\partial \langle \phi_m | T(ij) | \phi_n \rangle}{\partial \mathbf{R}_n} \frac{\partial \mathbf{R}_n}{\partial \mathbf{R}_X} + \frac{\partial \langle \phi_m | T(ij) | \phi_n \rangle}{\partial \mathbf{R}_i} \frac{\partial \mathbf{R}_i}{\partial \mathbf{R}_X} + \frac{\partial \langle \phi_m | T(ij) | \phi_n \rangle}{\partial \mathbf{R}_j} \frac{\partial \mathbf{R}_j}{\partial \mathbf{R}_X}$$

$$= \frac{\partial \langle \phi_m | T(ij) | \phi_n \rangle}{\partial \mathbf{R}_X} \delta_{mX} + \frac{\partial \langle \phi_m | T(ij) | \phi_n \rangle}{\partial \mathbf{R}_X} \delta_{nX} + \frac{\partial \langle \phi_m | T(ij) | \phi_n \rangle}{\partial \mathbf{R}_X} \delta_{iX} + \frac{\partial \langle \phi_m | T(ij) | \phi_n \rangle}{\partial \mathbf{R}_X} \delta_{jX},$$

$$\tag{A.41}$$

we have

$$\sum_{ijmn:i\neq j} L_{mi}L_{nj}\frac{\partial\langle\phi_m|T(ij)|\phi_n\rangle}{\partial\mathbf{R}_X}\rho_{ij}$$

$$= \sum_{ijn:i\neq j} L_{Xi}L_{nj}\frac{\partial\langle\phi_X|T(ij)|\phi_n\rangle}{\partial\mathbf{R}_X}\rho_{ij} + \sum_{ijm:i\neq j} L_{mi}L_{Xj}\frac{\partial\langle\phi_m|T(ij)|\phi_X\rangle}{\partial\mathbf{R}_X}\rho_{ij}$$

$$+ \sum_{jmn:j\neq X} L_{mX}L_{nj}\frac{\partial\langle\phi_m|T(Xj)|\phi_n\rangle}{\partial\mathbf{R}_X}\rho_{Xj} + \sum_{imn:i\neq X} L_{mi}L_{nX}\frac{\partial\langle\phi_m|T(iX)|\phi_n\rangle}{\partial\mathbf{R}_X}\rho_{iX}$$

$$= \sum_{ijn:i\neq j} L_{Xi}L_{nj}\frac{\partial\langle\phi_X|T(ij)|\phi_n\rangle}{\partial\mathbf{R}_X}\rho_{ij} + \sum_{ijn:i\neq j} L_{nj}L_{Xi}\frac{\partial\langle\phi_n|T(ji)|\phi_X\rangle}{\partial\mathbf{R}_X}\rho_{ji}$$

$$+ \sum_{jmn:j\neq X} L_{mX}L_{nj}\frac{\partial\langle\phi_m|T(Xj)|\phi_n\rangle}{\partial\mathbf{R}_X}\rho_{Xj} + \sum_{jmn:j\neq X} L_{nj}L_{mX}\frac{\partial\langle\phi_n|T(jX)|\phi_m\rangle}{\partial\mathbf{R}_X}\rho_{jX}$$

$$= 2\sum_{ijn:i\neq j} L_{Xi}L_{nj}\frac{\partial\langle\phi_X|T(ij)|\phi_n\rangle}{\partial\mathbf{R}_X}\rho_{ij} + 2\sum_{jmn:j\neq X} L_{mX}L_{nj}\frac{\partial\langle\phi_m|T(Xj)|\phi_n\rangle}{\partial\mathbf{R}_X}\rho_{Xj}, \qquad (A.42)$$

where we changed dummy variables in the second step, and the last step used the symmetry property

$$\frac{\partial\langle\phi_X|T(ij)|\phi_n\rangle}{\partial\mathbf{R}_X} = \frac{\partial\langle\phi_n|T(ji)|\phi_X\rangle}{\partial\mathbf{R}_X}. \qquad (A.43)$$

The last two terms on the right side of Eq. (A.40) can be proven equal:

$$\sum_{ijmn:i\neq j} L_{mi}\frac{\partial L_{nj}}{\partial\mathbf{R}_X}\langle\phi_m|T(ij)|\phi_n\rangle\rho_{ij} = \sum_{ijmn:i\neq j} L_{nj}\frac{\partial L_{mi}}{\partial\mathbf{R}_X}\langle\phi_n|T(ji)|\phi_m\rangle\rho_{ji}$$

$$= \sum_{ijmn:i\neq j} \frac{\partial L_{mi}}{\partial\mathbf{R}_X}L_{nj}\langle\phi_m|T(ij)|\phi_n\rangle\rho_{ij} \qquad (A.44)$$

in the first step we changed dummy variables $i \to j$, $m \to n$, the second step used Eq. (A.39).

Put Eq. (A.42) and Eq. (A.44) into Eq. (A.40), we get

$$\sum_{ij:i\neq j}\frac{\partial t_{ij}}{\partial \mathbf{R}_X}\rho_{ij} = 2\sum_{ijn:i\neq j}L_{Xi}L_{nj}\frac{\partial \langle \phi_X|T(ij)|\phi_n\rangle}{\partial \mathbf{R}_X}\rho_{ij} + 2\sum_{jmn:j\neq X}L_{mX}L_{nj}\frac{\partial \langle \phi_m|T(Xj)|\phi_n\rangle}{\partial \mathbf{R}_X}\rho_{Xj}$$

$$+ 2\sum_{ijmn:i\neq j}\frac{\partial L_{mi}}{\partial \mathbf{R}_X}L_{nj}\langle \phi_m|T(ij)|\phi_n\rangle\rho_{ij}. \tag{A.45}$$

The computation over all the $\mathbf{R}_X$ in the last term of Eq. (A.45) has $O(N^5)$ time complexity at first glance, but the summation can be re-formulated as

$$2\sum_{ijmn:i\neq j}\frac{\partial L_{mi}}{\partial \mathbf{R}_X}L_{nj}\langle \phi_m|T(ij)|\phi_n\rangle\rho_{ij} = 2\sum_{im}\frac{\partial L_{mi}}{\partial \mathbf{R}_X}\Big(\sum_{jn:j\neq i}L_{nj}\langle \phi_m|T(ij)|\phi_n\rangle\rho_{ij}\Big), \tag{A.46}$$

For a given $\{i, m\}$, this term

$$\sum_{jn:j\neq i}L_{nj}\langle \phi_m|T(ij)|\phi_n\rangle\rho_{ij} \tag{A.47}$$

requires $O(N^2)$ time complexity. Summing over $\{i, m\}$ requires another $O(N^2)$ time complexity, thus the overall time complexity is $O(N^4)$.

For on-site terms t_{ii}

$$t_{ii} = \langle w_i|K + V_{\text{ion}}(\mathbf{R}_i)|w_i\rangle = \sum_{mn}L_{mi}L_{ni}\langle \phi_m(\mathbf{r}-\boldsymbol{\nu}_{im})|K + V_{\text{ion}}(\mathbf{R}_i)|\phi_n(\mathbf{r}-\boldsymbol{\nu}_{in})\rangle, \tag{A.48}$$

define

$$\langle \phi_m|T(i)|\phi_n\rangle \equiv \langle \phi_m(\mathbf{r}-\boldsymbol{\nu}_{im})|K + V_{\text{ion}}(\mathbf{R}_i)|\phi_n(\mathbf{r}-\boldsymbol{\nu}_{in})\rangle, \tag{A.49}$$

we have

$$t_{ii} = \sum_{mn} L_{mi} L_{ni} \langle \phi_m | T(i) | \phi_n \rangle. \tag{A.50}$$

Similar to Eq. (A.39), we can prove the symmetry property

$$\langle \phi_m | T(i) | \phi_n \rangle = \langle \phi_n | T(i) | \phi_m \rangle. \tag{A.51}$$

The derivative

$$\sum_i \frac{\partial t_{ii}}{\partial \mathbf{R}_X} \rho_{ii} = \sum_{imn} L_{mi} L_{ni} \frac{\partial \langle \phi_m | T(i) | \phi_n \rangle}{\partial \mathbf{R}_X} \rho_{ii} + \sum_{imn} \frac{\partial L_{mi}}{\partial \mathbf{R}_X} L_{ni} \langle \phi_m | T(i) | \phi_n \rangle \rho_{ii}$$
$$+ \sum_{imn} \partial L_{mi} \frac{L_{ni}}{\partial \mathbf{R}_X} \langle \phi_m | T(i) | \phi_n \rangle \rho_{ii}. \tag{A.52}$$

The first term on the right side of Eq. (A.40) can be simplified, with

$$\frac{\partial \langle \phi_m | T(i) | \phi_n \rangle}{\partial \mathbf{R}_X} = \frac{\partial \langle \phi_m | T(i) | \phi_n \rangle}{\partial \mathbf{R}_m} \frac{\partial \mathbf{R}_m}{\partial \mathbf{R}_X} + \frac{\partial \langle \phi_m | T(i) | \phi_n \rangle}{\partial \mathbf{R}_n} \frac{\partial \mathbf{R}_n}{\partial \mathbf{R}_X} + \frac{\partial \langle \phi_m | T(i) | \phi_n \rangle}{\partial \mathbf{R}_i} \frac{\partial \mathbf{R}_i}{\partial \mathbf{R}_X}$$
$$= \frac{\partial \langle \phi_m | T(i) | \phi_n \rangle}{\partial \mathbf{R}_X} \delta_{mX} + \frac{\partial \langle \phi_m | T(i) | \phi_n \rangle}{\partial \mathbf{R}_X} \delta_{nX} + \frac{\partial \langle \phi_m | T(i) | \phi_n \rangle}{\partial \mathbf{R}_X} \delta_{iX}, \tag{A.53}$$

we have

$$\sum_{imn} L_{mi} L_{ni} \frac{\partial \langle \phi_m | T(i) | \phi_n \rangle}{\partial \mathbf{R}_X} \rho_{ii}$$

$$= \sum_{in} L_{Xi} L_{ni} \frac{\partial \langle \phi_X | T(i) | \phi_n \rangle}{\partial \mathbf{R}_X} \rho_{ii} + \sum_{im} L_{mi} L_{Xi} \frac{\partial \langle \phi_m | T(i) | \phi_X \rangle}{\partial \mathbf{R}_X} \rho_{ii} + \sum_{mn} L_{mX} L_{nX} \frac{\partial \langle \phi_m | T(X) | \phi_n \rangle}{\partial \mathbf{R}_X} \rho_{XX}$$

$$= \sum_{in} L_{Xi} L_{ni} \frac{\partial \langle \phi_X | T(i) | \phi_n \rangle}{\partial \mathbf{R}_X} \rho_{ii} + \sum_{in} L_{ni} L_{Xi} \frac{\partial \langle \phi_n | T(i) | \phi_X \rangle}{\partial \mathbf{R}_X} \rho_{ii} + \sum_{mn} L_{mX} L_{nX} \frac{\partial \langle \phi_m | T(X) | \phi_n \rangle}{\partial \mathbf{R}_X} \rho_{XX}$$

$$= 2 \sum_{in} L_{Xi} L_{ni} \frac{\partial \langle \phi_X | T(i) | \phi_n \rangle}{\partial \mathbf{R}_X} \rho_{ii} + \sum_{mn} L_{mX} L_{nX} \frac{\partial \langle \phi_m | T(X) | \phi_n \rangle}{\partial \mathbf{R}_X} \rho_{XX}. \tag{A.54}$$

The last two terms on the right side of Eq. (A.52) can also be proven equal, similar

to Eq. (A.44),

$$\sum_{imn} \frac{\partial L_{mi}}{\partial \mathbf{R}_X} L_{ni} \langle \phi_m | T(i) | \phi_n \rangle \rho_{ii} = \sum_{imn} \partial L_{mi} \frac{L_{ni}}{\partial \mathbf{R}_X} \langle \phi_m | T(i) | \phi_n \rangle \rho_{ii}. \quad (A.55)$$

Put Eq. (A.54) and Eq. (A.55) into Eq. (A.52), we get

$$\sum_{i} \frac{\partial t_{ii}}{\partial \mathbf{R}_X} \rho_{ii} = 2 \sum_{in} L_{Xi} L_{ni} \frac{\partial \langle \phi_X | T(i) | \phi_n \rangle}{\partial \mathbf{R}_X} \rho_{ii} + \sum_{mn} L_{mX} L_{nX} \frac{\partial \langle \phi_m | T(X) | \phi_n \rangle}{\partial \mathbf{R}_X} \rho_{XX}$$

$$+ 2 \sum_{imn} \frac{\partial L_{mi}}{\partial \mathbf{R}_X} L_{ni} \langle \phi_m | T(i) | \phi_n \rangle \rho_{ii}. \quad (A.56)$$

The derivative $\sum_{ij} \frac{\partial t_{ij}}{\partial \mathbf{R}_X} \rho_{ij}$ is the combination of Eq. (A.45) and Eq. (A.56),

$$\sum_{ij} \frac{\partial t_{ij}}{\partial \mathbf{R}_X} \rho_{ij} = \sum_{ij:i \neq j} \frac{\partial t_{ij}}{\partial \mathbf{R}_X} \rho_{ij} + \sum_{i} \frac{\partial t_{ii}}{\partial \mathbf{R}_X} \rho_{ii}. \quad (A.57)$$

A.4.2 electron-electron interaction terms

For the interaction terms, we only need to compute the U_i and V_{ijij} terms that are used in our Hubbard liquid model Eq. (5.37). First, the V_{ijij} term

$$V_{ijij} = \langle w_i(\mathbf{r}_1) | \langle w_j(\mathbf{r}_2 - \boldsymbol{\nu}_{ij}) | \frac{1}{|\mathbf{r}_1 - \mathbf{r}_2|} | w_i(\mathbf{r}_1) \rangle | w_j(\mathbf{r}_2 - \boldsymbol{\nu}_{ij}) \rangle$$

$$= \sum_{mnpq} L_{mi} L_{ni} L_{pj} L_{qj} \langle \phi_m(\mathbf{r}_1 - \boldsymbol{\nu}_{im}) | \langle \phi_p(\mathbf{r}_2 - \boldsymbol{\nu}_{ij} - \boldsymbol{\nu}_{jp}) | \frac{1}{|\mathbf{r}_1 - \mathbf{r}_2|} | \phi_n(\mathbf{r}_1 - \boldsymbol{\nu}_{in}) \rangle | \phi_q(\mathbf{r}_2 - \boldsymbol{\nu}_{ij} - \boldsymbol{\nu}_{jq}) \rangle$$

$$= \sum_{mnpq} L_{mi} L_{ni} L_{pj} L_{qj} (\phi_m(\mathbf{r}_1 - \boldsymbol{\nu}_{im}) \phi_n(\mathbf{r}_1 - \boldsymbol{\nu}_{in}) | \phi_p(\mathbf{r}_2 - \boldsymbol{\nu}_{ij} - \boldsymbol{\nu}_{jp}) \phi_q(\mathbf{r}_2 - \boldsymbol{\nu}_{ij} - \boldsymbol{\nu}_{jq}))_{ij}. \quad (A.58)$$

To simplify the notation, define

$$(\phi_m \phi_n | \phi_p \phi_q)_{ij} \equiv (\phi_m(\mathbf{r}_1 - \boldsymbol{\nu}_{im}) \phi_n(\mathbf{r}_1 - \boldsymbol{\nu}_{in}) | \phi_p(\mathbf{r}_2 - \boldsymbol{\nu}_{ij} - \boldsymbol{\nu}_{jp}) \phi_q(\mathbf{r}_2 - \boldsymbol{\nu}_{ij} - \boldsymbol{\nu}_{jq}))_{ij},$$

$$(A.59)$$

we have

$$V_{ijij} = \sum_{mnpq} L_{mi}L_{ni}L_{pj}L_{qj}(\phi_m\phi_n|\phi_p\phi_q)_{ij}. \tag{A.60}$$

We can prove the symmetry property

$$
\begin{aligned}
(\phi_m\phi_n|\phi_p\phi_q)_{ij} &= \langle\phi_m(\mathbf{r}_1 - \boldsymbol{\nu}_{im})|\langle\phi_p(\mathbf{r}_2 - \boldsymbol{\nu}_{ij} - \boldsymbol{\nu}_{jp})|\frac{1}{|\mathbf{r}_1 - \mathbf{r}_2|}|\phi_n(\mathbf{r}_1 - \boldsymbol{\nu}_{in})\rangle|\phi_q(\mathbf{r}_2 - \boldsymbol{\nu}_{ij} - \boldsymbol{\nu}_{jq})\rangle \\
&= \langle\phi_m(\mathbf{r}_1 + \boldsymbol{\nu}_{ij} - \boldsymbol{\nu}_{im})|\langle\phi_p(\mathbf{r}_2 - \boldsymbol{\nu}_{jp})|\frac{1}{|\mathbf{r}_1 - \mathbf{r}_2|}|\phi_n(\mathbf{r}_1 + \boldsymbol{\nu}_{ij} - \boldsymbol{\nu}_{in})\rangle|\phi_q(\mathbf{r}_2 - \boldsymbol{\nu}_{jq})\rangle \\
&= \langle\phi_m(\mathbf{r}_2 + \boldsymbol{\nu}_{ij} - \boldsymbol{\nu}_{im})|\langle\phi_p(\mathbf{r}_1 - \boldsymbol{\nu}_{jp})|\frac{1}{|\mathbf{r}_2 - \mathbf{r}_1|}|\phi_n(\mathbf{r}_2 + \boldsymbol{\nu}_{ij} - \boldsymbol{\nu}_{in})\rangle|\phi_q(\mathbf{r}_1 - \boldsymbol{\nu}_{jq})\rangle \\
&= \langle\phi_p(\mathbf{r}_1 - \boldsymbol{\nu}_{jp})|\langle\phi_m(\mathbf{r}_2 - \boldsymbol{\nu}_{ji} - \boldsymbol{\nu}_{im})|\frac{1}{|\mathbf{r}_1 - \mathbf{r}_2|}|\phi_q(\mathbf{r}_1 - \boldsymbol{\nu}_{jq})\rangle|\phi_n(\mathbf{r}_2 - \boldsymbol{\nu}_{ji} - \boldsymbol{\nu}_{in})\rangle \\
&= (\phi_p\phi_q|\phi_m\phi_n)_{ji}, \tag{A.61}
\end{aligned}
$$

where we swapped dummy variables $\mathbf{r}_1, \mathbf{r}_2$ in the second step, and used $\boldsymbol{\nu}_{ij} = -\boldsymbol{\nu}_{ji}$. Similarly,

$$(\phi_m\phi_n|\phi_p\phi_q)_{ij} = (\phi_n\phi_m|\phi_p\phi_q)_{ij} = (\phi_m\phi_n|\phi_q\phi_p)_{ij}. \tag{A.62}$$

The derivative with $i \neq j$

$$
\begin{aligned}
\sum_{ij:i\neq j}\frac{\partial V_{ijij}}{\partial \mathbf{R}_X} &= \sum_{ijmnpq:i\neq j} L_{mi}L_{ni}L_{pj}L_{qj}\frac{\partial(\phi_m\phi_n|\phi_p\phi_q)}{\partial \mathbf{R}_X} + \sum_{ijmnpq:i\neq j}\frac{\partial L_{mi}}{\partial \mathbf{R}_X}L_{ni}L_{pj}L_{qj}(\phi_m\phi_n|\phi_p\phi_q)_{ij} \\
&+ \sum_{ijmnpq:i\neq j} L_{mi}\frac{\partial L_{ni}}{\partial \mathbf{R}_X}L_{pj}L_{qj}(\phi_m\phi_n|\phi_p\phi_q)_{ij} + \sum_{ijmnpq:i\neq j} L_{mi}L_{ni}\frac{\partial L_{pj}}{\partial \mathbf{R}_X}L_{qj}(\phi_m\phi_n|\phi_p\phi_q)_{ij} \\
&+ \sum_{ijmnpq:i\neq j} L_{mi}L_{ni}L_{pj}\frac{\partial L_{qj}}{\partial \mathbf{R}_X}(\phi_m\phi_n|\phi_p\phi_q)_{ij}. \tag{A.63}
\end{aligned}
$$

The first term on the right side of Eq. (A.63) can be simplified, with

$$\frac{\partial(\phi_m\phi_n|\phi_p\phi_q)_{ij}}{\partial\mathbf{R}_X}$$

$$= \frac{\partial(\phi_m\phi_n|\phi_p\phi_q)_{ij}}{\partial\mathbf{R}_m}\frac{\partial\mathbf{R}_m}{\partial\mathbf{R}_X} + \frac{\partial(\phi_m\phi_n|\phi_p\phi_q)_{ij}}{\partial\mathbf{R}_n}\frac{\partial\mathbf{R}_n}{\partial\mathbf{R}_X} + \frac{\partial(\phi_m\phi_n|\phi_p\phi_q)_{ij}}{\partial\mathbf{R}_p}\frac{\partial\mathbf{R}_p}{\partial\mathbf{R}_X} + \frac{\partial(\phi_m\phi_n|\phi_p\phi_q)_{ij}}{\partial\mathbf{R}_q}\frac{\partial\mathbf{R}_q}{\partial\mathbf{R}_X}$$

$$= \frac{\partial(\phi_m\phi_n|\phi_p\phi_q)_{ij}}{\partial\mathbf{R}_X}\delta_{mX} + \frac{\partial(\phi_m\phi_n|\phi_p\phi_q)_{ij}}{\partial\mathbf{R}_X}\delta_{nX} + \frac{\partial(\phi_m\phi_n|\phi_p\phi_q)_{ij}}{\partial\mathbf{R}_X}\delta_{pX} + \frac{\partial(\phi_m\phi_n|\phi_p\phi_q)_{ij}}{\partial\mathbf{R}_X}\delta_{qX},$$

$$(A.64)$$

we have

$$\sum_{ijmnpq:i\neq j} L_{mi}L_{ni}L_{pj}L_{qj}\frac{\partial(\phi_m\phi_n|\phi_p\phi_q)_{ij}}{\partial\mathbf{R}_X}$$

$$= \sum_{ijnpq:i\neq j} L_{Xi}L_{ni}L_{pj}L_{qj}\frac{\partial(\phi_X\phi_n|\phi_p\phi_q)_{ij}}{\partial\mathbf{R}_X} + \sum_{ijmpq:i\neq j} L_{mi}L_{Xi}L_{pj}L_{qj}\frac{\partial(\phi_m\phi_X|\phi_p\phi_q)_{ij}}{\partial\mathbf{R}_X}$$

$$+ \sum_{ijmnq:i\neq j} L_{mi}L_{ni}L_{Xj}L_{qj}\frac{\partial(\phi_m\phi_n|\phi_X\phi_q)_{ij}}{\partial\mathbf{R}_X} + \sum_{ijmnp:i\neq j} L_{mi}L_{ni}L_{pj}L_{Xj}\frac{\partial(\phi_m\phi_n|\phi_p\phi_X)_{ij}}{\partial\mathbf{R}_X}$$

$$= 4\sum_{ijnpq:i\neq j} L_{Xi}L_{ni}L_{pj}L_{qj}\frac{\partial(\phi_X\phi_n|\phi_p\phi_q)_{ij}}{\partial\mathbf{R}_X}. \qquad (A.65)$$

The last four terms on the right side of Eq. (A.63) can be proven equal with symmetry property, together with Eq. (A.65), Eq. (A.63) is simplified as

$$\sum_{ij:i\neq j}\frac{\partial V_{ijij}}{\partial\mathbf{R}_X} = 4\sum_{ijnpq:i\neq j} L_{Xi}L_{ni}L_{pj}L_{qj}\frac{\partial(\phi_X\phi_n|\phi_p\phi_q)_{ij}}{\partial\mathbf{R}_X} + 4\sum_{ijmnpq:i\neq j}\frac{\partial L_{mi}}{\partial\mathbf{R}_X}L_{ni}L_{pj}L_{qj}(\phi_m\phi_n|\phi_p\phi_q)_{ij}.$$

$$(A.66)$$

For Hubbard U_i, the result is obtained simply by setting $i = j$

$$U_i = \sum_{mnpq} L_{mi}L_{ni}L_{pi}L_{qi}(\phi_m\phi_n|\phi_p\phi_q)_{ii}, \qquad (A.67)$$

$$\sum_i\frac{\partial U_i}{\partial\mathbf{R}_X}d_i = 4\sum_{inpq} L_{Xi}L_{ni}L_{pi}L_{qi}\frac{\partial(\phi_X\phi_n|\phi_p\phi_q)_{ii}}{\partial\mathbf{R}_X}d_i + 4\sum_{imnpq}\frac{\partial L_{mi}}{\partial\mathbf{R}_X}L_{ni}L_{pi}L_{qi}(\phi_m\phi_n|\phi_p\phi_q)_{ii}d_i,$$

$$(A.68)$$

where $d_i = \langle \hat{n}_{i\uparrow} \hat{n}_{i\downarrow} \rangle$ is the double occupancy.

A.4.3   inter-atomic potential

The inter-atomic potential ϕ_{ij} is defined in Eq. (5.27)

$$\phi_{ij} \equiv T_{ii}^{j} + T_{jj}^{i} + V_{ijij} + V_{ij}^{\text{coul}}, \quad (i \neq j)$$

For ion-ion Coulomb interactions

$$V_{ij}^{\text{coul}} = \frac{1}{|\mathbf{R}_i - \mathbf{R}_j - \boldsymbol{\nu}_{ij}L|},$$

$$\frac{\partial V_{ij}^{\text{coul}}}{\partial \mathbf{R}_i} = -\frac{\mathbf{R}_i - \mathbf{R}_j - \boldsymbol{\nu}_{ij}L}{|\mathbf{R}_i - \mathbf{R}_j - \boldsymbol{\nu}_{ij}L|^3}. \tag{A.69}$$

Using

$$\frac{\partial V_{ij}^{\text{coul}}}{\partial \mathbf{R}_X} = \frac{\partial V_{ij}^{\text{coul}}}{\partial \mathbf{R}_i}\frac{\partial \mathbf{R}_i}{\partial \mathbf{R}_X} + \frac{\partial V_{ij}^{\text{coul}}}{\partial \mathbf{R}_j}\frac{\partial \mathbf{R}_j}{\partial \mathbf{R}_X} = \frac{\partial V_{ij}^{\text{coul}}}{\partial \mathbf{R}_i}\delta_{iX} + \frac{\partial V_{ij}^{\text{coul}}}{\partial \mathbf{R}_j}\delta_{jX}, \tag{A.70}$$

we get

$$\sum_{ij:i \neq j} \frac{\partial V_{ij}^{\text{coul}}}{\partial \mathbf{R}_X} = \sum_{ij:i \neq j} \frac{\partial V_{ij}^{\text{coul}}}{\partial \mathbf{R}_i}\delta_{iX} + \sum_{ij:i \neq j} \frac{\partial V_{ij}^{\text{coul}}}{\partial \mathbf{R}_j}\delta_{jX}$$

$$= \sum_{j:j \neq X} \frac{\partial V_{Xj}^{\text{coul}}}{\partial \mathbf{R}_X} + \sum_{i:i \neq X} \frac{\partial V_{iX}^{\text{coul}}}{\partial \mathbf{R}_X}$$

$$= 2 \sum_{j:j \neq X} \frac{\partial V_{Xj}^{\text{coul}}}{\partial \mathbf{R}_X}. \tag{A.71}$$

For the on-site hopping term

$$T_{ii}^{j} = \langle w_i | V_{\mathrm{ion}}(\mathbf{R}_j + \boldsymbol{\nu}_{ij}L)|w_i\rangle$$

$$= \sum_{mn} L_{mi}L_{ni}\langle \phi_m(\mathbf{r} - \boldsymbol{\nu}_{im}L)|V_{\mathrm{ion}}(\mathbf{R}_j + \boldsymbol{\nu}_{ij}L)|\phi_n(\mathbf{r} - \boldsymbol{\nu}_{in}L)\rangle. \tag{A.72}$$

Define

$$\langle \phi_m|V(j)|\phi_n\rangle_i \equiv \langle \phi_m(\mathbf{r} - \boldsymbol{\nu}_{im}L)|V_{\mathrm{ion}}(\mathbf{R}_j + \boldsymbol{\nu}_{ij}L)|\phi_n(\mathbf{r} - \boldsymbol{\nu}_{in}L)\rangle \tag{A.73}$$

we have

$$T_{ii}^{j} = \sum_{mn} L_{mi}L_{ni}\langle \phi_m|V(j)|\phi_n\rangle_i. \tag{A.74}$$

It has the symmetry property

$$\langle \phi_m|V(j)|\phi_n\rangle_i = \langle \phi_n|V(j)|\phi_m\rangle_i. \tag{A.75}$$

The derivative

$$\sum_{ij:i\neq j} \frac{\partial T_{ii}^{j}}{\partial \mathbf{R}_X} = \sum_{mn} L_{mi}L_{ni}\frac{\partial \langle \phi_m|V(j)|\phi_n\rangle_i}{\partial \mathbf{R}_X} + \sum_{ijmn:i\neq j} \frac{\partial L_{mi}}{\partial \mathbf{R}_X}L_{ni}\langle \phi_m|V(j)|\phi_n\rangle_i$$

$$+ \sum_{ijmn:i\neq j} L_{mi}\frac{\partial L_{ni}}{\partial \mathbf{R}_X}\langle \phi_m|V(j)|\phi_n\rangle_i. \tag{A.76}$$

The first term in Eq. (A.76) can be simplified, using

$$\frac{\partial \langle \phi_m | V(j) | \phi_n \rangle_i}{\partial \mathbf{R}_X} = \frac{\partial \langle \phi_m | V(j) | \phi_n \rangle_i}{\partial \mathbf{R}_m} \frac{\partial \mathbf{R}_m}{\partial \mathbf{R}_X} + \frac{\partial \langle \phi_m | V(j) | \phi_n \rangle_i}{\partial \mathbf{R}_n} \frac{\partial \mathbf{R}_n}{\partial \mathbf{R}_X} + \frac{\partial \langle \phi_m | V(j) | \phi_n \rangle_i}{\partial \mathbf{R}_j} \frac{\partial \mathbf{R}_j}{\partial \mathbf{R}_X}$$

$$= \frac{\partial \langle \phi_m | V(j) | \phi_n \rangle_i}{\partial \mathbf{R}_X} \delta_{mX} + \frac{\partial \langle \phi_m | V(j) | \phi_n \rangle_i}{\partial \mathbf{R}_X} \delta_{nX} + \frac{\partial \langle \phi_m | V(j) | \phi_n \rangle_i}{\partial \mathbf{R}_X} \delta_{jX}. \quad \text{(A.77)}$$

we have

$$\sum_{ijmn:i\neq j} L_{mi} L_{ni} \frac{\partial \langle \phi_m | V(j) | \phi_n \rangle_i}{\partial \mathbf{R}_X}$$

$$= \sum_{ijn:i\neq j} L_{Xi} L_{ni} \frac{\partial \langle \phi_X | V(j) | \phi_n \rangle_i}{\partial \mathbf{R}_X} + \sum_{ijm:i\neq j} L_{mi} L_{Xi} \frac{\partial \langle \phi_m | V(j) | \phi_X \rangle_i}{\partial \mathbf{R}_X} + \sum_{imn:i\neq X} L_{mi} L_{ni} \frac{\partial \langle \phi_m | V(X) | \phi_n \rangle_i}{\partial \mathbf{R}_X}$$

$$= \sum_{ijn:i\neq j} L_{Xi} L_{ni} \frac{\partial \langle \phi_X | V(j) | \phi_n \rangle_i}{\partial \mathbf{R}_X} + \sum_{ijn:i\neq j} L_{ni} L_{Xi} \frac{\partial \langle \phi_n | V(j) | \phi_X \rangle_i}{\partial \mathbf{R}_X} + \sum_{imn:i\neq X} L_{mi} L_{ni} \frac{\partial \langle \phi_m | V(X) | \phi_n \rangle_i}{\partial \mathbf{R}_X}$$

$$= 2 \sum_{ijn:i\neq j} L_{Xi} L_{ni} \frac{\partial \langle \phi_X | V(j) | \phi_n \rangle_i}{\partial \mathbf{R}_X} + \sum_{imn:i\neq X} L_{mi} L_{ni} \frac{\partial \langle \phi_m | V(X) | \phi_n \rangle_i}{\partial \mathbf{R}_X}. \quad \text{(A.78)}$$

The last two terms in Eq. (A.76) can be proven equal,

$$\sum_{ijmn:i\neq j} \frac{\partial L_{mi}}{\partial \mathbf{R}_X} L_{ni} \langle \phi_m | V(j) | \phi_n \rangle_i = \sum_{ijmn:i\neq j} L_{mi} \frac{\partial L_{ni}}{\partial \mathbf{R}_X} \langle \phi_m | V(j) | \phi_n \rangle_i. \quad \text{(A.79)}$$

Put Eq. (A.78) and Eq. (A.79) into Eq. (A.76), we have

$$\sum_{ij:i\neq j} \frac{\partial T_{ii}^j}{\partial \mathbf{R}_X} = 2 \sum_{ijn:i\neq j} L_{Xi} L_{ni} \frac{\partial \langle \phi_X | V(j) | \phi_n \rangle_i}{\partial \mathbf{R}_X} + \sum_{imn:i\neq X} L_{mi} L_{ni} \frac{\partial \langle \phi_m | V(X) | \phi_n \rangle_i}{\partial \mathbf{R}_X}$$

$$+ 2 \sum_{ijmn:i\neq j} \frac{\partial L_{mi}}{\partial \mathbf{R}_X} L_{ni} \langle \phi_m | V(j) | \phi_n \rangle_i. \quad \text{(A.80)}$$

With Eq. (A.66), Eq. (A.71) and Eq. (A.80), we have the derivative

$$\sum_{ij:i\neq j} \frac{\partial V_{ij}^{\text{coul}}}{\partial \mathbf{R}_X} = \sum_{ij:i\neq j} \frac{\partial V_{ij}^{\text{coul}}}{\partial \mathbf{R}_X} + \sum_{ij:i\neq j} \frac{\partial V_{ijij}}{\partial \mathbf{R}_X} + 2 \sum_{ij:i\neq j} \frac{\partial T_{ii}^j}{\partial \mathbf{R}_X}. \quad \text{(A.81)}$$

Bibliography

[1] Masatoshi Imada, Atsushi Fujimori, and Yoshinori Tokura. "Metal-insulator transitions". In: *Rev. Mod. Phys.* 70 (4 Oct. 1998), pp. 1039–1263. DOI: 10.1103/RevModPhys.70.1039. URL: https://link.aps.org/doi/10.1103/RevModPhys.70.1039.

[2] V. Dobrosavljevic. "Introduction to Metal-Insulator Transitions". In: *arXiv:1112.6166* (2011). DOI: 10.48550/arXiv.1112.6166.

[3] A. H. Wilson. "The theory of electronic semi-conductors". In: *Proc. Roy. Soc. (London)* A133 (1931), p. 438. DOI: 10.1098/rspa.1931.0162.

[4] A. H. Wilson. "The theory of electronic semi-conductors. - II". In: *Proc. Roy. Soc. (London)* A134 (1931), p. 277. DOI: 10.1098/rspa.1931.0196.

[5] J. H. de Boer and E. J. W. Verwey. "Semi-conductors with partially and with completely filled 3d-lattice bands". In: *Proceedings of the Physical Society* 49.4S (Aug. 1937), p. 59. DOI: 10.1088/0959-5309/49/4S/307. URL: https://dx.doi.org/10.1088/0959-5309/49/4S/307.

[6] N. F. Mott and R. Peierls. "Discussion of the paper by de Boer and Verwey". In: *Proc. Phys. Soc.* 49 (1937), p. 72. DOI: 10.1088/0959-5309/49/4S/308.

[7] N. F. Mott. "The Basis of the Electron Theory of Metals, with Special Reference to the Transition Metals". In: *Proceedings of the Physical Society. Section A* 62.7 (July 1949), p. 416. DOI: 10.1088/0370-1298/62/7/303. URL: https://dx.doi.org/10.1088/0370-1298/62/7/303.

[8] N. F. Mott. "ON THE TRANSITION TO METALLIC CONDUCTION IN SEMICONDUCTORS". In: *Can. J. Phys.* 34 (1956), p. 1356. DOI: 10.1139/p56-151.

[9] N. F. Mott. "The transition to the metallic state". In: *The Philosophical Magazine: A Journal of Theoretical Experimental and Applied Physics* 6.62 (1961), pp. 287–309. DOI: 10.1080/14786436108243318.

[10] P. W. Anderson. "New Approach to the Theory of Superexchange Interactions". In: *Phys. Rev.* 115 (1 July 1959), pp. 2–13. DOI: 10.1103/PhysRev.115.2. URL: https://link.aps.org/doi/10.1103/PhysRev.115.2.

[11] J. Hubbard. "Electron correlations in narrow energy bands". In: *Proc. R. Soc. Lond.* A276 (1963), p. 238. DOI: 10.1098/rspa.1963.0204.

[12] J. Hubbard. "Electron correlations in narrow energy bands. II. The degenerate band case". In: *Proc. R. Soc. Lond.* A277 (1964), p. 237. DOI: 10.1098/rspa.1964.0019.

[13] J. Hubbard. "Electron Correlations in Narrow Energy Bands. III. An Improved Solution". In: *Proc. R. Soc. Lond.* A281 (1964), p. 401. DOI: 10.1098/rspa.1964.0190.

[14] J. Kanamori. "Electron Correlation and Ferromagnetism of Transition Metals". In: *Progress of Theoretical Physics* 30.3 (1963), p. 275. DOI: 10.1143/PTP.30.275.

[15] Elliott H. Lieb and F. Y. Wu. "Absence of Mott Transition in an Exact Solution of the Short-Range, One-Band Model in One Dimension". In: *Phys. Rev. Lett.* 20 (25 June 1968), pp. 1445–1448. DOI: 10.1103/PhysRevLett.20.1445. URL: https://link.aps.org/doi/10.1103/PhysRevLett.20.1445.

[16] Elbio Dagotto. "Correlated electrons in high-temperature superconductors". In: *Rev. Mod. Phys.* 66 (3 July 1994), pp. 763–840. DOI: 10.1103/RevModPhys.66.763. URL: https://link.aps.org/doi/10.1103/RevModPhys.66.763.

[17] Emanuel Gull et al. "Continuous-time Monte Carlo methods for quantum impurity models". In: *Rev. Mod. Phys.* 83 (2 May 2011), pp. 349–404. DOI: 10.1103/RevModPhys.83.349. URL: https://link.aps.org/doi/10.1103/RevModPhys.83.349.

[18] Ralf Bulla, Theo A. Costi, and Thomas Pruschke. "Numerical renormalization group method for quantum impurity systems". In: *Rev. Mod. Phys.* 80 (2 Apr. 2008), pp. 395–450. DOI: 10.1103/RevModPhys.80.395. URL: https://link.aps.org/doi/10.1103/RevModPhys.80.395.

[19] Antoine Georges et al. "Dynamical mean-field theory of strongly correlated fermion systems and the limit of infinite dimensions". In: *Rev. Mod. Phys.* 68 (1 Jan. 1996), pp. 13–125. DOI: 10.1103/RevModPhys.68.13. URL: https://link.aps.org/doi/10.1103/RevModPhys.68.13.

[20] G. Kotliar et al. "Electronic structure calculations with dynamical mean-field theory". In: *Rev. Mod. Phys.* 78 (3 Aug. 2006), pp. 865–951. DOI: 10.1103/RevModPhys.78.865. URL: https://link.aps.org/doi/10.1103/RevModPhys.78.865.

[21] Martin C. Gutzwiller. "Effect of Correlation on the Ferromagnetism of Transition Metals". In: *Phys. Rev. Lett.* 10 (5 Mar. 1963), pp. 159–162. DOI: 10.1103/PhysRevLett.10.159. URL: https://link.aps.org/doi/10.1103/PhysRevLett.10.159.

[22] Martin C. Gutzwiller. "Effect of Correlation on the Ferromagnetism of Transition Metals". In: *Phys. Rev.* 134 (4A May 1964), A923–A941. DOI: 10.1103/

`PhysRev.134.A923`. URL: `https://link.aps.org/doi/10.1103/PhysRev.134.A923`.

[23] Martin C. Gutzwiller. "Correlation of Electrons in a Narrow s Band". In: *Phys. Rev.* 137 (6A Mar. 1965), A1726–A1735. DOI: `10.1103/PhysRev.137.A1726`. URL: `https://link.aps.org/doi/10.1103/PhysRev.137.A1726`.

[24] Walter Metzner and Dieter Vollhardt. "Correlated Lattice Fermions in $d = \infty$ Dimensions". In: *Phys. Rev. Lett.* 62 (3 Jan. 1989), pp. 324–327. DOI: `10.1103/PhysRevLett.62.324`. URL: `https://link.aps.org/doi/10.1103/PhysRevLett.62.324`.

[25] W. Metzner. "Variational theory for correlated lattice fermions in high dimensions". In: *Z. Physik B* 77 (1989), p. 253. DOI: `10.1007/BF01313669`.

[26] Gabriel Kotliar and Andrei E. Ruckenstein. "New Functional Integral Approach to Strongly Correlated Fermi Systems: The Gutzwiller Approximation as a Saddle Point". In: *Phys. Rev. Lett.* 57 (11 Sept. 1986), pp. 1362–1365. DOI: `10.1103/PhysRevLett.57.1362`. URL: `https://link.aps.org/doi/10.1103/PhysRevLett.57.1362`.

[27] J. Bünemann and F. Gebhard. "Equivalence of Gutzwiller and slave-boson mean-field theories for multiband Hubbard models". In: *Phys. Rev. B* 76 (19 Nov. 2007), p. 193104. DOI: `10.1103/PhysRevB.76.193104`. URL: `https://link.aps.org/doi/10.1103/PhysRevB.76.193104`.

[28] Frank Lechermann et al. "Rotationally invariant slave-boson formalism and momentum dependence of the quasiparticle weight". In: *Phys. Rev. B* 76 (15 Oct. 2007), p. 155102. DOI: `10.1103/PhysRevB.76.155102`. URL: `https://link.aps.org/doi/10.1103/PhysRevB.76.155102`.

[29] Nicola Lanatà et al. "Slave Boson Theory of Orbital Differentiation with Crystal Field Effects: Application to UO_2". In: *Phys. Rev. Lett.* 118 (12 Mar. 2017), p. 126401. DOI: 10.1103/PhysRevLett.118.126401. URL: https://link.aps.org/doi/10.1103/PhysRevLett.118.126401.

[30] W. F. Brinkman and T. M. Rice. "Application of Gutzwiller's Variational Method to the Metal-Insulator Transition". In: *Phys. Rev. B* 2 (10 Nov. 1970), pp. 4302–4304. DOI: 10.1103/PhysRevB.2.4302. URL: https://link.aps.org/doi/10.1103/PhysRevB.2.4302.

[31] P. Hohenberg and W. Kohn. "Inhomogeneous Electron Gas". In: *Phys. Rev.* 136 (3B Nov. 1964), B864–B871. DOI: 10.1103/PhysRev.136.B864. URL: https://link.aps.org/doi/10.1103/PhysRev.136.B864.

[32] W. Kohn and L. J. Sham. "Self-Consistent Equations Including Exchange and Correlation Effects". In: *Phys. Rev.* 140 (4A Nov. 1965), A1133–A1138. DOI: 10.1103/PhysRev.140.A1133. URL: https://link.aps.org/doi/10.1103/PhysRev.140.A1133.

[33] Dieter Vollhardt. "Normal ^{3}He: an almost localized Fermi liquid". In: *Rev. Mod. Phys.* 56 (1 Jan. 1984), pp. 99–120. DOI: 10.1103/RevModPhys.56.99. URL: https://link.aps.org/doi/10.1103/RevModPhys.56.99.

[34] M. A. Paalanen et al. "Thermodynamic Behavior near a Metal-Insulator Transition". In: *Phys. Rev. Lett.* 61 (5 Aug. 1988), pp. 597–600. DOI: 10.1103/PhysRevLett.61.597. URL: https://link.aps.org/doi/10.1103/PhysRevLett.61.597.

[35] D. Belitz and T. R. Kirkpatrick. "The Anderson-Mott transition". In: *Rev. Mod. Phys.* 66 (2 Apr. 1994), pp. 261–380. DOI: 10.1103/RevModPhys.66.261. URL: https://link.aps.org/doi/10.1103/RevModPhys.66.261.

[36] V. Dobrosavljevi ć and G. Kotliar. "Mean Field Theory of the Mott-Anderson Transition". In: *Phys. Rev. Lett.* 78 (20 May 1997), pp. 3943–3946. DOI: `10.1103/PhysRevLett.78.3943`. URL: `https://link.aps.org/doi/10.1103/PhysRevLett.78.3943`.

[37] E. Miranda and V. Dobrosavljevi ć. "Localization-Induced Griffiths Phase of Disordered Anderson Lattices". In: *Phys. Rev. Lett.* 86 (2 Jan. 2001), pp. 264–267. DOI: `10.1103/PhysRevLett.86.264`. URL: `https://link.aps.org/doi/10.1103/PhysRevLett.86.264`.

[38] Riku Yamamoto et al. "Electronic Griffiths Phase in Disordered Mott-Transition Systems". In: *Phys. Rev. Lett.* 124 (4 Jan. 2020), p. 046404. DOI: `10.1103/PhysRevLett.124.046404`. URL: `https://link.aps.org/doi/10.1103/PhysRevLett.124.046404`.

[39] N. F. Mott. "The Electrical Properties of Liquid Mercury". In: *Philosophical Magazine* 13.125 (1966), pp. 989–1014. DOI: `10.1080/14786436608213149`.

[40] J. M. Ziman. "A theory of the electrical properties of liquid metals. I: The monovalent metals". In: *The Philosophical Magazine: A Journal of Theoretical Experimental and Applied Physics* 6.68 (1961), pp. 1013–1034. DOI: `10.1080/14786436108243361`. URL: `https://doi.org/10.1080/14786436108243361`.

[41] Morrel H. Cohen and Joshua Jortner. "Conduction regimes in expanded liquid mercury". In: *Phys. Rev. A* 10 (3 Sept. 1974), pp. 978–996. DOI: `10.1103/PhysRevA.10.978`. URL: `https://link.aps.org/doi/10.1103/PhysRevA.10.978`.

[42] Fumiko Yonezawa et al. "Electron correlations and metal-insulator transition in structurally disordered systems: General theory and application to supercritical alkali metals". In: *Phys. Rev. B* 10 (6 Sept. 1974), pp. 2322–2332. DOI:

`10.1103/PhysRevB.10.2322`. URL: `https://link.aps.org/doi/10.1103/PhysRevB.10.2322`.

[43] N. F. MOTT. "Metal-Insulator Transition". In: *Rev. Mod. Phys.* 40 (4 Oct. 1968), pp. 677–683. DOI: `10.1103/RevModPhys.40.677`. URL: `https://link.aps.org/doi/10.1103/RevModPhys.40.677`.

[44] S. R. Bickham et al. "Ab initio molecular dynamics of expanded liquid sodium". In: *Phys. Rev. B* 58 (18 Nov. 1998), R11813–R11816. DOI: `10.1103/PhysRevB.58.R11813`. URL: `https://link.aps.org/doi/10.1103/PhysRevB.58.R11813`.

[45] A Kietzmann et al. "Structure of expanded fluid Rb and Cs: a quantum molecular dynamics study". In: *Journal of Physics: Condensed Matter* 18.24 (June 2006), p. 5597. DOI: `10.1088/0953-8984/18/24/002`. URL: `https://dx.doi.org/10.1088/0953-8984/18/24/002`.

[46] F. Hensel. "The Liquid-Vapour Phase Transition in Fluid Metals". In: *Phil. Trans. R. Soc. A.* 356 (1998), p. 97. DOI: `10.1098/rsta.1998.0152`.

[47] S. Jüngst, B. Knuth, and F. Hensel. "Observation of Singular Diameters in the Coexistence Curves of Metals". In: *Phys. Rev. Lett.* 55 (20 Nov. 1985), pp. 2160–2163. DOI: `10.1103/PhysRevLett.55.2160`. URL: `https://link.aps.org/doi/10.1103/PhysRevLett.55.2160`.

[48] H Renkert, F Hensel, and E.U Franck. "Metal-nonmetal transition in dense cesium vapour". In: *Physics Letters A* 30.9 (1969), pp. 494–495. ISSN: 0375-9601. DOI: `https://doi.org/10.1016/0375-9601(69)90266-7`. URL: `https://www.sciencedirect.com/science/article/pii/0375960169902667`.

100

[49] P. P. Edwards. "The Metal-Nonmetal Transition: A Global Perspective". In: *J. Phys. Chem.* 99 (1995), p. 5228. DOI: 10.1021/j100015a002.

[50] W.-C. Pilgrim et al. "Monatomic-Molecular Transition in Expanded Rubidium". In: *Phys. Rev. Lett.* 78 (19 May 1997), pp. 3685–3688. DOI: 10.1103/PhysRevLett.78.3685. URL: https://link.aps.org/doi/10.1103/PhysRevLett.78.3685.

[51] K. Matsuda, K. Tamura, and M. Inui. "Instability of the Electron Gas in an Expanding Metal". In: *Phys. Rev. Lett.* 98 (9 Feb. 2007), p. 096401. DOI: 10.1103/PhysRevLett.98.096401. URL: https://link.aps.org/doi/10.1103/PhysRevLett.98.096401.

[52] K Tamura, K Matsuda, and M Inui. "Structural and electronic properties of expanding fluid metals". In: *Journal of Physics: Condensed Matter* 20.11 (Feb. 2008), p. 114102. DOI: 10.1088/0953-8984/20/11/114102. URL: https://dx.doi.org/10.1088/0953-8984/20/11/114102.

[53] W. Freyland. "Magnetic susceptibility of metallic and nonmetallic expanded fluid cesium". In: *Phys. Rev. B* 20 (12 Dec. 1979), pp. 5104–5110. DOI: 10.1103/PhysRevB.20.5104. URL: https://link.aps.org/doi/10.1103/PhysRevB.20.5104.

[54] U. El-Hanany, G. F. Brennert, and W. W. Warren. "Enhanced Paramagnetism and Spin Fluctuations in Expanded Liquid Cesium". In: *Phys. Rev. Lett.* 50 (7 Feb. 1983), pp. 540–544. DOI: 10.1103/PhysRevLett.50.540. URL: https://link.aps.org/doi/10.1103/PhysRevLett.50.540.

[55] W. W. Warren, G. F. Brennert, and U. El-Hanany. "NMR investigation of the electronic structure of expanded liquid cesium". In: *Phys. Rev. B* 39 (7

Mar. 1989), pp. 4038–4050. DOI: 10.1103/PhysRevB.39.4038. URL: https://link.aps.org/doi/10.1103/PhysRevB.39.4038.

[56]   B. Knuth and F. Hensel. "The optical properties of expanded liquid cesium". In: *High Pressure Research* 4.1-6 (1990), pp. 552–554. DOI: 10.1080/08957959008246185. URL: https://doi.org/10.1080/08957959008246185.

[57]   Gia-Wei Chern et al. "Mott Transition in a Metallic Liquid: Gutzwiller Molecular Dynamics Simulations". In: *Phys. Rev. Lett.* 118 (22 June 2017), p. 226401. DOI: 10.1103/PhysRevLett.118.226401. URL: https://link.aps.org/doi/10.1103/PhysRevLett.118.226401.

[58]   J. Bünemann, F. Gebhard, and W. Weber. "Gutzwiller-correlated wave functions for degenerate bands: exact results in infinite dimensions". In: *Journal of Physics: Condensed Matter* 9.35 (Sept. 1997), p. 7343. DOI: 10.1088/0953-8984/9/35/009. URL: https://dx.doi.org/10.1088/0953-8984/9/35/009.

[59]   J. Bünemann, W. Weber, and F. Gebhard. "Multiband Gutzwiller wave functions for general on-site interactions". In: *Phys. Rev. B* 57 (12 Mar. 1998), pp. 6896–6916. DOI: 10.1103/PhysRevB.57.6896. URL: https://link.aps.org/doi/10.1103/PhysRevB.57.6896.

[60]   Jörg Bünemann, Florian Gebhard, and Rüdiger Thul. "Landau-Gutzwiller quasiparticles". In: *Phys. Rev. B* 67 (7 Feb. 2003), p. 075103. DOI: 10.1103/PhysRevB.67.075103. URL: https://link.aps.org/doi/10.1103/PhysRevB.67.075103.

[61]   Michele Fabrizio. "Gutzwiller description of non-magnetic Mott insulators: Dimer lattice model". In: *Phys. Rev. B* 76 (16 Oct. 2007), p. 165110. DOI: 10.1103/PhysRevB.76.165110. URL: https://link.aps.org/doi/10.1103/PhysRevB.76.165110.

102

[62]   Nicola Lanatà, Paolo Barone, and Michele Fabrizio. "Fermi-surface evolution across the magnetic phase transition in the Kondo lattice model". In: *Phys. Rev. B* 78 (15 Oct. 2008), p. 155127. DOI: 10.1103/PhysRevB.78.155127. URL: https://link.aps.org/doi/10.1103/PhysRevB.78.155127.

[63]   Nicola Lanatà et al. "Efficient implementation of the Gutzwiller variational method". In: *Phys. Rev. B* 85 (3 Jan. 2012), p. 035133. DOI: 10.1103/PhysRevB.85.035133. URL: https://link.aps.org/doi/10.1103/PhysRevB.85.035133.

[64]   Wan-Sheng Wang et al. "Finite-temperature Gutzwiller projection for strongly correlated electron systems". In: *Phys. Rev. B* 82 (12 Sept. 2010), p. 125105. DOI: 10.1103/PhysRevB.82.125105. URL: https://link.aps.org/doi/10.1103/PhysRevB.82.125105.

[65]   Matteo Sandri, Massimo Capone, and Michele Fabrizio. "Finite-temperature Gutzwiller approximation and the phase diagram of a toy model for V_2O_3". In: *Phys. Rev. B* 87 (20 May 2013), p. 205108. DOI: 10.1103/PhysRevB.87.205108. URL: https://link.aps.org/doi/10.1103/PhysRevB.87.205108.

[66]   M. Allen and D. Tildesley. *Computer simulation of liquids*. New York: Oxford University Press, 1989.

[67]   D. C. Rapaport. *The art of molecular dynamics simulation*. Cambridge: Cambridge University Press, 2011.

[68]   N. F. Mott. *Metal-Insulator Transitions*. New York: Taylor & Francis, 1997.

[69]   V Dobrosavljević. *Introduction to Metal-Insulator Transitions*. Oxford: Oxford University Press, 2012.

[70]   Ferdinand Evers and Alexander D. Mirlin. "Anderson transitions". In: *Rev. Mod. Phys.* 80 (4 Oct. 2008), pp. 1355–1417. DOI: 10.1103/RevModPhys.80.1355. URL: https://link.aps.org/doi/10.1103/RevModPhys.80.1355.

[71]   Patrick A. Lee and T. V. Ramakrishnan. "Disordered electronic systems". In: *Rev. Mod. Phys.* 57 (2 Apr. 1985), pp. 287–337. DOI: 10.1103/RevModPhys.57.287. URL: https://link.aps.org/doi/10.1103/RevModPhys.57.287.

[72]   Dmitry A. Abanin et al. "Colloquium: Many-body localization, thermalization, and entanglement". In: *Rev. Mod. Phys.* 91 (2 May 2019), p. 021001. DOI: 10.1103/RevModPhys.91.021001. URL: https://link.aps.org/doi/10.1103/RevModPhys.91.021001.

[73]   S. Das Sarma and E. H. Hwang. "Charged Impurity-Scattering-Limited Low-Temperature Resistivity of Low-Density Silicon Inversion Layers". In: *Phys. Rev. Lett.* 83 (1 July 1999), pp. 164–167. DOI: 10.1103/PhysRevLett.83.164. URL: https://link.aps.org/doi/10.1103/PhysRevLett.83.164.

[74]   Igor F. Herbut. "The effect of parallel magnetic field on the Boltzmann conductivity and the Hall coefficient of a disordered two-dimensional Fermi liquid". In: *Phys. Rev. B* 63 (11 Feb. 2001), p. 113102. DOI: 10.1103/PhysRevB.63.113102. URL: https://link.aps.org/doi/10.1103/PhysRevB.63.113102.

[75]   H. Javan Mard et al. "Non-Gaussian Spatial Correlations Dramatically Weaken Localization". In: *Phys. Rev. Lett.* 114 (5 Feb. 2015), p. 056401. DOI: 10.1103/PhysRevLett.114.056401. URL: https://link.aps.org/doi/10.1103/PhysRevLett.114.056401.

[76]   F. Hensel and W. W. Warren. *Fluid Metals: The Liquid-Vapor Transition of Metals.* Princeton University Press, 2016.

[77]   F. Hensel et al. "Metal-Nonmetal Transition and the Critical Point Phase Transition in Fluid Cesium". In: *Localization and Metal-Insulator Transitions*. Ed. by H. Fritzsche and D. Adler. N.Y.: Springer New York, 1985, pp. 109–117. DOI: https://doi.org/10.1007/978-1-4613-2517-8.

[78]   R. Winter et al. "The static structure factor of cesium over the whole liquid range up to the critical point". In: *Berichte der Bunsengesellschaft für physikalische Chemie* 91.12 (1987), pp. 1327–1330. DOI: https://doi.org/10.1002/bbpc.19870911205. URL: https://onlinelibrary.wiley.com/doi/abs/10.1002/bbpc.19870911205.

[79]   F Hensel. "Experiments on Expanded Metals in the Metal-Nonmetal Transition Region". In: *Physica Scripta* 1989.T25 (Jan. 1989), p. 283. DOI: 10.1088/0031-8949/1989/T25/051. URL: https://dx.doi.org/10.1088/0031-8949/1989/T25/051.

[80]   V M Nield, M A Howe, and R L McGreevy. "The metal-nonmetal transition in expanded caesium". In: *Journal of Physics: Condensed Matter* 3.38 (Sept. 1991), p. 7519. DOI: 10.1088/0953-8984/3/38/023. URL: https://dx.doi.org/10.1088/0953-8984/3/38/023.

[81]   U. El-Hanany, G. F. Brennert, and W. W. Warren. "Enhanced Paramagnetism and Spin Fluctuations in Expanded Liquid Cesium". In: *Phys. Rev. Lett.* 50 (7 Feb. 1983), pp. 540–544. DOI: 10.1103/PhysRevLett.50.540. URL: https://link.aps.org/doi/10.1103/PhysRevLett.50.540.

[82]   D. Marx and J. Hutter. *Ab initio molecular dynamics: basic theory and advance methods.* Cambridge: Cambridge University Press, 2009.

[83]   Ryogo Kubo. "Statistical-Mechanical Theory of Irreversible Processes. I. General Theory and Simple Applications to Magnetic and Conduction Problems".

In: *Journal of the Physical Society of Japan* 12.6 (1957), pp. 570–586. DOI: 10.1143/JPSJ.12.570. URL: https://doi.org/10.1143/JPSJ.12.570.

[84] D A Greenwood. "The Boltzmann Equation in the Theory of Electrical Conduction in Metals". In: *Proceedings of the Physical Society* 71.4 (Apr. 1958), p. 585. DOI: 10.1088/0370-1328/71/4/306. URL: https://dx.doi.org/10.1088/0370-1328/71/4/306.

[85] L. Calderín, V.V. Karasiev, and S.B. Trickey. "Kubo-Greenwood electrical conductivity formulation and implementation for projector augmented wave datasets". In: *Computer Physics Communications* 221 (2017), pp. 118–142. ISSN: 0010-4655. DOI: https://doi.org/10.1016/j.cpc.2017.08.008. URL: https://www.sciencedirect.com/science/article/pii/S0010465517302539.

[86] G. D. Mahan. *Many-Particle Physics*. New York: Plenum, 1990.

[87] Indranil Paul and Gabriel Kotliar. "Thermal transport for many-body tight-binding models". In: *Phys. Rev. B* 67 (11 Mar. 2003), p. 115131. DOI: 10.1103/PhysRevB.67.115131. URL: https://link.aps.org/doi/10.1103/PhysRevB.67.115131.

[88] Pier Luigi Silvestrelli, Ali Alavi, and Michele Parrinello. "Electrical-conductivity calculation in ab initio simulations of metals:Application to liquid sodium". In: *Phys. Rev. B* 55 (23 June 1997), pp. 15515–15522. DOI: 10.1103/PhysRevB.55.15515. URL: https://link.aps.org/doi/10.1103/PhysRevB.55.15515.

[89] I. Kwon et al. "Electrical conductivities for hot, dense hydrogen". In: *Phys. Rev. E* 54 (3 Sept. 1996), pp. 2844–2851. DOI: 10.1103/PhysRevE.54.2844. URL: https://link.aps.org/doi/10.1103/PhysRevE.54.2844.

[90] V. Dobrosavljevi ć and G. Kotliar. "Hubbard models with random hopping in d=∞". In: *Phys. Rev. Lett.* 71 (19 Nov. 1993), pp. 3218–3221. DOI: 10. 1103/PhysRevLett.71.3218. URL: https://link.aps.org/doi/10.1103/ PhysRevLett.71.3218.

[91] V. Dobrosavljevi ć and G. Kotliar. "Strong correlations and disorder in d=∞ and beyond". In: *Phys. Rev. B* 50 (3 July 1994), pp. 1430–1449. DOI: 10.1103/ PhysRevB.50.1430. URL: https://link.aps.org/doi/10.1103/PhysRevB. 50.1430.

[92] N. F. Mott and E. A. Davis. *Electronic Processes in Non-Crystalline Materials.* Second. Oxford: Clarendon Press, 1979.

[93] Y. Frenkel. *Kinetic Theory of Liquids.* New York: Dover, 1955.

[94] U. Balucani and M. Zoppi. *Dynamics of the Liquid State.* Oxford: Clarendon Press, 1994.

[95] R. L. Liboff. *Kinetic Theory.* New York: Springer-Verlag, 2003.

[96] R. Zwanzig. "On the relation between self-diffusion and viscosity of liquids". In: *J. Chem. Phys.* 79 (1983), p. 4507. DOI: 10.1063/1.446338.

[97] E. L. Cussler. *Diffusion - Mass Transfer in Fluid Systems.* Cambridge: Cambridge University Press, 2009.

[98] P. M. Chaikin and T. C. Lubensky. *Principles of condensed matter physics.* Cambridge: Cambridge University Press, 1995.

[99] J.-P. Hansen and I. R. McDonald. *Theory of Simple Liquids 3rd Ed.* Academic Press, 2006.

[100] J. E. Lennard-Jones. "Cohesion". In: *Proc. Phys. Soc.* 43 (1941), p. 461. DOI: 10.1088/0959-5309/43/5/301.

[101]   A. J. Stone. *The Theory of Intermolecular Forces*. Oxford University Press, 2013.

[102]   Tullio Scopigno, Giancarlo Ruocco, and Francesco Sette. "Microscopic dynamics in liquid metals: The experimental point of view". In: *Rev. Mod. Phys.* 77 (3 Sept. 2005), pp. 881–933. DOI: 10.1103/RevModPhys.77.881. URL: https://link.aps.org/doi/10.1103/RevModPhys.77.881.

[103]   N. H. March. *Liquid Metals: Concepts and Theory*. Cambridge: Cambridge University Press, 1990.

[104]   Carlos Fiolhais et al. "Dominant density parameters and local pseudopotentials for simple metals". In: *Phys. Rev. B* 51 (20 May 1995), pp. 14001–14011. DOI: 10.1103/PhysRevB.51.14001. URL: https://link.aps.org/doi/10.1103/PhysRevB.51.14001.

[105]   L. E. Gonzalez et al. "A theoretical study of the static structure and thermodynamics of liquid lithium". In: *Journal of Physics: Condensed Matter* 5.26 (June 1993), p. 4283. DOI: 10.1088/0953-8984/5/26/003. URL: https://dx.doi.org/10.1088/0953-8984/5/26/003.

[106]   Manel Canales, Luis Enrique González, and Joan Àngel Padró. "Computer simulation study of liquid lithium at 470 and 843 K". In: *Phys. Rev. E* 50 (5 Nov. 1994), pp. 3656–3669. DOI: 10.1103/PhysRevE.50.3656. URL: https://link.aps.org/doi/10.1103/PhysRevE.50.3656.

[107]   J.-F. Wax and N. Jakse. "Large-scale molecular dynamics study of liquid K-Cs alloys: Structural, thermodynamic, and diffusion properties". In: *Phys. Rev. B* 75 (2 Jan. 2007), p. 024204. DOI: 10.1103/PhysRevB.75.024204. URL: https://link.aps.org/doi/10.1103/PhysRevB.75.024204.

[108] J W E Lewis and S W Lovesey. "Short-wavelength collective density excitations in monatomic liquids". In: *Journal of Physics C: Solid State Physics* 10.17 (Sept. 1977), p. 3221. DOI: 10.1088/0022-3719/10/17/007. URL: https://dx.doi.org/10.1088/0022-3719/10/17/007.

[109] Shaw Kambayashi and Yasuaki Hiwatari. "Molecular-dynamics study of dynamical properties of dense soft-sphere fluids: The role of short-range repulsion of the intermolecular potential". In: *Phys. Rev. E* 49 (2 Feb. 1994), pp. 1251–1259. DOI: 10.1103/PhysRevE.49.1251. URL: https://link.aps.org/doi/10.1103/PhysRevE.49.1251.

[110] M. Canales and J. A. Padró. "Static and dynamic structure of liquid metals: Role of the different parts of the interaction potential". In: *Phys. Rev. E* 56 (2 Aug. 1997), pp. 1759–1764. DOI: 10.1103/PhysRevE.56.1759. URL: https://link.aps.org/doi/10.1103/PhysRevE.56.1759.

[111] M. Canales and J. A. Padró. "Dynamic properties of Lennard-Jones fluids and liquid metals". In: *Phys. Rev. E* 60 (1 July 1999), pp. 551–558. DOI: 10.1103/PhysRevE.60.551. URL: https://link.aps.org/doi/10.1103/PhysRevE.60.551.

[112] N. Anento, J. A. Padró, and M. Canales. "Dynamic properties of simple liquids: Dependence on the softness of the potential core". In: *J. Chem. Phys.* 111 (1999), p. 10210. DOI: 10.1063/1.480371.

[113] David Chandler and John D. Weeks. "Equilibrium Structure of Simple Liquids". In: *Phys. Rev. Lett.* 25 (3 July 1970), pp. 149–152. DOI: 10.1103/PhysRevLett.25.149. URL: https://link.aps.org/doi/10.1103/PhysRevLett.25.149.

[114] J. D. Weeks, D. Chandler, and H. C. Andersen. "Role of Repulsive Forces in Determining the Equilibrium Structure of Simple Liquids". In: *J. Chem. Phys.* 54 (1971), p. 5237. DOI: 10.1063/1.1674820.

[115] P. Ascarelli and A. Paskin. "Dense-Gas Formulation of Self-Diffusion of Liquid Metals". In: *Phys. Rev.* 165 (1 Jan. 1968), pp. 222–224. DOI: 10.1103/PhysRev.165.222. URL: https://link.aps.org/doi/10.1103/PhysRev.165.222.

[116] D. Chandler. "Equilibrium Structure and Molecular Motion in Liquids". In: *Acc. Chem. Res.* 7 (1974), p. 246. DOI: 10.1021/ar50080a002.

[117] H. C. Andersen P. Protopapas and N. A. D. Parlee. "Theory of transport in liquid metals. I. Calculation of self-diffusion coefficients". In: *J. Chem. Phys.* 59 (1973), p. 15. DOI: 10.1063/1.1679784.

[118] E. Helfand. "Theory of the molecular friction constant". In: *Phys. Fluids* 4 (1961), p. 1. DOI: 10.1063/1.1706384.

[119] H. T. Davis and J. A. Palyvos. "Contribution to the friction coefficient from time correlations between hard and soft molecular interactions". In: *J. Chem. Phys.* 46 (1967), p. 4043. DOI: 10.1134/S0036029517080055.

[120] T Gaskell. "Velocity autocorrelation function and diffusion coefficient in a liquid". In: *Journal of Physics C: Solid State Physics* 4.12 (Aug. 1971), p. 1466. DOI: 10.1088/0022-3719/4/12/003. URL: https://dx.doi.org/10.1088/0022-3719/4/12/003.

[121] John E. Straub. "Analysis of the role of attractive forces in self-diffusion of a simple fluid". In: *Molecular Physics* 76.2 (1992), pp. 373–385. DOI: 10.1080/00268979200101391. URL: https://doi.org/10.1080/00268979200101391.

[122] N. F. Mott. *Metal-Insulator Transition, 2nd Ed.* London: Taylor & Francis, 1990.

[123] P. Tarazona, E. Chacón, and J. P. Hernandez. "Simple Model for the Phase Coexistence and Electrical Conductivity of Alkali Fluids". In: *Phys. Rev. Lett.* 74 (1 Jan. 1995), pp. 142–145. DOI: `10.1103/PhysRevLett.74.142`. URL: `https://link.aps.org/doi/10.1103/PhysRevLett.74.142`.

[124] M. P. Allen and D. J. Tildesley. *Computer Simulation of Liquids.* Oxford: Clarendon Press, 1987.

[125] R. Iftimie, P. Minary, and M. E. Tuckerman. "Ab initio molecular dynamics: Concepts, recent developments, an future trends". In: *Proc. Natl. Acad. Sci. U.S.A.* 102 (2005), p. 6654. DOI: `10.1073/pnas.0500193102`.

[126] G.-W. Chern. "Kinetics of thermal Mott transitions in the Hubbard model". In: *arXiv:1907.05880* (2019). DOI: `10.48550/arXiv.1907.05880`.

[127] Philip M. Morse. "Diatomic Molecules According to the Wave Mechanics. II. Vibrational Levels". In: *Phys. Rev.* 34 (1 July 1929), pp. 57–64. DOI: `10.1103/PhysRev.34.57`. URL: `https://link.aps.org/doi/10.1103/PhysRev.34.57`.

[128] Yatendra Pal Varshni. "Comparative Study of Potential Energy Functions for Diatomic Molecules". In: *Rev. Mod. Phys.* 29 (4 Oct. 1957), pp. 664–682. DOI: `10.1103/RevModPhys.29.664`. URL: `https://link.aps.org/doi/10.1103/RevModPhys.29.664`.

[129] S. Chapman and T. Cowling. *The Mathematical Theory of Non-Uniform Gases.* Cambridge University Press, 1970.

[130] D. A. McQuarrie. *Statistical Mechanics.* New York: Harper and Row, 1976.

[131] R. J. Speedy et al. "Diffusion in simple fluids". In: *Molecular Physics* 66 (1989), p. 577. DOI: 10.1080/00268978900100341.

[132] K. M. Ho, J. Schmalian, and C. Z. Wang. "Gutzwiller density functional theory for correlated electron systems". In: *Phys. Rev. B* 77 (7 Feb. 2008), p. 073101. DOI: 10.1103/PhysRevB.77.073101. URL: https://link.aps.org/doi/10.1103/PhysRevB.77.073101.

[133] XiaoYu Deng et al. "Local density approximation combined with Gutzwiller method for correlated electron systems: Formalism and applications". In: *Phys. Rev. B* 79 (7 Feb. 2009), p. 075114. DOI: 10.1103/PhysRevB.79.075114. URL: https://link.aps.org/doi/10.1103/PhysRevB.79.075114.

[134] Ming-Feng Tian et al. "Intermediate-pressure phases of cerium studied by an LDA + Gutzwiller method". In: *Phys. Rev. B* 84 (20 Nov. 2011), p. 205124. DOI: 10.1103/PhysRevB.84.205124. URL: https://link.aps.org/doi/10.1103/PhysRevB.84.205124.

[135] Giovanni Borghi, Michele Fabrizio, and Erio Tosatti. "Gutzwiller electronic structure calculations applied to transition metals: Kinetic energy gain with ferromagnetic order in bcc Fe". In: *Phys. Rev. B* 90 (12 Sept. 2014), p. 125102. DOI: 10.1103/PhysRevB.90.125102. URL: https://link.aps.org/doi/10.1103/PhysRevB.90.125102.

[136] Graeme J. Ackland. "Bearing down on hydrogen". In: *Science* 348.6242 (2015), pp. 1429–1430. ISSN: 0036-8075. DOI: 10.1126/science.aac6626.

[137] N W Ashcroft. "The hydrogen liquids". In: *Journal of Physics: Condensed Matter* 12.8A (Feb. 2000), A129. DOI: 10.1088/0953-8984/12/8A/314. URL: https://dx.doi.org/10.1088/0953-8984/12/8A/314.

112

[138] Jeffrey M. McMahon et al. "The properties of hydrogen and helium under extreme conditions". In: *Rev. Mod. Phys.* 84 (4 Nov. 2012), pp. 1607–1653. DOI: 10.1103/RevModPhys.84.1607. URL: https://link.aps.org/doi/10.1103/RevModPhys.84.1607.

[139] S. A. Bonev et al. "A quantum fluid of metallic hydrogen suggested by first-principles calculations". In: *Nature* 431 (2004), p. 669. DOI: 10.1038/nature02968.

[140] C. F. Richardson and N. W. Ashcroft. "High Temperature Superconductivity in Metallic Hydrogen: Electron-Electron Enhancements". In: *Phys. Rev. Lett.* 78 (1 Jan. 1997), pp. 118–121. DOI: 10.1103/PhysRevLett.78.118. URL: https://link.aps.org/doi/10.1103/PhysRevLett.78.118.

[141] E. Babaev, A. Sudbo, and N. W. Ashcroft. "A superconductor to superfluid phase transition in liquid metallic hydrogen". In: *Nature* 431 (2004), p. 666. DOI: 10.1038/nature02910.

[142] P. Cudazzo et al. "Ab Initio Description of High-Temperature Superconductivity in Dense Molecular Hydrogen". In: *Phys. Rev. Lett.* 100 (25 June 2008), p. 257001. DOI: 10.1103/PhysRevLett.100.257001. URL: https://link.aps.org/doi/10.1103/PhysRevLett.100.257001.

[143] E. Wigner and H. B. Huntington. "On the possibility of a metallic modification of hydrogen". In: *Journal of Chemical Physics* 3 (1935), p. 764. DOI: 10.1063/1.1749590.

[144] S. T. Weir, A. C. Mitchell, and W. J. Nellis. "Metallization of Fluid Molecular Hydrogen at 140 GPa (1.4 Mbar)". In: *Phys. Rev. Lett.* 76 (11 Mar. 1996), pp. 1860–1863. DOI: 10.1103/PhysRevLett.76.1860. URL: https://link.aps.org/doi/10.1103/PhysRevLett.76.1860.

[145]   M. Eremets and I. Troyan. "Conductive dense hydrogen". In: *Nature Mater* 10 (2011), p. 927. DOI: 10.1038/nmat3175.

[146]   Vasily Dzyabura, Mohamed Zaghoo, and Isaac F. Silvera. "Evidence of a liquid–liquid phase transition in hot dense hydrogen". In: *Proceedings of the National Academy of Sciences* 110.20 (2013), pp. 8040–8044. DOI: 10.1073/pnas.1300718110. eprint: https://www.pnas.org/doi/pdf/10.1073/pnas.1300718110. URL: https://www.pnas.org/doi/abs/10.1073/pnas.1300718110.

[147]   R. P. Dias and I. F. Silvera. "Observation of the Wigner-Huntington transition to metallic hydrogen". In: *Science* 355 (2017), p. 715. DOI: 10.1126/science.aal1579.

[148]   G. Mazzola, S. Yunoki, and S. Sorella. "Unexpectedly high pressure for molecular dissociation in liquid hydrogen by electronic simulation". In: *Nat Commun* 5 (2014), p. 3487. DOI: 10.1038/ncomms4487.

[149]   Miguel A. Morales et al. "Nuclear Quantum Effects and Nonlocal Exchange-Correlation Functionals Applied to Liquid Hydrogen at High Pressure". In: *Phys. Rev. Lett.* 110 (6 Feb. 2013), p. 065702. DOI: 10.1103/PhysRevLett.110.065702. URL: https://link.aps.org/doi/10.1103/PhysRevLett.110.065702.

[150]   Jeremy McMinis et al. "Molecular to Atomic Phase Transition in Hydrogen under High Pressure". In: *Phys. Rev. Lett.* 114 (10 Mar. 2015), p. 105305. DOI: 10.1103/PhysRevLett.114.105305. URL: https://link.aps.org/doi/10.1103/PhysRevLett.114.105305.

[151]   Carlo Pierleoni et al. "Liquid–liquid phase transition in hydrogen by coupled electron–ion Monte Carlo simulations". In: *Proceedings of the National*

114

Academy of Sciences 113.18 (2016), pp. 4953–4957. ᴅᴏɪ: 10 . 1073 / pnas . 1603853113. eprint: https : / / www . pnas . org / doi / pdf / 10 . 1073 / pnas . 1603853113. ᴜʀʟ: https : / / www . pnas . org / doi / abs / 10 . 1073 / pnas . 1603853113.

[152] Guglielmo Mazzola, Ravit Helled, and Sandro Sorella. "Phase Diagram of Hydrogen and a Hydrogen-Helium Mixture at Planetary Conditions by Quantum Monte Carlo Simulations". In: *Phys. Rev. Lett.* 120 (2 Jan. 2018), p. 025701. ᴅᴏɪ: 10.1103/PhysRevLett.120.025701. ᴜʀʟ: https://link.aps.org/doi/ 10.1103/PhysRevLett.120.025701.

[153] J. C. Slater and G. F. Koster. "Simplified LCAO Method for the Periodic Potential Problem". In: *Phys. Rev.* 94 (6 June 1954), pp. 1498–1524. ᴅᴏɪ: 10 . 1103 / PhysRev . 94 . 1498. ᴜʀʟ: https : / / link . aps . org / doi / 10 . 1103 / PhysRev.94.1498.

[154] J. L. Fry et al. "Two-center approximation in the quantum theory of solids". In: *Phys. Rev. B* 15 (12 June 1977), pp. 5811–5820. ᴅᴏɪ: 10.1103/PhysRevB. 15.5811. ᴜʀʟ: https://link.aps.org/doi/10.1103/PhysRevB.15.5811.

[155] Y. X. Yao et al. "Correlation matrix renormalization approximation for total-energy calculations of correlated electron systems". In: *Phys. Rev. B* 89 (4 Jan. 2014), p. 045131. ᴅᴏɪ: 10 . 1103 / PhysRevB . 89 . 045131. ᴜʀʟ: https : //link.aps.org/doi/10.1103/PhysRevB.89.045131.

[156] Attila Szabo and Neil S. Ostlund. *Modern quantum chemistry : introduction to advanced electronic structure theory*. Mineola, NY: Dover, 1989.

[157] Lucjan Piela. "Appendix J - Orthogonalization". In: *Ideas of Quantum Chemistry (Second Edition)*. Ed. by Lucjan Piela. Second Edition. Oxford: Elsevier, 2014, e99–e103. ɪsʙɴ: 978-0-444-59436-5. ᴅᴏɪ: https://doi.org/10.1016/

`B978-0-444-59436-5.00030-1`. URL: `https://www.sciencedirect.com/science/article/pii/B9780444594365000301`.

[158] G. W. Pratt and S. F. Neustadter. "Maximal Orthogonal Orbitals". In: *Phys. Rev.* 101 (4 Feb. 1956), pp. 1248–1250. DOI: `10.1103/PhysRev.101.1248`. URL: `https://link.aps.org/doi/10.1103/PhysRev.101.1248`.

[159] Martin Head-Gordon and John A. Pople. "Optimization of wave function and geometry in the finite basis Hartree-Fock method". In: *The Journal of Physical Chemistry* 92.11 (1988), pp. 3063–3069. DOI: `10.1021/j100322a012`. eprint: `https://doi.org/10.1021/j100322a012`. URL: `https://doi.org/10.1021/j100322a012`.